Improved and Practical Energy Management Systems for Isolated Microgrids

by

Bharatkumar Solanki

A thesis
presented to the University of Waterloo
in fulfillment of the
thesis requirement for the degree of
Doctor of Philosophy
in
Electrical and Computer Engineering

Waterloo, Ontario, Canada, 2018

Examining Committee Membership

The following served on the Examining Committee for this thesis. The decision of the Examining Committee is by majority vote.

External Examiner:	Alberto Berizzi Professor, Politecnico di Milano Department of Energy
Supervisors:	Kankar Bhattacharya Professor, University of Waterloo Department of Electrical and Computer Engineering
	Claudio Cañizares Professor, University of Waterloo Department of Electrical and Computer Engineering
Internal Member:	Mehrdad Kazerani Professor, University of Waterloo Department of Electrical and Computer Engineering
Internal Member:	Kshirasagar Naik Professor, University of Waterloo Department of Electrical and Computer Engineering
Internal-external Member:	Kumaraswamy Ponnambalam Professor, University of Waterloo Department of Electrical and Computer Engineering

I hereby declare that I am the sole author of this thesis. This is a true copy of the thesis, including any required final revisions, as accepted by my examiners. I understand that my thesis may be made electronically available to the public.

Abstract

There are many remote communities around the world which do not have interconnection with the power grid because of technical and/or economic constraints, and thus have to manage their energy requirements independently, mainly from fossil-fuel-based and in some cases renewable-based generation, operating as isolated microgrids. The reliable and economic operation of a microgrid is handled by an Energy Management System (EMS), which includes scheduling and dispatching Distributed Energy Resources (DERs) such as Distributed Generators (DG), Energy Storage Systems (ESS), with controllable loads and demand response (DR), while maintaining appropriate reserve levels, and considering uncertainty in the forecast of renewables. Thus, this thesis focuses on developing comprehensive EMSs that consider Unit Commitment (UC), and Optimal Power Flow (OPF) constraints, smart load models for DR, and possible deviations in the forecast of renewable-based DGs.

First, a mathematical model of smart loads in DR schemes is developed, based on a centralized and integrated UC and OPF EMS for isolated microgrids, to optimally dispatch generation and smart loads. These smart loads are modeled by a neural network (NN) load estimator as a function of the ambient temperature, time of day, Time of Use (TOU) price, and a peak demand constraint that the microgrid operator may set. A novel Microgrid EMS (MEMS) approach based on a Model Predictive Control (MPC) technique to manage forecast uncertainties is formulated; this tool yields optimal dispatch decisions of DGs, and ESS, and obtains optimal peak demand constraints for smart loads, considering power flow and UC constraints simultaneously. The impact of DR on the microgrid operation with the developed MEMS is studied using a CIGRE benchmark system that includes DERs and renewable-based generation, demonstrating its feasibility and advantages over existing EMS approaches, and showing the benefits of controllable loads in microgrids.

In isolated microgrids, the network losses and voltage drops across feeders are relatively small. This feature is utilized through a novel linearization approach applied to the unbalanced power flow equations to propose practical EMSs. The proposed EMS models are Mixed Integer Quadratic Programming (MIQP) problems, requiring less computation time and thus suitable for online applications. The proposed practical EMS models are compared with a typical decoupled UC-OPF based EMS with and without consideration of system unbalancing. These EMS models, along with "standard" EMS models, are tested and validated, using an MPC approach to account for forecast deviations, on the CIGRE medium voltage benchmark system and the real isolated microgrid of Kasabonika Lake First Nation (KLFN) in Northern Ontario, Canada. The presented results demonstrate the effectiveness, and practicability of the proposed models.

In the third stage of the thesis, the impact of Electric Thermal Storage (ETS) systems on the operation of Northern Communities' microgrids is analyzed. A mathematical model of the ETS system is developed, in collaboration with a colleague from Karlsruhe Institute of Technology, and integrated into an EMS for isolated microgrids, in which the problem is divided into UC and OPF subproblems, to dispatch fossil-fuel-based generators, ESS, and ETS charging. To account for the deviations in the forecast of renewables and demand, an MPC technique is used. The proposed ETS-EMS framework is tested and studied on a modified CIGRE medium voltage benchmark system, which comprises various kinds of DERs, and on the real KLFN isolated microgrid system. It is shown that the ETS significantly reduces operating costs, and allows for better integration of intermittent wind and solar sources.

Finally, equivalent CO_2 emission models for fossil-fuel-based DG units are developed considering their individual emission characteristic and fuel consumption. These models are then integrated within a microgrid EMS model, together with constant energy, and demand shifting load models, to examine the possible impact of DR on the total system emissions and economics of a microgrid, using again an MPC approach to manage forecast uncertainties. The impact of including the developed emission models on the operation of an isolated microgrid, equivalent CO_2 emissions, and costs are examined considering five different operating strategies. The proposed operating strategies are validated on a modified CIGRE medium voltage benchmark system, with the obtained results highlighting the effectiveness of the proposed EMS and also demonstrate the impact of DR on emissions and costs.

Acknowledgements

I take this opportunity to thank my research supervisors Professor Kankar Bhattacharya and Professor Claudio Canizares for their invaluable support, guidance and patience during the course of my PhD studies. Under their supervision, I have learned beyond the boundaries of power and energy systems. It has been my privilege to have completed my studies under their supervisions, and they continue to be my role models in professionalism throughout my life.

I also thank Professors Mehrdad Kazerani, Sagar Naik and Kumaraswamy Ponnambalam, for their support and co-operation. I acknowledge the financial support received from Natural Sciences and Engineering Research Council of Canada (NSERC) Smart Microgrid Network and other funds from NSERC. I also acknowledge the cooperation received from all the staff members of the Office of Graduate Studies, Department of Electrical and Computer Engineering, University of Waterloo.

I am always grateful for the support of my friends through the up and downs of these past few years. Special thanks to Indrajit, Chandrari, Rahil, Nishank, Naman, Arpit, Malhar, Shivam, Nitin and Sreedevi. I would like to thank my colleagues and friends, in the Electricity Market Simulation and Optimization Lab at the ECE Department: Isha, Nafeesa, Mostafa, Mauricio, Amir, Fabian, Ivan, Juan Carlos, Edris, Victor, Edson, David, Sofia, Chioma, Alfredo, Akash, Dario, Fabricio, Felipe, Jose, Enrique, and Shubha for maintaining an interesting research environment in the lab. I also thank Satyam Panchal for making my stay very friendly and pleasant.

My parents have suffered a lot in their life without letting me know, and have always encouraged me. I would like to express my sincere gratitude towards my parents for all sacrifices they made, to see me prosper. I will never ever forget that it has costed a lot to reach where I am today. It is my parents' years of love and affection that I am submitting my PhD thesis on this day.

I don't have any words to acknowledge the contribution of my wife Ishanee to my PhD thesis. I extend my hearty appreciation for her understanding and support. I am very grateful to my father and mother in laws for their trust, patience and moral support. I also thank my sisters, and brother in laws for their continual support. Finally, my sincere gratitude to my spiritual master for giving us the strength to accomplish the dreams.

Dedication

This is dedicated to my parents - grand parents and my wife Ishanee.

Table of Contents

List of Tables

List of Figures

Nomenclature

Functions

$F(.)$	Linear or non-linear function
$g(.)$	Linear or non-linear function
$h(.)$	Linear or non-linear function
$J(.)$	Linear or non-linear objective function

Indices and superscripts

g	Generating units
i	Bus or objective number or device number
j	Bus number
k	Time-step [min]
l, m	Phase (a,b,c)
n	ESS units
p	Pollutant type (CO_2, CO and NO_x)
t	Time [min]
x	Input layer neurons of NN
y	Hidden layer neurons of NN
^{c}	Commercial
^{r}	Residential
$^{\rightarrow}$	phasor

Sets

G_i	Generator units connected to bus i
N_i	ESS units connected to bus i

Parameters

A	Parameter matrix
A_1	Aspiration level for operating cost [$]
A_2	Aspiration level for emission cost [$]
d^{em}	Quadratic term of emission function of DG unit [tonne/(kWh)^2]
d_g	Quadratic term of cost function [$/kWh^2]
B	Parameter vector
B^{op}	NN bias at the output neuron
B_y^{ip}	NN bias at the hidden layer neuron
e^{em}	Linear term of emission function of DG unit [tonne/kWh]
e_g	Linear term of cost function [$/kWh]
C	Parameter vectors
C^{em-sdn}	CO_2 emission associated with shut-down of DG unit [tonne]
C^{em-sup}	CO_2 emission associated with start-up of DG unit [tonne]
C^{LC}	Load curtailment cost [$/kWh]
C_g^{sdn}	Shut-down cost generating units [$]
C_g^{sup}	Start-up cost generating units [$]
f^{em}	Constant term of emission function of DG unit [tonne/h]
f_g	Constant term of cost function [$/h]
$IP_{x,t}$	NN input
$IW_{x,y}$	Hidden layer weights of NN

$K_{1,2}$	Reactive power load factors [kVAR/kW]
LW_y	Output layer weights of NN
$PD_{i,k}$	Active power demand [p.u.]
$PW_{i,k}$	Wind turbine output [p.u.]
$\overline{PESS}_n$	Maximum charging/discharging power limit of ESS [p.u.]
P^{TH}	Thermal demand served by electric heating [p.u.]
P_S^{TH}	Thermal discharge set point [p.u.]
$PV_{i,k}$	Photovoltaic unit output [p.u.]
R_g^{dn}	Ramp down rate of generating units [p.u./h]
R_g^{up}	Ramp up rate of generating units [p.u./h]
T^0	Ambient temperature [^{0} C]
T_g^{dn}	Minimum down time of generating units [h]
T_g^{up}	Minimum up time of generating units [h]
T_r	Room temperature [^{0} C]
T_s	Temperature set point [^{0} C]
w	Weight applied to D_1 and D_2
χ_i	Number of electric heating units at bus i
Y	Admittance [p.u.]
α_k	Voltage exponent for active load
β_k	Voltage exponent for reactive load
Δt_k	Absolute time between step k_t and step k_{t+1} [h]
η_{ETS}	ETS electric-thermal energy conversion efficiency
η_n^{ch}	Charging efficiency of ESS

η_n^{dch}	Discharging efficiency of ESS
η_S	Thermal storage efficiency of ETS
Γ	Social cost of CO_2 emissions [$/tonne]
$\gamma_{l,m}$	Angle difference between two balanced phases ($\pm 120^0$)
λ_k	Errors in the output of the RCLPE [p.u.]
μ_i	% electric heating units replaced by ETS at bus i
ψ	Emission Factor for a pollutant of DG unit [tonne/MBTU]
0	3-by-3 zero matrix
I	3-by-3 identity matrix
θ	Angle for line admittance [radian]
$\underline{\ },\bar{\ }$	Minimum, maximum variable limits
$\tilde{\ }$	Normalized variable
ξ	Global Warming Potential Index
Z	Impedance [p.u.]

Variables

D_1, D_2	Deviations from aspiration level for operating and equivalent CO_2 emission costs, respectively [$]
$\mathcal{E}$	Internal voltage of generator [p.u.]
E	Pollutant p emission from DG unit [tonne]
$E^{\mathrm{CO_2}}$	Equivalent CO_2 emission of pollutant from DG unit [tonne]
E^{ETS}	ETS thermal energy level [p.u.]
I	Current [p.u.]
J_{cp}	Normalized distance function
J_{em}	Equivalent CO_2 emission cost [$]

J_{gp}	Weighted sum of D_1 and D_2 [$]
J_{oc}	Sum of J_{op} and J_{em} [$]
J_{op}	Operating cost [$]
L	Fuel consumption of DG unit [MBTU]
$L^{ETS^{TH}}$	ETS effective thermal energy self-discharge [p.u.]
$P_{g,k}$	Active power from generating units [p.u.]
$\Delta P, \Delta Q$	Slack variables used for active and reactive power balance [p.u.]
$P_{n,k}^{ch}$	ESS charging power [p.u.]
$P_{n,k}^{dch}$	ESS discharging power [p.u.]
P^{ETS}	ETS charging power [p.u.]
P_k^{LC}, Q_k^{LC}	Load curtailed [p.u.]
P_k^{max}	Demand limit - DR control [kW]
PD_k^{rc}	Residential controllable active power demand [p.u.]
PD_k^{rs}	Residential shiftable active power demand [p.u.]
$Q_{g,k}$	Reactive power from generating units [p.u.]
$QC_{n,k}$	ESS reactive power output [p.u.]
$\mathcal{S}_{i,j,k}$	Apparent power transfer between i and j [p.u.]
$S_{g,k}$	Shut-down decision (1 = shut-down, 0 = otherwise)
$SOC_{n,k}$	State of charge of ESS [p.u.]
U^{ch}	ESS charging binary decision (1 = charge)
U^{dch}	ESS discharging binary decision (1 = discharge)
u_t	vector of control variables, $u_t \in U$
$U_{g,k}$	Start-up decision (1 = start-up, 0 = otherwise)

$V_{i,k}$	Bus voltage [p.u.]
$W_{g,k}$	ON/OFF decision (1 = ON, 0 = OFF)
$\delta^{\mathcal{E}}$	Inter voltage angle of generator, [radian]
$\delta_{i,k}$	Voltage angle [radian]
z	Decision variables, $z \in \mathcal{Z}$
z_1	Continuous variables, $z_1 \in \mathcal{Z}_1$
z_2	Integer variables, $z_2 \in \mathcal{Z}_2$

List of Acronyms

AMI	Advanced Metering Infrastructure.
CPP	Critical Peak Pricing.
CHP	Combined Heat and Power.
DER	Distributed Energy Resources.
DG	Distributed Generator.
DLC	Direct Load Control.
DMEMS	Decomposed Microgrid Energy Management System.
DOPF	Distribution Optimal Power Flow.
DR	Demand Response.
DSM	Demand Side Management.
EHMS	Energy Hub Management System.
EMS	Energy Management System.
ESS	Energy Storage System.
ETS	Electric Thermal Storage.
GHG	Green House Gases.
GWPI	Global Warming Potential Index.
HAS	Home Automation System.
HEMS	Home Energy Management System.

ISO	Independent System Operator.
LP	Linear Programming.
KIT	Karlsruhe Institute of Technology.
KLFN	Kasabonika Lake First Nation.
MEMS	Microgrid Energy Management System.
MGO	Microgrid operator.
MINLP	Mixed Integer Non-Linear Programming.
MIP	Mixed Integer Programming.
MIQP	Mixed Integer Quadratic Programming.
MLP	Multi-Layer Perceptron.
MOPF	Microgrid Optimal Power Flow.
MPC	Model Predictive Control.
MUC	Microgrid Unit Commitment.
NLP	Non-Linear Programming.
NN	Neural Network.
OPF	Optimal Power Flow.
pdf	Probability Density Function.
PV	Photo-Voltaic.
RCLPE	Residential Controllable Load Profile Estimator.

RES	Renewable Energy Sources.
RTP	Real Time Pricing.
TOU	Time of Use.
UC	Unit Commitment.

Chapter 1

Introduction

1.1 Motivation

There are many remote communities around the world which do not have interconnection with the power grid because of technical and/or economic constraints, and thus have to manage their energy requirements independently, mainly from fossil-fuel-based and, in some cases, renewable energy sources (RES)-based generation. These communities supply their energy need with isolated microgrids.

A microgrid is a group of interconnected loads and Distributed Energy Resources (DERs) such as distributed generators (DGs), energy storage systems (ESS), and controllable loads, within a clearly defined and local electrical boundary that can act as a single controllable entity with respect to the grid [1]. Canada has around 280 remote communities which are not connected with the power grid and manage their electricity demand through isolated microgrids mostly based on fossil-fuel-based generation [2], [3]. Diesel generation accounts for about 50% of the total installed capacity of these microgrids [3]. Because of the high transportation cost of fuel, these communities face high electricity costs as compared to the rest of Canada. For example, the approximate electricity costs for a remote community with road access is about 0.45 $/kWh, while communities located in the Arctic region of Canada pay as high as 2.5 $/kWh; on the other hand, the average electricity tariff in rest of Canada is in the range of 0.07-0.17 $/kWh [3]. Additionally, in some remote communities, peak demands are close to their generation capacities [2], [3]. In order to cope with these issues, there is a need to introduce RES, which would require a proper Energy Management System (EMS) to maintain appropriate reserve margins in the microgrid. In this context, there is also a need to consider uncertainty in the forecast of RES and a proper coordination of DERs and demand response (DR) mechanisms in the EMS [4], [5].

Customer participation in energy management, enabled by DR mechanisms [6], can improve the operational efficiency of isolated microgrids and facilitate the integration of RES by reducing the demand at critical instances, and/or shifting the demand to off-peak

hours or to when sufficient generation from RES is available. The works reported so far to account for DR in EMS generally model the controllable loads either by price elasticity coefficients or using a power curtailment variable with an associated cost. However, such representations fail to capture the load behaviour in response to various DR controls such as peak demand limits or externalities such as weather conditions. Therefore, there is a need to represent the controllable loads in terms of various DR controls, so that they can be integrated in the EMS for optimal dispatch along with other DERs.

Centralized EMS for microgrids, based on Unit Commitment (UC) and Optimal Power Flow (OPF) models, have been reported in the literature. The UC-based EMS models consider the DER operational constraints such as ramp-up, ramp-down, and minimum up/down-time constraints, but not the network flows. On the other hand, OPF based EMS models do consider network flows, but not the other relevant operational constraints. In order to yield optimal solutions, EMS models need to simultaneously consider the network flow and the operational constraints associated with DERs. However, there is very little work reported on microgrid EMS models that simultaneously considers UC and OPF constraints.

Since integrated EMSs consider together operational constraints, active and reactive power balance, and reserve constraints, these models are mixed integer non-linear programming (MINLP) problems, which are difficult to implement online. However, depending on the desired functionalities and characteristics of the microgrid, the EMS model can be developed considering different levels of detail. Thus, since it has been found from practical measurements in actual remote microgrids that the voltage drops and feeder losses are negligible because of short length and large size of the feeders, network constraints for these microgrids can be re-evaluated and better represented in integrated and approximate EMS models, which, with increasing share of RES in the system, would allow to appropriately consider reactive power dispatch concurrently with active power dispatch. Furthermore, the loads in such isolated microgrids are very sensitive to voltage variations, which need be accounted for, as well. Thus, there is a need for an integrated and practical EMS for such isolated microgrids to deal with these specific issues.

Remote communities of Canada, working as isolated microgrids, are located in the Northern parts of the country, faced with significant heating demand. This large heating demand is generally supplied by wood pallets, fuel oil, gas, and electricity [3]. To mitigate the high cost of energy and reduce the environmental impact, Electrical Thermal Storage (ETS) systems can be used. Other storage systems such as a typical battery based ESS are expensive, whereas ETS systems are cheaper and can meet the thermal heating demand, thereby allowing the efficient use of diesel- and RES-based DG units. Therefore, there is a need to properly model ETS systems and examine their integration in and impact on

microgrid EMS models.

Finally, and as mentioned earlier, isolated microgrids rely on fossil-fuel-based DG units to meet electricity demand, and are known to be high emitters of green house gases (GHG). High levels of diesel-based generation in isolated communities are causes of environmental and socio-economic concerns. While there is a need to explore non-polluting energy supply options to reduce the impact on the environment [3], DR is a viable option for isolated microgrids for emissions and cost reductions, since they are readily implementable and available, as well as environmentally friendly and cheaper than investments in generation resources. Although the positive impact of DR on the operation and costs of isolated microgrids has been analyzed, there is a need to study the effect of DR on the pollutant emissions of isolated microgrids, and to develop an operating strategy so that both emission and operating costs can be minimized in the presence of DR.

1.2 Literature Review

This section presents a brief review of relevant works pertaining to the issues addressed in this thesis, to properly justify the relevance and need of the main contributions of this work.

1.2.1 Microgrid Energy Management Systems

Microgrid EMS obtains the optimal dispatch and schedules of the DERs considering certain selected objectives. Two different types of EMS architecture for microgrids, both centralized and decentralized, are usually found in practice [5]. In the centralized approach, the central controller is responsible for gathering the data from all the DERs and obtain the optimal set points for them, while in the decentralized approach, centralized and local both controllers participate to obtain the optimal set points for the DERs [5]. In decentralized approach, the central controller coordinates the aggregated operation of the DERs and loads, while local controllers manage DERs within the microgrid, interacting with the central controller to meet local and global objectives [5]. The decentralized approach can integrate the new DERs without needing continuous changes in the controller and thus, has plug and play feature; however, it fails to provide high level of coordination between the DERs and controller [5]. On the other hand, the centralized approach, because of its architecture, can manage and coordinate DERs more efficiently; thus, is more suitable for isolated microgrids, which require a critical demand-supply balance [5]. Since the main

focus of this thesis is on EMS models for isolated microgrids, the works which consider the centralized approach are presented and reviewed next.

The concept of centralized EMS for microgrids, based on UC and OPF models, have been reported in several papers. Thus, in [7], a UC based EMS for grid connected microgrids comprising ESS, micro-turbines, fuel cells, and renewables based DGs is presented. The proposed EMS uses the genetic algorithm (GA) approach to minimize the microgrid operation cost of DERs considering their associated constraints; moreover, to predict the generation from solar Photo-Voltaic (PV) units, a Neural Network (NN) based forecasting model is developed. A multi-objective UC problem is proposed in [8] for microgrid EMS seeking to minimize the operating cost and pollutant emissions. A two stage, day-ahead UC and real-time economic dispatch problems are presented in [9] for grid connected microgrids, considering all types of DERs. The EMSs in [7], [8], and [9] consider UC based dispatch of DERs, but do not take into account reactive power management and voltage regulation aspects nor forecasting errors, which are important in microgrid with RES. Therefore, detailed power flow equations need to be included in the EMS formulation, i.e., OPF models are required, and forecasting errors management strategies are also needed.

In [10], an OPF based EMS for grid connected industrial microgrids is proposed, which considers a revenue maximization based non-linear programming (NLP) optimization problem, including network and ESS constraints, and plug-in electric vehicles. Different microgrid configurations are considered, such as a stand alone microgrid and a grid connected microgrid. Similarly, a multi-objective OPF for optimal dispatch of DGs and ESS in the presence of RES-based generation for isolated microgrids, simultaneously minimizing the operation cost and pollutant emissions is presented in [11]. A phase-decoupled three phase OPF model for grid connected microgrid is presented in [12], considering ESS, and generation from RES. In [13], an OPF based EMS model is proposed, considering the dispatchable and non-dispatchable DG units, and electric vehicles for isolated microgrids. However, [10]–[13] do not take into account the UC constraints associated with DERs, which are important in an EMS, nor forecasting errors.

Since the integration of UC and OPF problems result in an MINLP problem, which is computationally challenging, specially for online applications, approximate integrated UC-OPF approaches have been proposed. Thus, in [14], a two-stage EMS problem for grid-connected microgrid is proposed, where the first stage is a unified linearized UC-OPF problem, while the second stage is a three-phase OPF problem; the power flow equations in the first stage are linearized using a Taylor series expansion. A linearized UC-OPF problem is presented in [15] for isolated microgrids, where the network equations are linearized as piece-wise functions, although the typical UC constraints such as ramp-up and -down, and minimum-up and -down time constraints are ignored. However, both [14] and [15] do

not consider the voltage dependency of the loads, which is important because loads are voltage dependent in isolated microgrids. Furthermore, the results in [14] and [15] do not consider deviations from the forecast of RES and demand, which needs to be accounted for in isolated microgrids because of the critical need for a constant demand supply balance.

For isolated microgrids with a high penetration of RES based DGs, deviations in the forecast of renewables can significantly affect the dispatch of other resources and hence the operating costs [5]. Therefore, to address this issue, Model Predictive Control (MPC) has been used in systems with uncertain inputs, wherein the optimization problem is solved at discrete time steps considering updated forecasted inputs over a rolling time horizon, with the obtained optimal decisions being valid for the next time step only [16]. In [17] and [18], the energy management problem of an isolated microgrid is decomposed into UC and OPF subproblems. In [17], an MPC technique is used to solve the UC and OPF models every 5 min, considering updated forecasted inputs of wind and solar PV generation, while in [18], the stochastic UC subproblem is modeled using stochastic programming and a receding horizon approach is used to solve the OPF subproblem to consider forecasting errors of RES and demand. Furthermore, in both [17] and [18], the OPF subproblem yields an optimal dispatch considering the unbalanced network representation and unbalanced loading; if a deficit in reactive power supply is observed in the OPF, the UC subproblem is solved again by turning on the next cheaper available DG unit, thus arriving at a sub-optimal dispatch. However, the proposed EMS does not consider load curtailment or other load control mechanisms.

From the discussed papers, it is clear that very few works have considered microgrid EMS models that accounts for unbalanced network conditions, which increase the computational burden significantly. Furthermore, only few works take into account the deviations in the forecast of RES and demand, while for isolated microgrids, deviations in the forecast of RES can significantly affect the optimal dispatch decisions of other DERs. Since it is important to consider the network constraints for isolated microgrids along with the UC constraints, because of the system's specific feeder and loading characteristics, integrated UC-OPF but practical EMS models that properly account for forecasting errors need to be developed for these microgrids, for online applications that provide an economic, efficient, and realistic dispatch of microgrid DERs.

1.2.2 Demand Response and Emissions in Microgrids

DSM and DR schemes allow customers to participate in energy management by shaving and/or shifting loads during critical periods, and provide benefits to both customers and

the utility. In order to take full advantage of the responsiveness of the electricity demand, EMS formulations need to represent DR.

The different DR options, such as peak shaving and demand shifting, are modeled in [19] by using associated cost and price elasticity coefficients in order to analyze their impact on the operation of a microgrid with high penetration of RES; it is noted that for such microgrids, a demand shifting scheme can be more useful to level out the variations in the generation from RES. Although this work considers DR and RES-based DGs in the EMS framework, it does not include ESS.

A double-layer coordinated control approach comprising the UC based scheduling layer and an OPF based dispatching layer for microgrid EMS is presented in [20], for both grid connected and isolated microgrids with fossil-fuel- and RES-based DERs and ESS. In order to balance the load and generation, a load shedding scheme is included in the EMS in the case of isolated microgrids, whereas active and reactive power purchase/sell decisions are considered for grid connected operation. An unbalanced three phase linearized OPF-based EMS model is presented in [21] for a grid connected microgrid which includes ESS, DG units and curtailable loads. Although [19]–[21] consider DR options in the microgrid EMS, these works do not consider the uncertainties associated with the forecast of electricity demand and/or generation from RES based DG units.

In [22] and [23], UC-based EMS models for microgrids which are meeting their demand mainly from RES, are presented; the variation in the forecast of RES and demand is accounted for by applying an MPC approach. A component of the electricity demand is considered shiftable to other hours in [22], which is a form of DR. On the other hand, in [23], two types of loads are represented: critical loads, which are fixed, and controllable loads, which can be curtailed based on a cost that accounts for user discomfort. Additionally, it is shown in [22] that, by using MPC, average operation costs are reduced because of the reduction in the energy deficit and better use of the ESS. Similarly, in [23], the EMS with and without MPC, as well as a heuristic based EMS approach are compared, and the results are in line with those discussed in [22].

In [19], [20], [22], and [23], DR is included in the EMS by modeling controllable loads as either shiftable demand or curtailable demand with an associated cost. However, such representations fail to capture the load behaviour in response to various DR controls such as peak demand limits, or externalities such as weather conditions. Hence, in this thesis, models of smart, controllable loads are developed from measured and simulated data and integrated into the EMS to study their impact and benefits for remote microgrids.

Large-scale use of diesel-based generation in isolated communities raises environmental and other socio-economic concerns. In order to reduce emissions and costs, DR can be a

viable option for isolated microgrids, since it is readily implementable and available, as well as environmentally friendly and cheaper than investments in generation resources. In [24], several different objectives from the system operation perspectives are considered along with their weighted sum to determine the optimal dispatch of the DERs in a grid-connected microgrid. The emissions from the DG units are modeled as quadratic functions of the DG power output, considering fuel consumption and the corresponding pollutant emission; moreover, load curtailment is considered with associated costs of energy curtailment.

Heuristic-based UC models are presented in [25] and [26] for day-ahead operation of grid-connected microgrids. In [25], the operating and emission costs are minimized to obtain the optimal dispatch of DERs including ESS and electric vehicles, considering predetermined emission characteristics of the DG units from [27] and generation from RES. In [26], the operating and emission costs are minimized in a grid-connected microgrid considering curtailable demand, vehicle-to-grid (electricity from electric vehicles can be sold back to the grid), and DG units, with their respective predetermined emission characteristics from [28]; ESS and generation from RES are not considered.

The UC models for grid-connected microgrids in [24]–[26] do not take into account start-up and shut-down operation costs and associated pollutant emissions, nor consider forecast deviations of RES and demand. In these works, the impact of DR on emissions is not analyzed. Thus, there is no reported attempt to develop a detailed UC model for isolated microgrids with all DER related constraints, including pollutant emission models, while accounting for deviations in the forecast of the RES and demand, and various DR schemes. Hence, in this thesis, a novel mathematical model of such a comprehensive UC, which simultaneously minimizes operating costs and pollutant emissions considering demand-shifting load models, is presented to analyze the impact of DR on pollutant emissions from the dispatchable DG units.

1.2.3 ETS Applications in Microgrids

ETS systems have been used for decades as a mean of efficient use of electricity, since thermal storage allows the charging electric power and thermal heat output to be managed separately. Thus, ETS systems store thermal energy, converted from electric energy during off-peak hours, and discharge it as required by the thermal demand [29]. ETS systems are available for both residential and commercial applications.

The potential of ETS systems in remote community electricity grids in Northern Canada is discussed in, for example, [30], [31], and [32]. In [30], a rule based algorithm to manage ETS charging from wind-generated electricity is presented, considering issues related with

the integration of RES and the high thermal demand in Prince Edward Island, Canada. In [31], a methodology for ETS charging, which serves as a secondary load for frequency regulation, is proposed for microgrids of Alaska, USA, with effective use of wind generation. In [32], the economic assessment of a smart grid program in Summerside, Canada, considers ETS systems as a solution to mitigate the issue of surplus generation from wind turbines at low electricity rates.

The use of ETS systems as controllable demand in the context of DR services for single residential or commercial customers is reported in [33] and [34]. In [33], a physically based load model of ETS is presented and integrated in a load management program; the ETS is scheduled to charge only at predetermined time periods. An MPC based thermal storage management problem is presented in [34] for commercial buildings, considering a physical based model of thermal storage. Furthermore, various approaches to ETS system management for a cluster of residential customers, from the perspective of an aggregator, are reported in [35]–[37]. A stochastic optimization problem to schedule ETS along with a micro-combined heat and power (CHP) generator is proposed in [35] for retailers to minimize the import/export electricity and gas cost over the day; it considers the dead-band on the thermostat set-point to control the discharging of the ETS. In [36], electric space heating with partial thermal storage for a DR control strategy based on dynamic electricity pricing is presented, highlighting the benefits of DR to the aggregators. Day-ahead ETS operation strategies for an aggregator with different objectives, including electricity cost minimization, load shifting, and frequency regulation, are presented in [37], considering day-ahead hourly electricity prices. Although [33]–[37] present different approaches to manage ETS either for residential or commercial customers or for an aggregator, none of these study the integration of the ETS into a microgrid EMS to determine the optimal schedules of DERs, and the ETS system.

The authors in [38] present an optimization based medium-term planning model to determine the optimal mix of ETS and wind resources, and a rule-based short-term operations model for isolated microgrids in Yukon, Canada. However, the proposed short-term operations model does not consider the operational constraints of fossil-fuel-based generators, grid constraint, or ESS.

In [39], a coordinated scheduling model is presented for the introduction of combined cooling heating and power and ice-storage air-conditioners into grid connected microgrids with RES. The proposed model is decomposed into a stochastic day ahead scheduling model and a real-time dispatch model, which are solved using an Improved Particle Swarm Optimization algorithm. However, this work does not include constraints associated with DG units, reserve constraints, and power flow equations in neither day-ahead scheduling nor real-time dispatch, which need to be considered in microgrid EMS [5] .

The ETS systems represented in [30] and [31] are not mathematical models, but are rather rule-based control schemes. The mathematical models in [33], [34], and [36], on the other hand, are detailed models that include thermal modeling of whole buildings, which are too complex for an online capable EMS. In [34] and [37], cooling ETS systems are modeled, have different physical characteristics than ETS for heating. The ETS model in [35] includes CHP, but, as in [38], it does not include heat losses effectively. Therefore, a simpler ETS model for heating is proposed in this thesis, so that it can be readily integrated in an online EMS, considering the effective heat losses.

1.3 Research Objectives

The existing literature review reveals that there is a need to consider different aspects of isolated microgrids in the formulation of EMS models. Accordingly, the main research objectives of the research presented in this thesis are the following:

- Develop an appropriate mathematical model to estimate the controllable load component of an isolated microgrid as a function of the ambient temperature, electricity price, time of the day, and peak demand constraint imposed by the microgrid operator (MGO).
- Incorporate the estimated load model into an integrated microgrid EMS framework to study the impact and potential of DR. To this effect, a comprehensive mathematical formulation of the EMS framework for isolated microgrids that simultaneously considers power flow and UC operational constraints is developed, using an MPC approach to take into account the errors in forecasts of uncertainties associated with the intermittency of RES and electricity demand.
- Develop a practical microgrid EMS model that considers the issues of unbalanced loading conditions by including detailed three-phase models of DERs, and excluding the network, given the little impact of feeders observed in actual isolated microgrids, but considering the voltage dependency of loads. This model is validated with the real isolated microgrid from the remote Ontario community of Kasabonika Lake First Nation (KLFN).
- Develop a new mathematical model of heating ETS systems considering stored thermal energy, charging electric input, thermal demand, and effective heating loss for microgrid EMS models, to analyze the impact of ETS systems on the operation of isolated microgrids. A novel ETS-EMS model is developed for isolated microgrids taking

into account operating UC constraints, network equations with grid constraints, deviations in the forecast of generation and demand, and the proposed ETS model.

- Develop and integrate the emission models of DERs along with the shiftable demand models in the EMS model to investigate the effect of DR in emission reductions in a microgrid.

1.4 Thesis Outline

The rest of the thesis is structured as follows: Chapter 2 presents a review of the relevant background topics for the discussed research, which includes a description of the conceptual definitions and features of microgrids, followed by an overview of microgrid EMS, DR, ETS, and optimization methods.

Chapter 3 explains the proposed microgrid EMS model in detail, along with the proposed NN-based smart load model. Results are presented both for a proposed integrated UC+OPF EMS model and a typical decoupled UC-OPF EMS model, considering various penetration levels for DR control, and using a modified CIGRE benchmark test system; analysis are carried out to demonstrate the positive impact of the proposed approach.

Chapter 4 presents novel, practical, and realistic EMS models for isolated microgrids. These EMS models, and the commonly used decoupled UC-OPF approach, are tested and validated on a modified CIGRE benchmark test system and also on the real isolated microgrid of KLFN. The results obtained are analyzed and discussed, and the effectiveness and applicability of the proposed models are demonstrated.

Chapter 5 presents the mathematical model of a heating ETS system, which is then integrated into a decoupled UC-OPF based EMS model. The ETS-EMS model is tested and validated on a modified CIGRE benchmark test system and also on the real isolated microgrid of KLFN. The results obtained are analyzed and discussed, highlighting the impact of ETS on operation of the microgrid.

Chapter 6 describes emission models of generators, and five operating strategies to consider both emission and operating costs of an isolated microgrid in a single objective function; a DR model with shiftable demand is also included. Results obtained by testing and validating the UC problem with the proposed operating strategies, for a modified CIGRE system are studied and discussed, demonstrating the impact of DR on emissions and operation of the microgrid with different operating strategies.

Finally, Chapter 7 summarizes the main conclusions and contributions of this thesis, and suggests possible future research work.

Appendices A and B present detailed data of the test system components.

Chapter 2

Background Review

This chapter presents a review of the background of the main concepts and tools relevant to this thesis. In Section 2.1, the fundamental concept of a microgrid is presented, which is followed by a description of the microgrid EMS in Section 2.2, and a brief outline of different DR programs in Section 2.3. The heating ETS system and its architecture is discussed in Section 2.4, followed by an overview of different optimization methods applicable to the proposed research, in Section 2.5, and a brief outline of the MPC technique in Section 2.6. Section 2.7 summarizes the chapter.

2.1 Microgrids

The concept of a microgrid has evolved in order to address the problems arising from interfacing DERs such as RES, micro-turbines, fuel cells, and ESS, at low voltage levels [1]. A microgrid has been defined as a cluster of small sources, storage systems and loads which presents itself to the grid as a single entity [1], [5], as shown in Figure 2.1. DERs play an important role in microgrids to meet an increasing electricity demand and reduce carbon emissions, where the term DER is used to refer to RES and fossil-fuel-based DG units, ESS, and controllable loads. As per the definition of the U.S. Department of Energy (DoE), a microgrid is a group of interconnected loads and DERs within clearly defined electrical boundaries that act as a single controllable entity with respect to the grid [40]. Certain features of the smart grid, such as bi-directional communication between customer and utility, using Advanced Metering Infrastructure (AMI) to strengthen the EMS, are also applicable to microgrids.

Microgrids can be permanently connected to the grid or can be islanded/isolated from the grid. There are many remote communities around the world which do not have interconnection with the main grid due to economical, geographical, socio-political, or technical reasons, meeting their electricity demand mostly from fossil fuel based DG units; these can be considered isolated microgrids. In Canada, there exists around 280 such isolated microgrids [2].

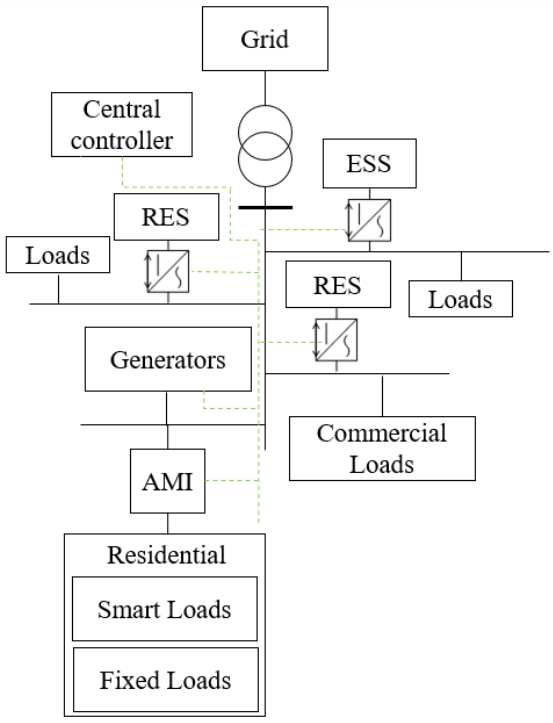

Figure 2.1: Concept of a microgrid.

The integration of various DERs in microgrid introduces many challenges in their operation, which can be tackled by proper design of the control system, including features such as [4], [5]:

- Track and ensure proper control of DER outputs.
- Maintain adequate power balance in the microgrid by accounting for sudden changes in demand or in the output of RES, so that voltage and frequency deviations are within prescribed limits.
- Economic dispatch to ensure DERs operate at minimum costs.

Typically, the microgrid control system includes controls with different time constants; for example, the economic dispatch follows slower dynamics, while the DG unit output control presents a fast dynamic behaviour. Hence, the microgrid control system can be divided into different hierarchical levels: primary control, secondary control, and tertiary control [5], as

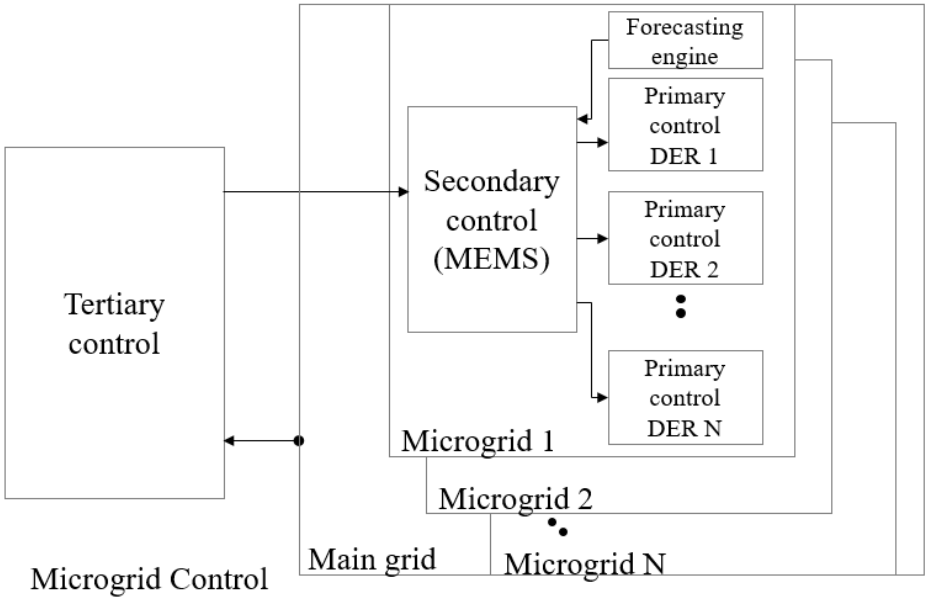

Figure 2.2: Microgrid control.

shown in Figure 2.2. The primary control is also referred to as local control, and represents the first level of control, which is essentially based on droops, and follows fast dynamics. The secondary control is referred to as the microgrid EMS, which takes care of the reliable and economic operation of the microgrid. The tertiary control represents the highest level of the central hierarchy, coordinating multiple microgrids to properly interact with one another in the system; these controls are not relevant to isolated microgrids. In this thesis, the main focus of the research is on the design of secondary control mechanisms, i.e., the EMS, for isolated microgrids.

2.2 Microgrid Energy Management System

The EMS is responsible for the reliable and economic operation of the microgrid, and is a collection of control strategies and operational practices, together with the hardware and software needed to accomplish these objectives. An EMS includes the acquisition of data for control, and yields information for planning and design purposes. Because of the presence of intermittent and non-dispatchable generating resources, the task of a microgrid EMS is very challenging [5]. To utilize the DERs efficiently, the microgrid EMS needs to

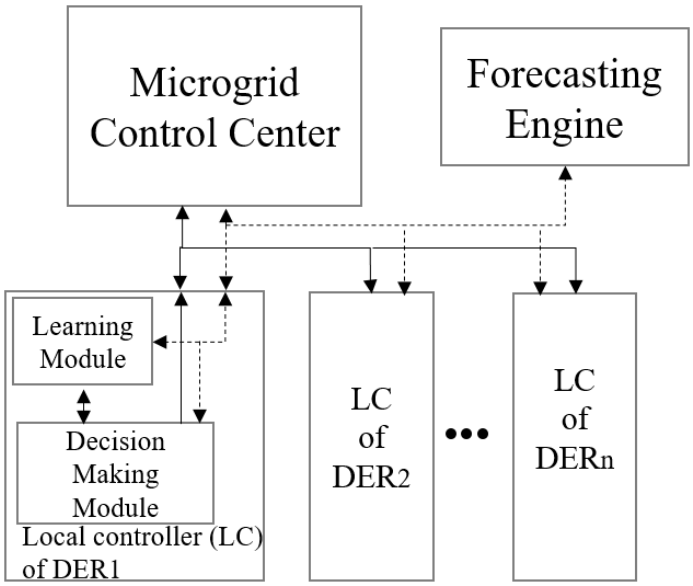

Figure 2.3: Decentralized EMS approach.

consider the supply and demand uncertainty, and appropriate levels of reserves, along with DSM and/or DR schemes [4], [5].

The EMS in a microgrid can adopt a centralized or a decentralized control strategy to perform its functions. In centralized control, the EMS minimizes the operation costs and hence determines the optimal control set points of the DERs, whereas in the decentralized control approach, the local controllers of the DERs interact with each other and with a central controller to operate the microgrid, based on a distributed decision making process, as depicted in Figure 2.3. For isolated microgrids, a high level of coordination is required to balance the demand and supply, which can be better achieved with a centralized approach. On the other hand, for grid connected microgrids with multiple owners and changing number of DERs, the decentralized approach is preferable, as it provides the highest possible autonomy to DERs. In centralized control, as shown in Figure 2.4, the EMS receives the forecast inputs for demand and generation from the renewable-based DG units, to determine their UC and economic dispatch. The central controller uses online calculations, a look-up table based on off-line calculations for different scenarios, or a heuristic approach.

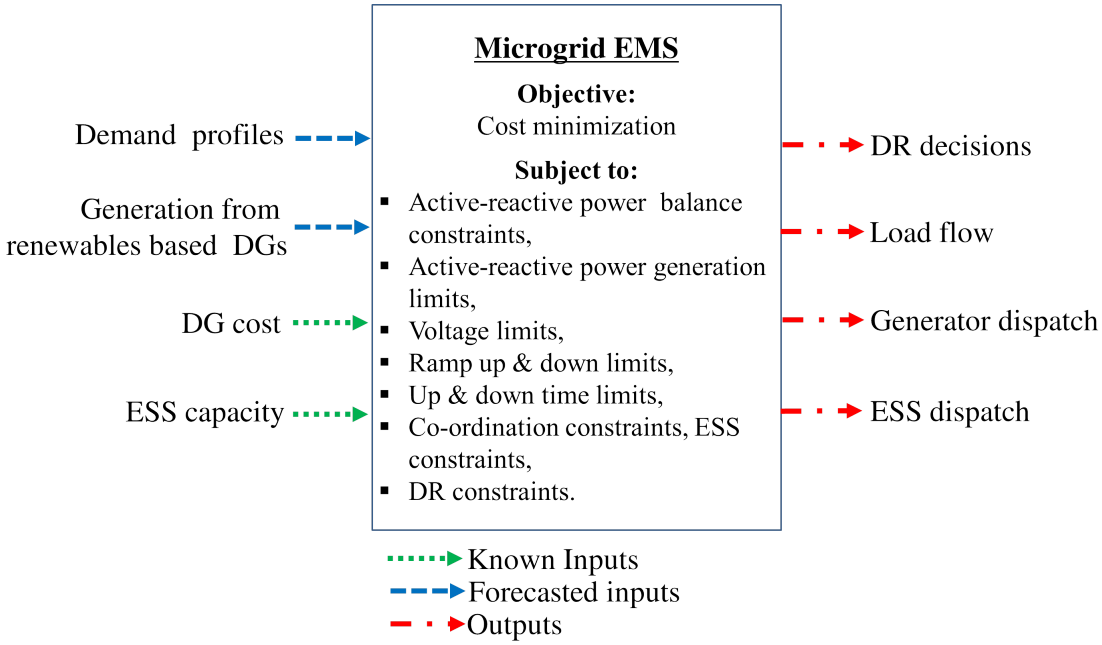

Figure 2.4: Centralized EMS approach for isolated microgrids.

2.2.1 Unit Commitment

UC is a scheduling and energy management problem carried out for a time horizon ranging from 24 hours to 168 hours ahead of real-time operation [22]. The microgrid UC problem minimizes the operating cost of the microgrid including generation costs, start-up and shut-down costs, and costs associated with load curtailment, as follows [22]:

$$J = \sum_{g,t}[(d_g P_{g,t}^2 \Delta t + e_g P_{g,t} + f_g W_{g,t})\Delta t + C_g^{sup} U_{g,t} + C_g^{sdn} S_{g,t}] + \sum_{i,t} P_{i,t}^{LC} C^{LC} \Delta t \qquad (2.1)$$

where all variables, parameters, and indices in this and other equations in this chapter are defined in the Notation section. The model constraints are the following, and are based on [22]:

- *Demand-supply Balance:* This constraint ensures that the total generation is equal to the total power demand at every time interval, as follows:

$$\sum_g P_{g,t} + \sum_i (PV_{i,t} + PW_{i,t}) + \sum_n (P_{n,t}^{dch} - P_{n,t}^{ch}) = \sum_i (PD_{i,t} - P_{i,t}^{LC}) \qquad \forall t \qquad (2.2)$$

- *Reserve Constraints:* These constraints ensure that the spinning reserve requirement at all time intervals, are provided by the committed generators, as follows:

$$\sum_{g}(\bar{P}_g W_{g,t} - P_{g,t}) \geq R^{sv} \sum_{i} PD_{i,t} \qquad \forall t \tag{2.3}$$

- *Generalized UC Constraints:* The following constraints include active power generation limits, ramp-up and ramp-down constraints, minimum up-time and down-time constraints, and coordination constraints:

$$\underline{P}_g W_{g,t} \leq P_{g,t} \leq \bar{P}_g W_{g,t} \qquad \forall g,t \tag{2.4}$$
$$P_{g,t+1} - P_{g,t} \leq R_g^{up} + U_{g,t+1}\underline{P}_g \qquad \forall g, t \geq 1 \tag{2.5}$$
$$P_{g,t} - P_{g,t+1} \leq R_g^{dn} + S_{g,t+1}\underline{P}_g \qquad \forall g, t \geq 1 \tag{2.6}$$
$$(G_{g,t-1}^{on} - T_g^{up})(W_{g,t-1} - W_{g,t}) \geq 0 \qquad \forall g, t \geq 1 \tag{2.7}$$
$$(G_{g,t-1}^{off} - T_g^{dn})(W_{g,t} - W_{g,t-1}) \geq 0 \qquad \forall g, t \geq 1 \tag{2.8}$$
$$U_{g,t} - S_{g,t} = W_{g,t} - W_{g,t-1} \qquad \forall g, t \geq 1 \tag{2.9}$$
$$U_{g,t} + S_{g,t} \leq 1 \qquad \forall g,t \tag{2.10}$$

Constraints (2.4) represent the active power generation limits; (2.5) and (2.6) represent ramp-up and ramp-down limits; (2.7) and (2.8) present minimum up-time and down-time constraints; and (2.9) and (2.10) are coordination equations.

- *Energy Storage System:* The ESS constraints include the energy balance equation and constraints to prevent simultaneous charging/discharging, limits on the State of Charge (SOC) and charging/discharging power, as follows:

$$SOC_{n,t+1} - SOC_{n,t} = \left(P_{n,t}^{ch}\eta_n^{ch} - \frac{P_{n,t}^{dch}}{\eta_n^{dch}}\right)\Delta t \qquad \forall n, t \geq 1 \tag{2.11}$$
$$U_{n,t}^{ch} + U_{n,t}^{dch} \leq 1 \qquad \forall n,t \tag{2.12}$$
$$\underline{SOC}_n \leq SOC_{n,t} \leq \overline{SOC}_n \qquad \forall n,t \tag{2.13}$$
$$P_{n,t}^{ch} \leq \overline{PESS}_n U_{n,t}^{ch} \qquad \forall n,t \tag{2.14}$$
$$P_{n,t}^{dch} \leq \overline{PESS}_n U_{n,t}^{dch} \qquad \forall n,t \tag{2.15}$$

2.2.2 Optimal Power Flow

In order to take into account voltage regulation and reactive power management, it is necessary to consider the network flow constraints, and hence an OPF model is needed. Typically, the microgrid OPF model comprises an objective function minimizing the operating costs of the microgrid, subject to constraints such as active and reactive power balance at each node, limits on active and reactive power generation of the controllable DERs, constraints (2.11)-(2.15) associated with the ESS, and grid operational constraints. These constraints and objective function are the following:

- *Objective Function:* Minimize the operating cost of the microgrid, including generation costs and costs associated with load curtailment, as follows:

$$J = \sum_{g,t}[(d_g P_{g,t}^2 \Delta t + e_g P_{g,t} + f_g)\Delta t] + \sum_{i,t} P_{i,t}^{LC} C^{LC} \Delta t \tag{2.16}$$

- *Power Balance:* The real power balance at a bus considers the output from DG units, solar PV and wind units, net of the power demand of loads from commercial and residential customers, taking into account ESS charging and discharging, as follows:

$$\sum_{g\in G_i} P_{g,t} + PV_{i,t} + PW_{i,t} - PD_{i,t} + P_{i,t}^{LC} + \sum_{n\in N_i}(P_{n,t}^{dch} - P_{n,t}^{ch}) = \sum_j V_{i,t}V_{j,t}Y_{i,j}\cos(\theta_{i,j} + \delta_{j,t} - \delta_{i,t}) \qquad \forall t,i,j \tag{2.17}$$

  The reactive power balance at a bus considers the reactive power injected by DG units and ESS, and the reactive demand at the bus, as follows:

$$\sum_{g\in G_i} Q_{g,t} - QD_{i,t} + \sum_{n\in N_i}(QC_{n,t}) = -\sum_j V_{i,t}V_{j,t}Y_{i,j}\sin(\theta_{i,j} + \delta_{j,t} - \delta_{i,t}) \quad \forall t,i,j \tag{2.18}$$

- *Grid Operational Constraints:* These constraints impose limits on the active and reactive power generation and voltage at each node, as follows:

$$\underline{P}_g \le P_{g,t} \le \bar{P}_g \qquad \forall g,t \tag{2.19}$$

$$\underline{Q}_g \le Q_{g,t} \le \bar{Q}_g \qquad \forall g,t \tag{2.20}$$

$$\underline{V} \le V_{i,t} \le \bar{V} \qquad \forall i,t \tag{2.21}$$

2.3 Demand Response and Smart Loads

"Demand Side Management (DSM) is the planning and implementation of those utility activities designed to influence the customer's use of electricity in ways that will produce the desired changes in the utility's load shape, i.e., changes in the pattern and magnitude of a utility's load" [41]. It comprises the whole range of management schemes linked with demand-side activities, and it can be divided into DR programs and energy efficiency programs.

DR is defined as "changes in electric use by demand-side resources from their normal consumption patterns in response to changes in the price of electricity, or to incentive payments designed to induce lower electricity use at times of high wholesale market prices or when system reliability is jeopardized" [42],[43]. DR can be classified as incentive based programs and price based programs. Typically, DR schemes to curtail and/or shift the demand are adopted in microgrids, and are discussed next.

- *DR programs to curtail the demand:* In this DR schemes, a portion of the microgrid demand is curtailed to achieve demand-supply balance during peak load hours. The customers whose loads are curtailed may receive a payment from the MGO to account for their discomfort. Direct Load Control (DLC) can also represent load curtailment or reduction, in which the MGO remotely turns off the equipment or changes the temperature set point of the air conditioner and water heater, on short notice during critical periods. The customers may be paid an incentive in the form of electricity bill credits. Program participants are generally residential and small commercial customers. One of such programs implemented in Ontario was the PeaksaverPLUS® program in which a residential customer's equipment such as air conditioner and water heater are remotely controlled by the Independent Electricity System Operator (IESO) during critical periods [44]. Also, in the Hartley Bay microgrid, Ontario, Canada, the DLC program has been in operation for controlling water heaters, baseboard heaters, and heating, ventilating and air conditioning systems during critical hours [45].

- *DR programs to shift the demand:* In this DR scheme, part of the microgrid demand is considered as shiftable to off-peak hours by encouraging customers to alter their load pattern, so that the system load profile is modified. The demand shift may be activated by a signal from the MGO, such as dynamic pricing, peak load caps, etc. Dynamic pricing includes TOU rates, critical peak pricing (CPP), and real-time pricing (RTP). TOU rates are pre-set tariff rates, depending on the time of the day

Table 2.1: Ontario TOU rates

Season	Period	Hours	Electricity rate
Winter	On-peak	7 AM - 11 AM, 5 PM - 7 PM	13.2 Cents/kWh
	Mid-peak	11 AM - 5 PM	9.5 Cents/kWh
	Off-peak	7 PM - 7 AM	6.5 Cents/kWh
Summer	Mid-peak	7 AM - 11 AM, 5 PM - 7 PM	9.5 Cents/kWh
	On-peak	11 AM - 5 PM	13.2 Cents/kWh
	Off-peak	7 PM - 7 AM	6.5 Cents/kWh

and season of the year, designed to reduce the electricity use at certain time-periods. In Ontario, TOU pricing have three different rate levels defined for three different periods: peak hours when energy demand is high; mid-peak hours when energy demand is moderate; and off-peak hours when energy demand is low. For winter (November to April) and summer (May to October) seasons, the peak, mid-peak, and off-peak periods are given in Table 2.1 [46].

Based on the aforementioned DR programs, the MGO can achieve its DSM/DR objectives, which include peak clipping, load shifting, strategic conservation, and flexible load shape. In order to implement these objectives, the following approaches can be used [41]:

- Customer equipment direct control, which comprises the control of cooling and heating equipment such as air conditioners, commercial and industrial chillers, water heaters, as well as pumps and other loads.
- Utility equipment control such as voltage regulation, feeder control, and power factor control for net-VAr optimization.
- Thermal Energy storage such as waste heat utilization and cool storage.
- Performance improvement of equipment and systems such as high efficiency motors and pumps.

With the introduction of smart meters with bidirectional communication capabilities, an effective DR program can be implemented, which can benefit both the MGO and customers. A proper forecast of customer electricity consumption patterns in response to electricity prices is important for effective application of DR schemes.

Smart systems such as Home Energy Management Systems (HEMS) interact with the MGO and customers through household appliance management, so that, both customer's

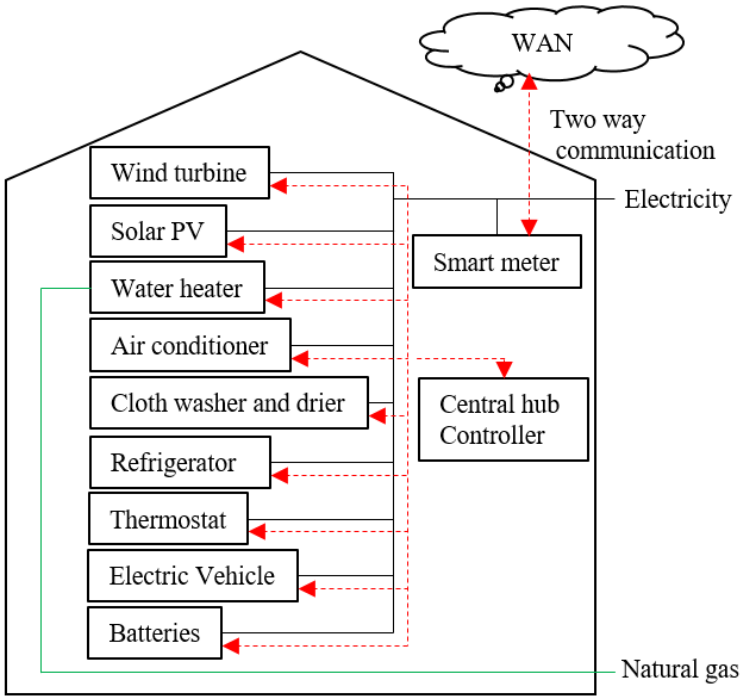

Figure 2.5: Residential Energy Micro Hub.

and MGO's needs are met [47]. In this context, the concept of an energy hub is useful. Such hubs are systems with a defined boundary, where energy activities such as energy conversion, energy production, storage and consumption take place [48], and it can be viewed as represents an interface between different energy infrastructure and/or loads; this concept facilitates the transition from the existing grid toward a smart grid.

In order to implement DLC and DR at the residential level simultaneously, automation in demand control is essential. An HEMS can facilitate both of these schemes [47], since it can receive DR signals, such as TOU prices or peak load caps, and DLC signals from the MGO, while considering customer's preferences in the form of set points, and based on this, it can schedule the operation of household appliances. An HEMS can be implemented through an optimization approach to either minimize the electricity bill or maximize customer satisfaction, considering electricity price and DR signals to manage appliance consumption [47], as discussed next.

Figure 2.5 depicts a residential energy micro hub proposed in [49], comprising of various appliances, ESS such as batteries, and power generation facilities such as wind and solar PV

units. This micro hub also includes a central hub controller that comprises a mathematical model of hub, and an associated optimization solver, and is an example of an HEMS referred to the Energy Hub Management System (EHMS). The mathematical model is an optimization model of the hub, with an objective function subject to the constraints associated with the operation of the appliances, customer preferences, weather externalities, electricity prices and peak demand cap for a scheduling horizon. By setting an appropriate demand limit control signal at each time interval, the MGO can reduce the demand during peak hours or shift it to off-peak hours, thus implementing DR. The optimization problem can be represented in general form as follows:

$$\begin{aligned} \min \quad & J = \text{Objective Function} \\ \text{s. t.} \quad & \sum_{h} P_{i,k} \leq P_k^{max} && \forall k \\ & \text{Device } i \text{ operational constraints} && \forall i \end{aligned} \tag{2.22}$$

Another example of an HEMS is the Home Automation System (HAS), which allows customers to schedule the operation of appliances by providing information on electricity prices, weather forecasts, history of energy consumption, etc. [50], [51]. With the help of HAS, customers can effectively shift the operation of appliances, i.e., demand, to low electricity price hours to reduce their electricity bill. However, such technologies for residential load management requires modeling the residential loads appropriately, so that these can be integrated into microgrid EMS.

Since HEMS basically shift the operation of appliances to non-critical hours with low electricity price, such systems can be generally modeled as constant energy demand shifting models. Thus, using these load models to represent such systems in microgrid EMS, allows to model controllable loads in EMS.

2.4 Electric Thermal Storage System

There are several kinds of heating ETS systems based on the storage medium, placement of the storage, and the conversion of electric energy. The storage medium can be liquid or solid. The location of the storage can be directly in the room that is heated or somewhere central to heat the whole house (e.g., in the basement). The conversion of electric energy into thermal energy can be done either by an electric heating element, i.e., a big resistance, or by a heat pump, which is more efficient but also more expensive.

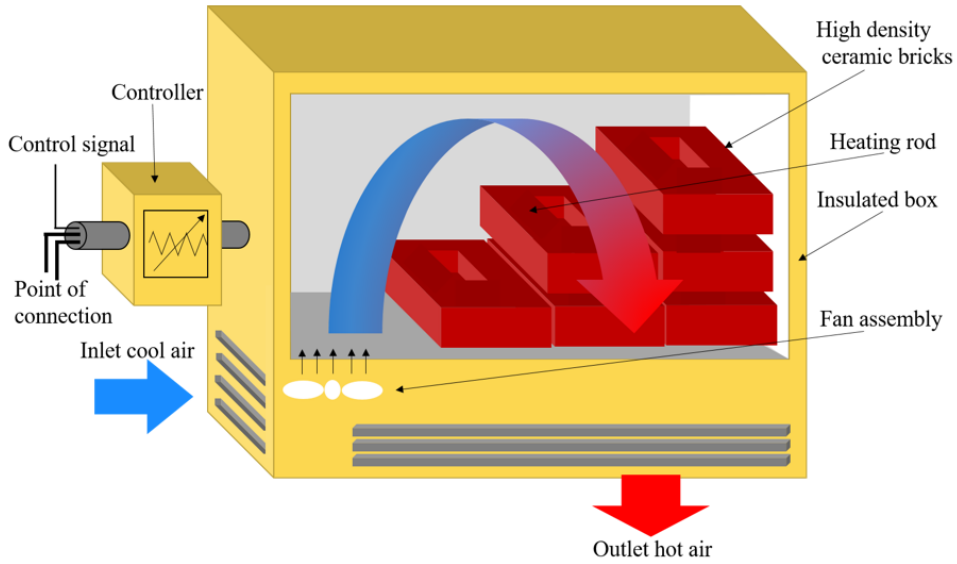

Figure 2.6: Brick-core ETS system.

In this thesis, brick-core ETS systems are considered. In these systems, the conversion of the electric energy is done by heating rods that are placed between high-density bricks in which the thermal energy is stored, as illustrated in Figure 2.6. These bricks are in a well-insulated box to ensure low self-discharge. To discharge the heat from the thermal storage, there is a controlled fan that blows air through air channels in the bricks. The conventional ETS systems are charged during off-peak hours when electricity prices are low [52].

For different room sizes of residential buildings, there are different sizes of brick core ETS systems available, which differ in the maximum electric power and the thermal storage size. Typical systems vary in size from 1.32 to 10.8 kW and 13.5 to 40 kWh [52].

2.5 Optimization Models and Methods

A mathematical optimization problem comprises an objective function to be minimized subject to a set of constraints. The optimization solution determines the values of the variables which minimize the objective function. The constraints ensure that the values of the variables are within specified limits and satisfy the stated conditions. Depending on the optimization model, an appropriate optimization algorithm is needed to solve it [53].

2.5.1 Linear Programming

A Linear Programming (LP) model consist of the minimization of a linear objective function subjected to a set of linear equality and inequality constraints [53]. It can be represented in general form as follows:

$$\begin{aligned} \min \quad & C^T z \\ \text{s.t.} \quad & Az \leq B \\ & z \in \mathcal{Z} \end{aligned} \tag{2.23}$$

where z is a n-dimensional decision vector in feasible region $\mathcal{Z}$, while A is a $m \times n$ parameter matrix, C is a n-dimensional parameter vector, and B is m-dimensional parameter. This model creates a feasible region which comprises the set of all points that satisfy all the constraints. An optimal solution of the LP problem is a point in the feasible region with the smallest value of the objective function. The most commonly used techniques for solving the LP problems are the simplex method or interior point methods [54]. In the simplex method, the solution process starts at one of the vertices of the polytopes, and travels from vertex to vertex in such a way that the objective function value decreases; when this value does not decrease any more, the process stops. On the other hand, in the interior point methods, the solution process starts at the interior of the feasible region and travels towards the boundary to converge at the optimum [53].

2.5.2 Mixed Integer Linear Programming

In LP models, all the decision variables are continuous or, in other words, the values of the variables are real numbers, and, when any of the variables is an integer, the LP problem is transformed into as a Mixed Integer Linear Programming (MILP) problem, which is generally solved using Branch and Bound methods or cutting plane based methods [55]. In the Branch and Bound method, the feasible region is subdivided to develop bounds on the value of the objective function. A relaxed integer program, where the integer variables are treated as continuous, thus transforming the problem into an LP problem, is solved first; this solution specifies the upper bound to the objective function. Based on the obtained non-integer value of relaxed integer variable, the integer variable limits are divided in subdivisions. A subdivision is then branched into another subdivisions based on the obtained non-integer value. In the cutting plane algorithm, the MILP problem is modified into an LP problem by adding new constraints until an integer solution is reached. The addition of the new constraints reduces the feasible region until the final optimal integer solution is obtained [55]. The microgrid UC problem with a piece-wise-

linear operating cost objective function is an MILP optimization problem, which can be solved by using highly efficient commercial grade software packages, such as CPLEX [56].

2.5.3 Mixed Integer Quadratic Programming

In Mixed Integer Quadratic Programming (MIQP) problems, the optimization problem includes a quadratic objective function and linear constraints which can be represented as follows:

$$\begin{aligned} \min \quad & J(z) = z^T C z \\ \text{s.t.} \quad & Az \leq B, z = [z_1, z_2]^T, z_1 \in Z_1, z_2 \in Z_2 \end{aligned} \tag{2.24}$$

where J is a quadratic objective function, $\mathcal{Z}_1$ is a bounded polyhedral set, and $\mathcal{Z}_2$ is the set of integer variables. MIQP problems can be solved by using Branch and Bound or Outer Approximation algorithms. In this thesis, the proposed microgrid UC and linearized UC-OPF models are MIQP problems, which are solved by using commonly used commercial grade solvers such as CPLEX [56].

2.5.4 Non-Linear Programming

Optimization problems comprising a non-linear objective function and/or constraints are referred to as Non-Linear Programming (NLP) problems [53], which can be formulated in general form as follows:

$$\begin{aligned} \min \quad & J(z) \\ \text{s.t.} \quad & g(z) \leq 0 \\ & h(z) = 0 \quad z \in \mathcal{Z} \end{aligned} \tag{2.25}$$

where, J, g and h are linear or non-linear functions, and z represents the decision variables in feasible region $\mathcal{Z}$. NLP problems are more difficult to solve than LP problems. First order derivative based methods or conjugate direction methods can be used to solve NLP problems. Since the partial derivative of the objective function at an optimal point is zero, the solution process in first-order-derivative-based methods relies on first derivative information. However, these methods face numerical difficulties near an optimal and require a longer time to converge to an optimal solution. On the other hand, in the conjugate direction algorithm, the solution process relies on the inverse of a matrix of second order partial derivatives, and converges quickly, but at increased computational costs [53]. The

OPF models proposed in this thesis are NLP problems, because of their non-linear power flow equations, and are solved by using commercially available solvers such as SNOPT, CONOPT, MINOS, and COIN-IPOPT [56].

2.5.5 Mixed Integer Non-Linear Programming

Many optimization problems comprise discrete decisions and non-linear constraints. Such models, referred to as MINLP problems, include discrete as well as continuous decision variables, and a non-linear objective function and/or non-linear constraints. Thus, the MINLP problem includes an NLP and an MILP subproblem [57], and can be represented as follows:

$$\begin{aligned} \min \quad & J(z_1, z_2) \\ \text{s.t.} \quad & g(z_1, z_2) \leq 0 \quad z_1 \in \mathcal{Z}_1, z_2 \in \mathcal{Z}_2 \end{aligned} \tag{2.26}$$

where, J and g are linear or non-linear functions, Z_1 is a bounded polyhedral set, and Z_2 is the set of integer variables. Such an MINLP problem can be solved using the Branch and Bound method, generalized Benders Decomposition, outer-approximation, LP/NLP based Branch and Bound, and extended cutting plane methods [58]. Large scale MINLP problems are typically difficult to solve because of the expansive search tree; in such cases, a good solution may be sufficient, as opposed to finding an optimal solution, given the computation time restrictions [58].

One of the microgrid EMS mathematical models developed in this work is an MINLP problem, which is coded in GAMS [59] using the DICOPT solver. This solver is based on the outer approximation method, in which the solution process begins by solving an NLP problem with relaxed discrete variables [56]. If it yields a solution with integer values for all the discrete variables, the solution process stops, otherwise, the process continues, solving the NLP subproblem and the MILP master problem sequentially and iteratively, until it satisfies a stopping rule. From the solution of the MILP master problem, the binary variables are fixed to solve the NLP subproblem at each iteration. There are various stopping criteria, one of them is the worsening of the NLP subproblem solution. In DICOPT, the NLP subproblems can be solved using the SNOPT, CONOPT, MINOS, or COIN-IPOPT solvers [56], while the MILP master problem can be solved using solvers such as CPLEX, XA, or BDMLP [56]. Although DICOPT obtains global optimal solutions for both convex and non-convex models [56], there is no guarantee that such global optimal can be obtained. Nevertheless, sub-optimal solutions obtained for the EMS models are all that is needed in practice for microgrid operation. MINLP problems coded in GAMS can

also be solved using solvers such as SBB, BARON and KNITRO [56].

2.5.6 Multiobjective Optimization Problems

Multiobjective optimization models consider several objectives at the same time, usually coupled together using a functional form as follows:

$$\begin{aligned} \min \quad & J(z) = g(h_1(z), h_2(z), ...) \\ \text{s.t.} \quad & z \in \mathcal{Z} \end{aligned} \tag{2.27}$$

where $J(z)$ is the objective function for the multi-objective optimization problem, with $h_i(z)$ being the individual objectives, and $z = (z_1, z_2, ..)$ are the decision variables in feasible region $\mathcal{Z}$. Such a model may include conflicting objectives and requires finding a Pareto optimal solution. The Pareto optimal solution is a set of efficient, non-dominated, and non-inferior solutions; in other words, for Pareto optimal solution, there is no other feasible solution vector which may improve some objective without deteriorating at least one other objective. In this type of problems, the objectives are combined to form a scalar equivalent function, which is then solved to identify the best compromising alternative; such single objective optimization problems can be solved using the above mentioned conventional mathematical programming algorithms [60].

There are three conventional and most used optimization approaches to the multi-objective optimization problem: the weighting and constraints methods, the distance-based methods (such as compromise programming and goal programming), and interactive methods. The distance-based methods consider pre-specified preferences for objectives, while in the interactive methods, the preferences for objectives can be provided during the solution process. The weighting and constraint methods are most commonly used to handle spatial multiobjective problems. In these methods, a weight, $w_1, w_2, ..$ is assigned to each objective function $h_i(z)$. The multiobjective function can be converted into a single objective by algebraic summation of the weighted objectives, as follows:

$$\begin{aligned} \min \quad & J(z) = \sum_i w_i h_i(z) \\ \text{s.t.} \quad & z \in \mathcal{Z} \end{aligned} \tag{2.28}$$

where the weights are positive number with $\sum_i w_i = 1$. To obtain the best compromised solution, the weighted single-objective model need to be solved by systematically varying the weights.

In constraint methods, only one objective is maximized while the rest of the objectives are converted into inequality constraints, as follows:

$$\begin{aligned} \min \quad & h_s(z) \\ \text{s.t.} \quad & c_i \leq h_i(z) \quad \forall i \neq s, z \in \mathcal{Z} \end{aligned} \tag{2.29}$$

where c_i is a lower bound on the objective i. The best compromised solutions can be determined by solving the problem by systematically varying the c_i values.

The weighting and constraint methods provide important information about the best solutions along with possible decision outcomes and trade-offs. However, there is no generic rule to identify the best combination of weights or constraint intervals to obtain the best possible compromise [60].

The distance-based methods seek to minimize the distance between the target objective value and achieved solutions. The most commonly used distance-based methods are goal programming, compromise programming, and the reference point method [60]. In goal programming methods, the summation of deviations from the aspiration or target value for the objectives are minimized, with the decision maker specifying the aspiration level for each objective [60]. The model for goal programming can be mathematically represented as follows:

$$\begin{aligned} \min \quad & \Big[\sum_i (w_i^- d_i^- + w_i^+ d_i^+)^p\Big]^{(1/p)} \\ \text{s.t.} \quad & h_i(z) + d_i^- + d_i^+ = A_i \quad \forall i, z \in \mathcal{Z} \\ & d_i^-, d_i^+ \geq 0 \quad \forall i \end{aligned} \tag{2.30}$$

where A_i represents the aspiration level for the objective i; w_i^-, w_i^+ are the weights associated with the objectives, reflecting the preferences set by the decision maker; and d_i^-, d_i^+ are negative and positive goal deviations, respectively. The goal programming methodology is computationally efficient, and for $p = 1$, it corresponds to a linear programming problem, which can be efficiently solved. However, in this method, it is important to know the aspiration levels for the objectives. There is also a possibility of missing the best compromise solution as it searches for solutions that are near their aspiration levels.

The compromise programming method considers the point of reference which is the ideal solution or the optimal value for that objective only. The mathematical representation of

the compromise programming problems is as follows:

$$\begin{aligned} \min \quad & \left[\sum_i \left(\frac{\bar{h}_i - h_i(z)}{\bar{h}_i - \underline{h}_i} \right)^p \right]^{(1/p)} \\ \text{s.t.} \quad & z \in \mathcal{Z} \end{aligned} \tag{2.31}$$

where $\bar{h}_i$ is the anti-ideal value for the objective i; $\underline{h}_i$ is the ideal value for the objective i; and p is a parameter which can be any integer from 1 to infinity, and reflects the importance of the deviation from the ideal point. This method has a simple structure, and can yield the best compromised solution, with clear information about the trade-off between the different objectives [60].

In this thesis, the weighting and distance-based multi-objective optimization methods are adopted in the formulation of the UC-based EMS models to minimize operating costs and pollutant emissions simultaneously for isolated microgrids. Such EMS models are MIQP problems, can be solved by using the commercially available software packages, such as CPLEX [56]

2.6 Model Predictive Control

The MPC technique is applied to the operation of systems which rely on input prediction. This methodology is an open-loop problem, such as a control or optimization problem, for a finite time horizon that is solved at each time interval to account for deviations in the predicted inputs [16]. Since the solution of the open-loop problem relies on the predicted inputs, which can differ due to external disturbances, the solution with updated predicted inputs is re-calculated periodically, but the solution is implemented only for one time interval. At each interval, the input forecast and solution are repeated while shifting forward the time horizon.

Consider for example the following dynamic model of a discrete-time system:

$$z_{t+1} = F(z_t, u_t) \qquad\qquad z_t \in \mathcal{Z}, u_t \in \mathcal{U} \tag{2.32}$$

For such a dynamic system, the open-loop optimal control problem for a finite time horizon

τ_t can be formulated as follows:

$$\begin{aligned} \min \quad & \sum_{t \in \tau_t} J(z_t, u_t) \\ \text{s.t.} \quad & z_{t+1} = F(z_t, u_t) \quad z_t \in \mathcal{Z}, u_t \in \mathcal{U}, \forall t \in \tau_t \end{aligned} \tag{2.33}$$

The optimal solution obtained from this control problem, i.e., z_t^*, u_t^*, is based on the predicted inputs received for the considered time horizon. From this solution, z_{t_0} and u_{t_0} is implemented, while at recalculation instant $t = t + 1$, the predicted set of inputs are re-calculated, and the optimization problem is re-solved over the shifted time horizon τ_{t+1} [16].

In the MPC approach, the recalculation time and the time horizon are important parameters that influence the performance of the system, and thus should be chosen carefully. The recalculation time can be a few minutes to hours depending on the solution time of the problem and its horizon time resolution. The longer the time horizon, the better the performance of the MPC approach; however, this increases the size of the optimization problem and the computational burden, as well as the prediction errors [17], [22].

Since many microgrids of today are generally supplied by a mix of renewables based generation resources and the output of such sources are uncertain, the MPC approach is an attractive solution for microgrid operational problems. Hence, in this thesis, the MPC method is applied to all proposed EMS models.

2.7 Summary

In this chapter, the concept of a microgrid and its EMS were presented, various DR strategies and schemes were discussed, and the concept and examples of HEMS for residential customers were outlined. A summary of ETS systems including their various features were presented, and a brief review of mathematical programming problems and the solution methods used in microgrid EMS were provided. Finally, the MPC approach was introduced, since it is an essential feature of the EMS proposed in this thesis.

Chapter 3

Including Smart Loads in Integrated EMS for Isolated Microgrids

Based on the literature review presented in Chapter 1, there is a need to develop a mathematical model to estimate the controllable load component of an isolated microgrid as a function of the ambient temperature, electricity price, time of the day, and peak demand constraints that are imposed by the MGO, so that it can be included in a microgrid EMS. Furthermore, in order to manage the voltage and reactive power, the mathematical formulation of the EMS has to simultaneously consider power flow and UC operational constraints. Hence, these issues are addressed in the chapter.

This chapter thus first presents the mathematical modeling of smart loads, using NN, as a function of the ambient temperature, time of day, TOU price, and a peak demand cap imposed by the MGO; to develop the NN-based smart load estimator, realistic data from an actual EHMS installation is used for supervised training. Thereafter, a novel microgrid EMS (MEMS) framework based on an MPC approach is proposed that includes the developed NN model of smart loads, which yields optimal dispatch decisions of dispatchable generators, ESS, and peak demand for controllable loads, considering power flow and UC constraints simultaneously. To study the impact of DR on the microgrid operation with the proposed MEMS framework, the CIGRE benchmark microgrid system is used, which includes DERs with RES based generation. The results show the feasibility and benefits of the proposed models and approach, compared to a standard decoupled UC and OPF based EMS.

3.1 Proposed Microgrid EMS

The proposed MEMS architecture for an isolated microgrid is shown in Figure 3.1, comprising smart loads and the MEMS itself. The introduced controllable smart load demand PD^{rc} is a function of the ambient temperature T^0, TOU price, peak demand constraint

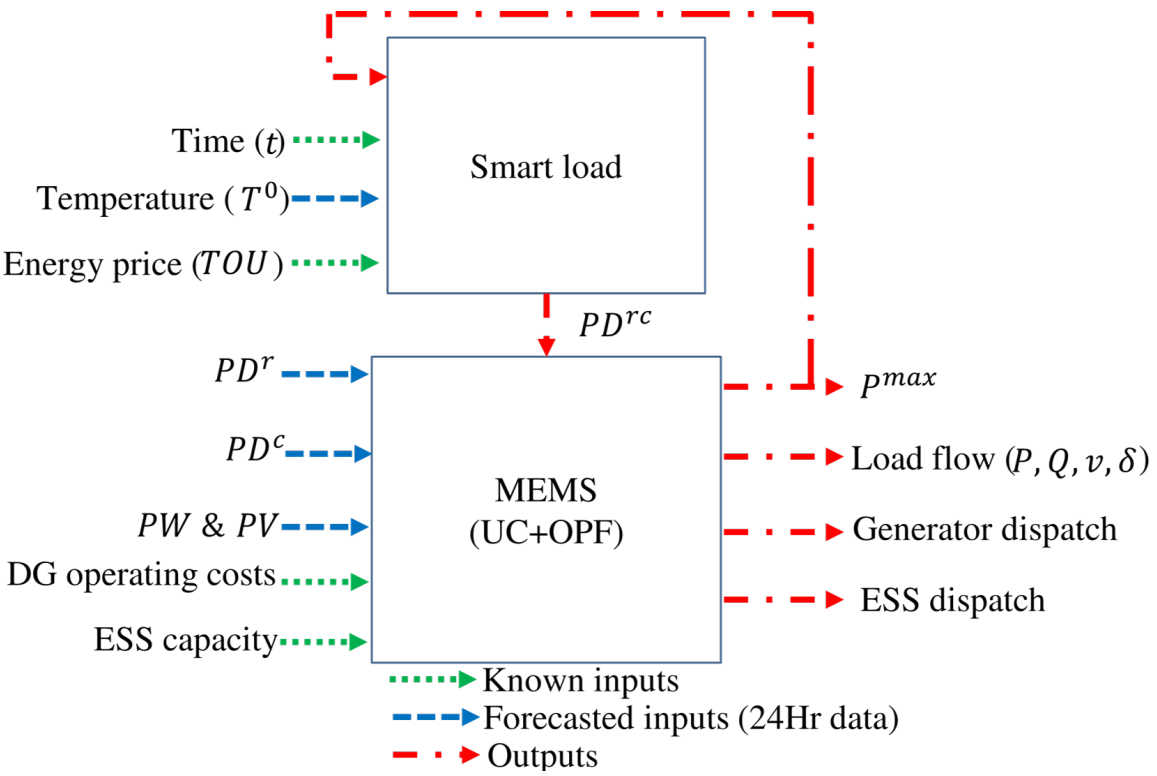

Figure 3.1: Proposed MEMS architecture.

P^{max}, and the time of day; among these, the time of the day and the TOU prices are known inputs, T^0 is a forecasted input, and P^{max} is a variable determined optimally by the MEMS. One of the main outputs of the MEMS model is the dispatch of the smart load demand as an available resource. The other MEMS outputs are the dispatch of available resources in the microgrid, considering the operational limits and constraints related to the dispatchable units, power flows, ESS energy balance, and spinning reserve requirements.

The mathematical model of MEMS is comprised of an objective function that represents the microgrid operational cost, including generation costs, start up and shut down costs, and costs associated with load curtailment, as follows:

$$J = \sum_{g,k}[(d_g P_{g,k}^2 \Delta t_k + e_g P_{g,k} + f_g W_{g,k})\Delta t_k + C_g^{sup} U_{g,k} + C_g^{sdn} S_{g,k}] + \sum_{i,k} P_{i,k}^{LC} C^{LC} \Delta t_k \quad (3.1)$$

where all variables, parameters, and indices in this and all equations in this chapter are

defined in the Nomenclature Section. It is assumed that the MGO owns all the DERs, and fully controls them. Furthermore, load curtailment is considered in (3.1) with significant high cost. The above objective function is subject to the followings constraints:

- *Real and Reactive Power Balance:* The real power balance at a bus considers the output from DG, solar PV, and wind power units, and the net power of the loads from commercial and residential customers, taking into account ESS charging and discharging, and the network flows, as follows:

$$\sum_{g\in G_i} P_{g,k} + PV_{i,k} + PW_{i,k} - PD^{c}_{i,k} V^{\alpha^c_k}_{i,k} - [PD^{r}_{i,k} + PD^{rc}_{i,k}(P^{max}_{k}) - P^{LC}_{i,k}] V^{\alpha^r_k}_{i,k} + \sum_{n\in N_i} (P^{dch}_{n,k} - P^{ch}_{n,k}) = \sum_{j} V_{i,k} V_{j,k} Y_{i,j} \cos(\theta_{i,j} + \delta_{j,k} - \delta_{i,k}) \quad \forall k, i, j \quad (3.2)$$

$$\sum_{g\in G_i} Q_{g,k} - PD^{c}_{i,k} K_1 V^{\beta^c_k}_{i,k} - [PD^{r}_{i,k} + PD^{rc}_{i,k}(P^{max}_{k}) - P^{LC}_{i,k}] K_2 V^{\beta^r_k}_{i,k} + \sum_{n\in N_i} (QC_{n,k}) = -\sum_{j} V_{i,k} V_{j,k} Y_{i,j} \sin(\theta_{i,j} + \delta_{j,k} - \delta_{i,k}) \quad \forall k, i, j \quad (3.3)$$

  The residential loads comprise fixed and controllable components; the fixed components PD^r are obtained from a forecasting engine; and the controllable components $PD^{rc}(P^{max})$ represent the dispatchable demand included in the MEMS model as a function of P^{max}, which is estimated using the RCLPE discussed in Section 3.3. Furthermore, residential and commercial loads are considered as a mix of constant impedance (Z), constant current (I), and constant power (P), or ZIP loads, and are included in the MEMS model as exponential functions of the voltage, as shown in (3.2) and (3.3). Note that customers are not paid any incentives for DR participation by the MGO, but are assumed to be controlled by an intelligent HEMS designed to individually optimize their costs and/or energy consumption, as explained in detail in [49].

- *Reserve Constraint:* This constraint ensures that the spinning reserve requirement

for the microgrid is provided by the dispatched generators as follows:

$$\sum_g (\bar{P}_g W_{g,k} - P_{g,k}) \geq R^{sv} \sum_i [PV_{i,k} + PW_{i,k} + PD^c_{i,k} V^{\alpha^c_k}_{i,k} + [PD^r_{i,k} + PD^{rc}_{i,k}(P^{max}_k) - P^{LC}_{i,k}] V^{\alpha^r_k}_{i,k}] \quad \forall k \quad (3.4)$$

where a reserve margin R^{sv} of 5% change in demand and generation from renewables is considered. Note that this is a small value, as typically reserves of 10% are used, which are increased to 25% of solar PV power output and 50% for wind power output; these are very conservative values preferred by utilities, that significantly affect dispatches and costs. Considering the fast response of ESS, these large reserves may not be necessary to maintain frequency stability in the microgrid.

- *Generalized UC Constraints:* The following constraints include active and reactive power generation limits, ramp-up and ramp-down constraints, minimum up-time and down-time constraints, and coordination constraints:

$$\underline{P}_g W_{g,k} \leq P_{g,k} \leq \bar{P}_g W_{g,k} \quad \forall g,k \quad (3.5)$$
$$\underline{Q}_g W_{g,k} \leq Q_{g,k} \leq \bar{Q}_g W_{g,k} \quad \forall g,k \quad (3.6)$$
$$P_{g,k+\Delta t_k} - P_{g,k} \leq R^{up}_g \Delta t_k + U_{g,k+\Delta t_k} \underline{P}_g \quad \forall g,k \quad (3.7)$$
$$P_{g,k} - P_{g,k+\Delta t_k} \leq R^{dn}_g \Delta t_k + S_{g,k+\Delta t_k} \underline{P}_g \quad \forall g,k \quad (3.8)$$
$$(G^{on}_{g,k-\Delta t_k} - T^{up}_g)(W_{g,k-\Delta t_k} - W_{g,k}) \geq 0 \quad \forall g,k \quad (3.9)$$
$$(G^{off}_{g,k-\Delta t_k} - T^{dn}_g)(W_{g,k} - W_{g,k-\Delta t_k}) \geq 0 \quad \forall g,k \quad (3.10)$$
$$U_{g,k} - S_{g,k} = W_{g,k} - W_{g,k-\Delta t_k} \quad \forall g,k \quad (3.11)$$
$$U_{g,k} + S_{g,k} \leq 1 \quad \forall g,k \quad (3.12)$$

- *Energy Storage System:* The ESS constraints include the energy balance and constraints to prevent simultaneous charging/discharging, plus limits on SOC and charg-

ing/discharging power, as follows:

$$SOC_{n,k+\Delta t_k} - SOC_{n,k} = \left(P^{ch}_{n,k}\eta^{ch}_n - \frac{P^{dch}_{n,k}}{\eta^{dch}_n} \right) \Delta t_k \qquad \forall n,k \tag{3.13}$$

$$P^{ch}_{n,k} P^{dch}_{n,k} = 0 \qquad \forall n,k \tag{3.14}$$

$$\underline{SOC}_n \leq SOC_{n,k} \leq \overline{SOC}_n \qquad \forall n,k \tag{3.15}$$

$$P^{ch}_{n,k} \leq \overline{PESS}_n \qquad \forall n,k \tag{3.16}$$

$$P^{dch}_{n,k} \leq \overline{PESS}_n \qquad \forall n,k \tag{3.17}$$

- *Grid Constraints:* The following represent the grid operational constraints to ensure that bus voltages and apparent power transfers are within specified limits:

$$\underline{V} \leq V_{i,k} \leq \bar{V} \quad \forall i,k \tag{3.18}$$

$$\mathcal{S}_{i,j,k}(|V_{i,k}|, |V_{j,k}|, |\delta_{i,k}|, |\delta_{j,k}|) \leq \overline{\mathcal{S}}_{i,j} \quad \forall i,j,k \tag{3.19}$$

- *DR Cap:* The following constraint imposes a limit on the maximum demand P^{max} at a given time interval:

$$\underline{P}^{max} \leq P^{max}_k \leq \bar{P}^{max} \quad \forall k \tag{3.20}$$

  where the minimum value $\underline{P}^{max}$ represents the minimum loading condition defined in agreement with DR participants, while the maximum value $\bar{P}^{max}$ specifies the maximum peak demand desired by the utility.

3.2 Microgrid EMS Implementation

Equations (3.1)-(3.20) represent the proposed MEMS model, and correspond to an MINLP problem. This optimization problem can be solved using existing MINLP solvers, in particularly the DICOPT solver [56], and a warm start procedure, i.e., the previous feasible solution is used as the starting point for the next solution. If the problem is infeasible during the solution process, it has been determined by trial-and-error that reinitializing the binary decision variables W_{g,k_t} to the ON state allows obtaining a feasible solution.

It is important to note that DGs in microgrids generally have fast start-up, shut-down, and ramp characteristics, with times in the order of a few minutes. In spite of that,

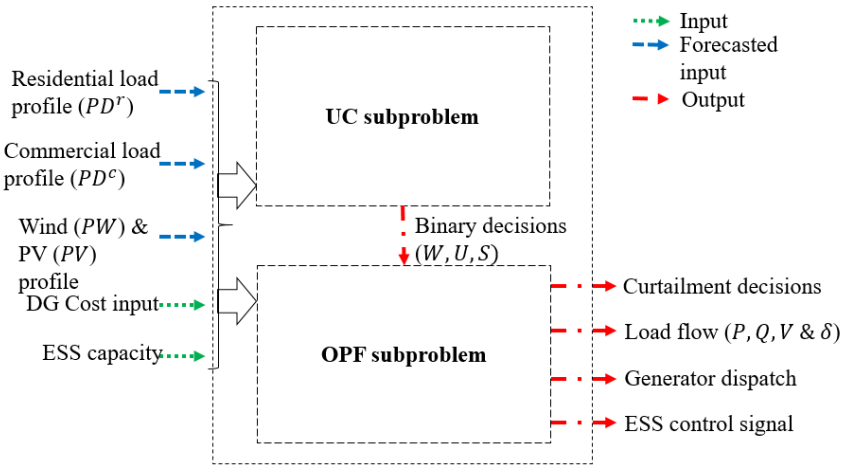

Figure 3.2: Decomposed Microgrid EMS architecture.

constraints (3.7)-(3.10) need be considered because of the MPC recalculation time, which is less than the minimum up- or down-times, or the time required to ramp up to full capacity of the respective DGs. In the present work, the minimum up- and down-times of the diesel generators are assumed 30 minutes, and full capacity ramp-up and ramp-down rates of 10 minutes are used, which are typical values for diesel generators [61].

3.2.1 Decomposition Approach

The microgrid EMS problem can also be decomposed into UC and OPF subproblems and solved sequentially, as proposed in [17]. The Decomposed Microgrid Energy Management System (DMEMS) starts with the Microgrid UC (MUC) subproblem, which is solved considering the inputs which include the output of the forecasting engine and smart loads, to obtain the commitment decisions, as shown in Figure 3.2. To accomplish this, the real power demand, supply balance, and reserve constraints are modified as follows:

$$\sum_g P_{g,k} + \sum_i (PV_{i,k} + PW_{i,k}) + \sum_n (P^{dch}_{n,k} - P^{ch}_{n,k}) = \sum_i [PD^c_{i,k} + PD^r_{i,k} + PD^{rc}_{i,k}(P^{max}_k) - P^{LC}_{i,k}] \quad \forall k_t \quad (3.21)$$

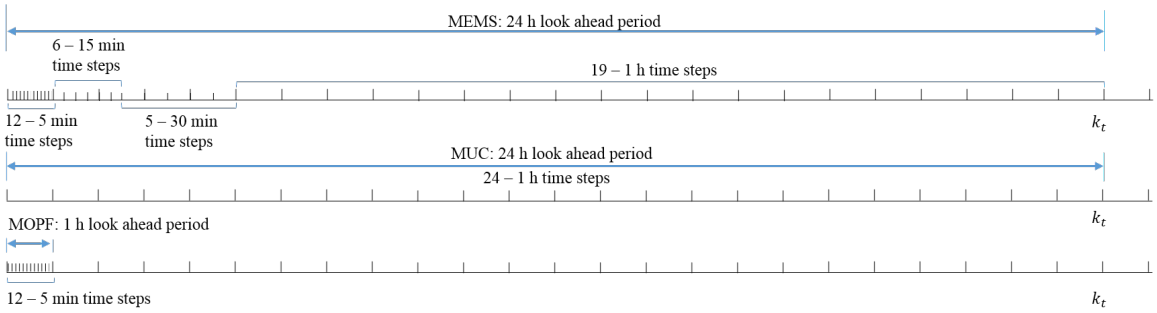

Figure 3.3: Time horizons of MEMS, MUC, and MOPF models.

$$\sum_{g}(\bar{P}_g W_{g,k} - P_{g,k}) \geq R^{sv} \sum_{i}[PV_{i,k} + PW_{i,k} + PD^{c}_{i,k} + PD^{r}_{i,k} + PD^{rc}_{i,k}(P^{max}_{k}) - P^{LC}_{i,k}] \quad \forall k \tag{3.22}$$

Hence, the MUC subproblem is comprised of (3.1), (3.5)-(3.17), (3.20), (3.21) and (3.22), and the optimal decisions thus obtained are then applied to the Microgrid OPF (MOPF) subproblem, comprised of (3.1)-(3.8), (3.13)-(3.20), to obtain the optimal dispatch decisions that are implemented as set points for controllable DERs. If the MOPF is infeasible, due to, for example, lack of enough reactive power support, the commitment decisions of the MUC subproblem can be modified by forcing the commitment of the next available cheaper generator. This process is repeated until a feasible MOPF solution is obtained that satisfies all the active and reactive power demand-supply balance and network constraints [17]. This approach provides a local optimal solution, which may or may not be the global optimal solution. However, as discussed in [5], sub-optimal solutions for EMS models are adequate for practical purposes in microgrid operation.

3.2.2 Time Horizons

Solving the MEMS problem considering a uniform time horizon of 5 min intervals over 24 hours, i.e., $T = 288$ intervals, is the computationally expensive. In this work, therefore, a non-uniform time scale comprising a higher resolution for the first few minutes and a reduced resolution in the later stages is used for the MEMS model, as in [17]. This accounts for the fact that the accuracy of forecasts vary over the forecasting horizon; thus, the shorter the horizon, the more accurate the forecast than for an extended horizon. The considered non-uniform time horizon is shown in Figure 3.3, yielding 12 time steps of 5 min, followed by 6 time steps of 15 min, 5 time steps of 30 min, and finally 19 time steps

of 1 hour, all adding up to 24 hours.

For the DMEMS framework, the MUC problem is solved for a 24 hour look ahead time window with a uniform time resolution of one hour, as shown in Figure 3.3, since decisions related to UC problem presents slower dynamics. The MOPF problem is, on the other hand, solved with a look-ahead period of one hour and uniform time resolutions of 5 min.

3.2.3 MPC Implementation

The optimal decisions obtained by solving the MEMS model over the horizon 0 to T relies on the forecasted inputs of intermittent energy sources and demand. In isolated microgrids, renewable power generation forecasts can vary significantly over a 24 hour time horizon. Hence, the optimal decision of the MEMS must be re-calculated with updated forecasted inputs every 5 min, based on the MPC approach discussed in Section 2.6. In this case, the optimal results obtained by solving the MEMS model are applied only to the next time interval, after which the forecast inputs are updated and the MEMS model is re-solved over the next 24 hour horizon, repeating this process every 5 min [16], [17].

3.3 Residential Controllable Load Profile Estimator

In this work, the smart residential DR options described in [49] is considered, in which a household owns an EHMS, i.e., an intelligent HEMS as discussed in Chapter 2, for optimally managing the household loads to reduce electricity costs and/or consumption. It is assumed here that such EHMS is connected to the microgrid with a bi-directional communication network, so that the MGO can send DR control signals, in particular P^{max}, to the household. Thus, the EHMS would schedule the operation of the household based on the DR signal, weather conditions, and customer preferences. This EHMS is comprised of an objective function seeking to minimize the customer's energy cost and/or consumption, subject to operational constraints of the household appliances and constraints associated with DR controls, as explained in Section 2.3. The DR control signal P^{max} is determined by the MGO using the proposed MEMS model to limit PD^{rc} of each house with an EHMS, within certain limits.

For efficient energy management of a microgrid in the presence of DR, the PD^{rc} profile needs to be properly estimated, so that an adequate DR model can be integrated in the MEMS framework. Therefore, based on the universal approximation theorem [62], which

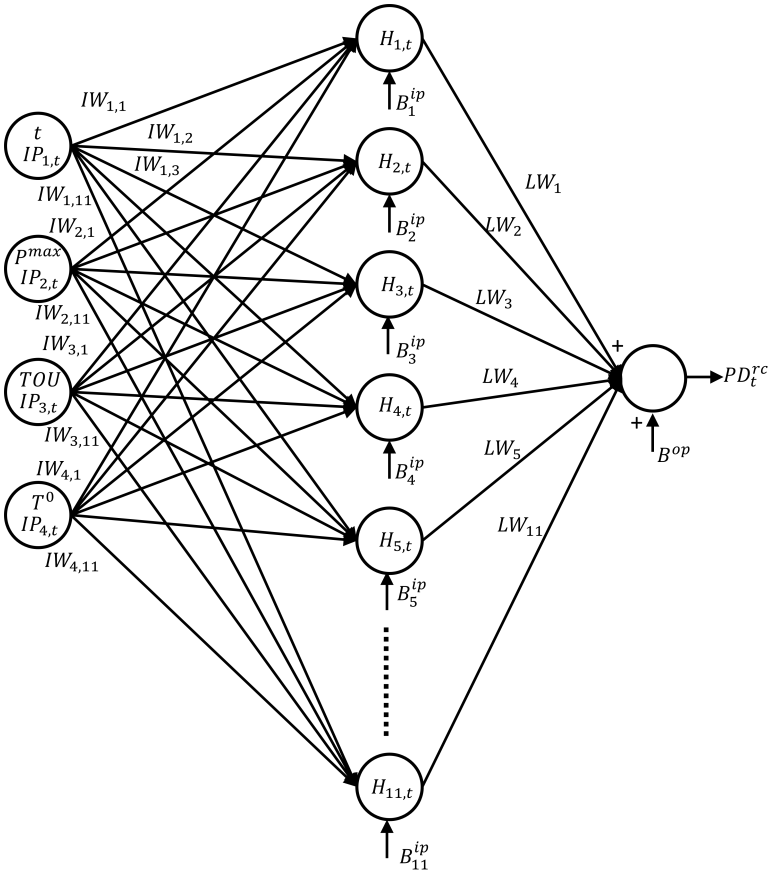

Figure 3.4: Smart load NN model obtained from the RCLPE.

states that a single hidden layer NN can be used to approximate any arbitrary continuous function, a Residential Controllable Load Profile Estimator (RCLPE) is developed to estimate the PD^{rc} from ambient temperature, TOU price, time of day and P^{max} inputs.

A supervised learning technique is applied to train the NN with measured data from smart meters and simulated data for an actual EHMS. These data were obtained for the months of May, June, and July of 2012 for weekdays, with a resolution of 5 min, and includes actual temperature profiles, TOU prices, and load profiles for different P^{max} values. An input 121,537 x 4 matrix and a 121,537 output vector is used for training the NN. By varying the number of hidden layer neurons and training the NN with the available data, the best result is obtained with 11 hidden layer neurons, using the Levenberg-Marquardt learning technique in MATLAB$^{\text{TM}}$, because of its robust nature [63]. The resulting RCLPE structure, shown in Figure 3.4, has an R^2 of 0.87 for the complete dataset, indicating that

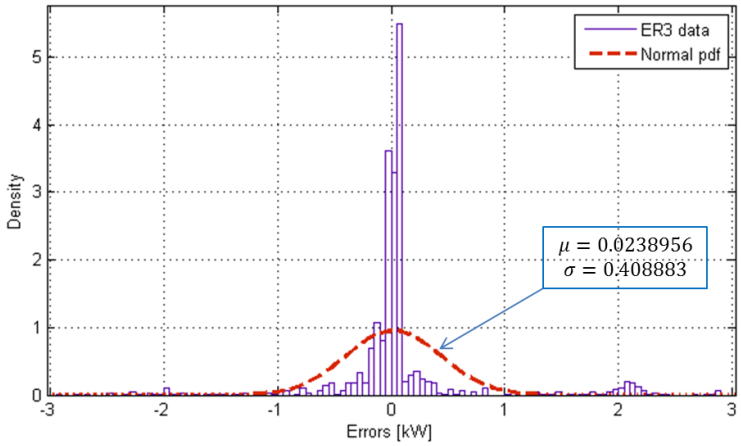

Figure 3.5: Validation error histogram for RCLPE model.

the output of the NN and the data used for training have a high correlation. Note that the complexity of the NN-model obtained reflects the complex relations between the various inputs to the load model and the power demand.

After the training procedure, the NN model is validated and tested with the datasets that are not used for training, to evaluate the performance of the NN. Figure 3.5 shows the validation error histogram for the proposed NN model in Figure 3.4, depicting the maximum and minimum possible error and their number of occurrences; observe that the model is quite accurate, with about 80% of errors being within the range of $\pm$ 0.2 kW for a peak power of about 5 kW.

Ultimately, the estimated PD^{rc} NN can be expressed as a function of time, ambient temperature, TOU price, and P^{max}, as follows:

$$PD_t^{rc} = f(t, P^{max}, TOU, T^0) \tag{3.23}$$

Thus, the following mathematical model can be used in the proposed MEMS model to represent the smart load demand PD^{rc}:

$$PD_t^{rc} = \sum_y \left(\frac{2}{1+e^{-2H_{y,t}}} - 1 \right) LW_y + B^{op} \quad \forall t \tag{3.24}$$

where

$$H_{y,t} = \sum_x IP_{x,t} IW_{x,y} + B_y^{ip} \quad \forall y \tag{3.25}$$

Table 3.1: DER ratings for the modified CIGRE system.

Node	DER type	Pmax [kW]
1	Diesel Generator	800
9	CHP diesel	310
1	Diesel Generator	1400
1	Diesel Generator	2500
3	Photovoltaic	600
4	Photovoltaic	33
5	Photovoltaic	30
5	Battery	750
5	Residential fuel cell	41.25
6	Photovoltaic	50
8	Photovoltaic	200
9	Photovoltaic	212
9	Fuel cell	265
10	Photovoltaic	214
10	Battery	250
10	Residential fuel cell	17.5
13	CHP Microturbine	500
7	Wind turbine (inverter-interfaced)	1000
7	Wind turbine (SCIG)	500

It should be mentioned that other types of controllable/smart loads, beside the EHMS, could be modeled in a similar way, with an appropriate NN model. Therefore, the proposed approach can be considered generic in this regard, with the only requirement for the smart load being that it should be able to respond to peak demand commands, as, for example, the case of Peak Saver Plus loads [44].

3.4 Results and Discussions

To validate the proposed MEMS for a significantly complex isolated microgrid, the modified CIGRE medium voltage benchmark network shown in Figure 3.6, which is based on a real system [64], is considered, based on the test microgrid used in [17] but with 25% more total ESS capacity, and including limits for the main transformer. The 3 diesel units at Bus 1 have a combined capacity of 4,700 kW, and the total installed capacity in the microgrid is 9,216 kW, including ESS, intermittent energy sources, and various other DGs, as shown in Table 3.1; the feeder data can be found in Appendix A. In order to account for the uncertainties and errors in the forecast of the RES and demand, normal probability

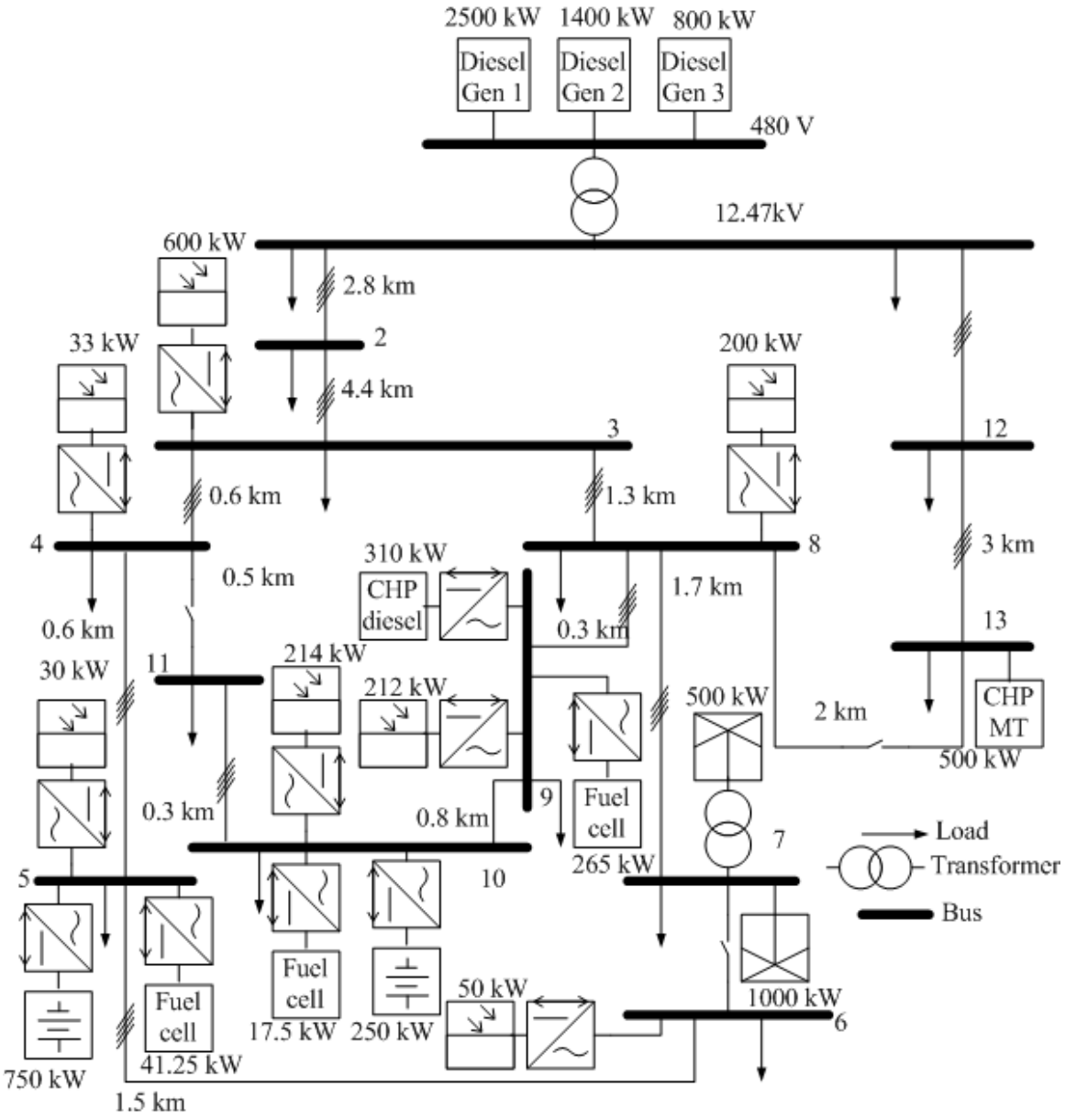

Figure 3.6: Modified CIGRE microgrid benchmark.

density functions (pdfs) for 24h- and 1h-ahead are used to obtain the wind, PV, and demand power profiles, based on linear approximations of the difference between the 24h- and 1h-ahead forecast errors with respect to time.

In the RCLPE, the EHMS is considered to be managing four household appliances, namely, the dish washer, cloth dryer, washer, and air conditioner. It is assumed that 50% of the total energy demand of households, which corresponds to 30% of the total energy demand of the microgrid, is from controllable loads. The proposed integrated MEMS approach could also be tested on the real microgrid system of KLFN; however, the modified CIGRE benchmark system is more complex, and represents a more challenging case to test the proposed approach. Hence, if the proposed approach provides feasible and more optimal dispatch results for the CIGRE test system, the same can be expected for the simpler KLFN system, and thus, here, results are only obtained for the former system in this Chapter.

3.4.1 Case Studies

The proposed MPC based MEMS framework is validated for 24 h of operation, with a recalculation time of 5 min. The MEMS model and the MUC and MOPF models, as part of the DMEMS framework, were coded in GAMS [59]. The MEMS and MUC models are MINLP problems, due to the smart load NN model in the MUC, and are thus solved using the DICOPT solver [56]. The MOPF is a NLP problem that is solved using the SNOPT solver [56].

To investigate the impact of DR on microgrid operation, different cases, from no controllable loads to 100% EHMS loads (30% of total demand), are considered, where EHMS loads in the microgrid are controlled through P^{max}. Note that 20% controllable loads means that 6% of the total energy demand of the microgrid is being controlled.

The proposed MEMS model using the MPC approach required on average 28 s to obtain a solution for a single 24 h variable time-step horizon, in a Intel® Xeon® CPU L7555 1.87GHz (4 processors) server; this is well within the 5 min MPC re-calculation time. The process was repeated 288 times by shifting the time horizon forward by 5 min, for 24 hours, thus simulating the MEMS operation for a full day; this computation took 180 min. On the other hand, the DMEMS framework required a total computation time of around 30 min, with an average of 6.25 s per iteration. Although, the MEMS framework requires a longer simulation time than the DMEMS framework, it is still feasible for real-time applications.

Table 3.2 presents a summary of the results obtained from the MEMS application, which shows that as DR control increases, the load curtailed by the MGO decreases, with no need for curtailment for 100% DR control. Consequently, the total operating costs are high without DR control, because of the high cost of load curtailment, decreasing as

Table 3.2: Summary of Results with MEMS

DR control [%]	Objective function [$]	Energy served by ESS [kWh]	Load curtailed [kWh]	Load factor	Peak demand [kW]
0	83,781	3,037	528	0.580	7,575
20	62,447	2,870	351	0.589	7,431
40	42,464	2,808	185	0.6	7,287
60	25,099	2,760	41	0.611	7,141
100	19,941	2,416	0	0.631	6,851

Table 3.3: Summary of Results with DMEMS

DR control [%]	Objective function [$]	Energy served by ESS [kWh]	Load curtailed [kWh]	Load factor	Peak demand [kW]
0	315,354	1,097	2,468	0.568	7,576
20	289,379	1,067	2,252	0.578	7,431
40	263,168	1,064	2,034	0.589	7,286
60	241,396	1,033	1,853	0.6	7,141
100	195,833	1,053	1,474	0.622	6,851

DR is increased. Furthermore, the load factor, which represents the ratio of average daily demand with respect to peak demand, increases from 0.580 to 0.631, indicating that the load profile gets flatter as DR control increases. Finally, and as expected, the peak demand decreases from 7.5 MW to 6.8 MW with increased DR control.

In Figure 3.7, the 24 h optimal P^{max} profile obtained from the MEMS and the TOU price profiles are depicted for 100% DR control. Figure 3.8 depicts 24 h PD^{rc} profiles of the RCLPE obtained with optimal P^{max} from the MEMS with and without DR control.

From the summary of results presented for the DMEMS framework in Table 3.3, it can be observed that with increased DR control, peak demand decreases from 7.5 MW to 6.8 MW, and the load factor increases from 0.568 to 0.622, which are similar to the results presented in Table 3.2 for the proposed MEMS approach. However, note that even though the total cost in DMEMS decreases with increased DR control, it is considerably higher than the total cost obtained with the MEMS approach, due to significantly higher load curtailment. Furthermore, observe that the total energy served by ESS with the MEMS approach is higher than with the DMEMS, which indicates the MEMS method makes effective use of the ESS in the dispatch, resulting in less load curtailment.

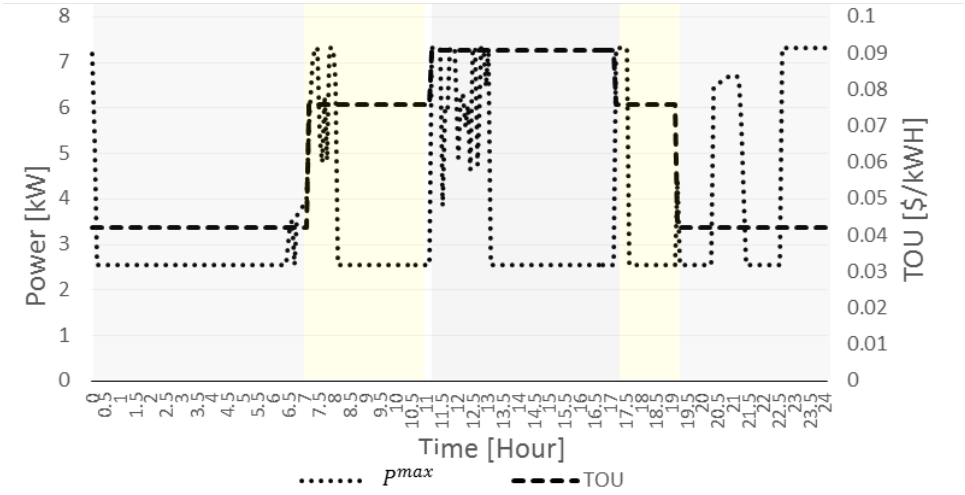

Figure 3.7: Optimal P^{max} obtained from the MEMS and TOU prices for 100% DR control.

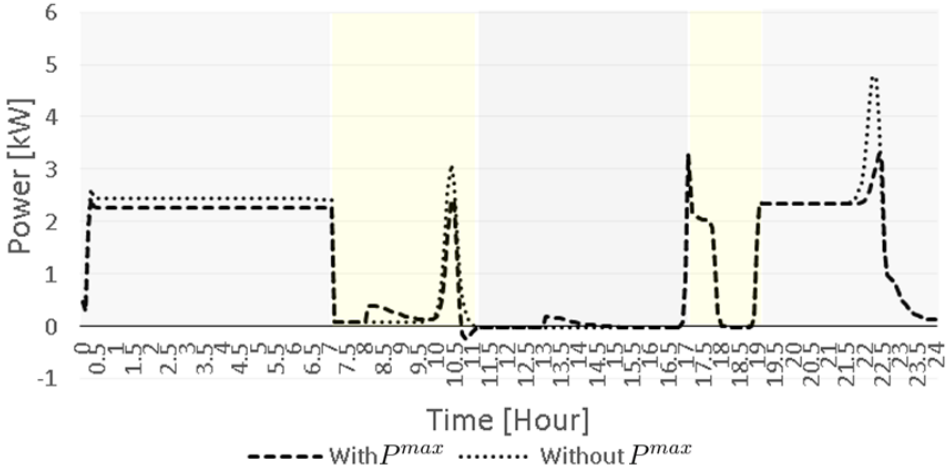

Figure 3.8: Optimal PD^{rc} obtained from the MEMS with and without 100% DR control.

The optimal dispatch of the DERs determined from the two EMS MPC approaches for a 24 h interval, considering P^{max} feedback or not, are presented in Figures 3.9 and 3.10. The negative area shows the total charging energy absorbed by the ESS, and white spaces under the demand (PD) line show the curtailed energy, confirming the better use of ESS and less load curtailment with the proposed MEMS approach. Particularly, two important time windows are highlighted in Figures 3.9 and 3.10:

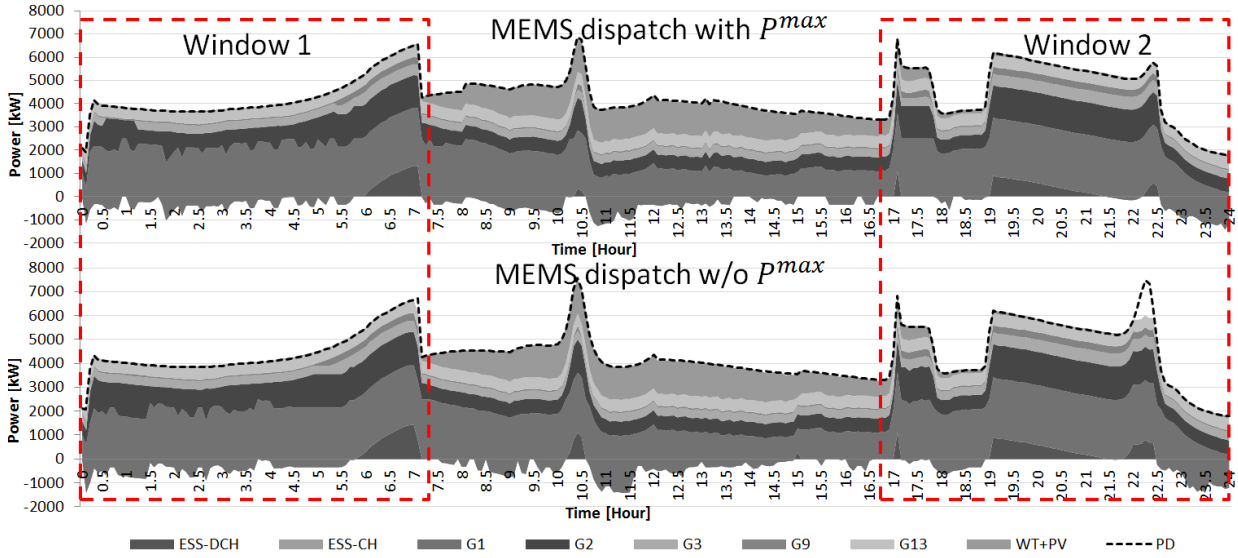

Figure 3.9: Optimal dispatch obtained from the MEMS approach with and without P^{max}.

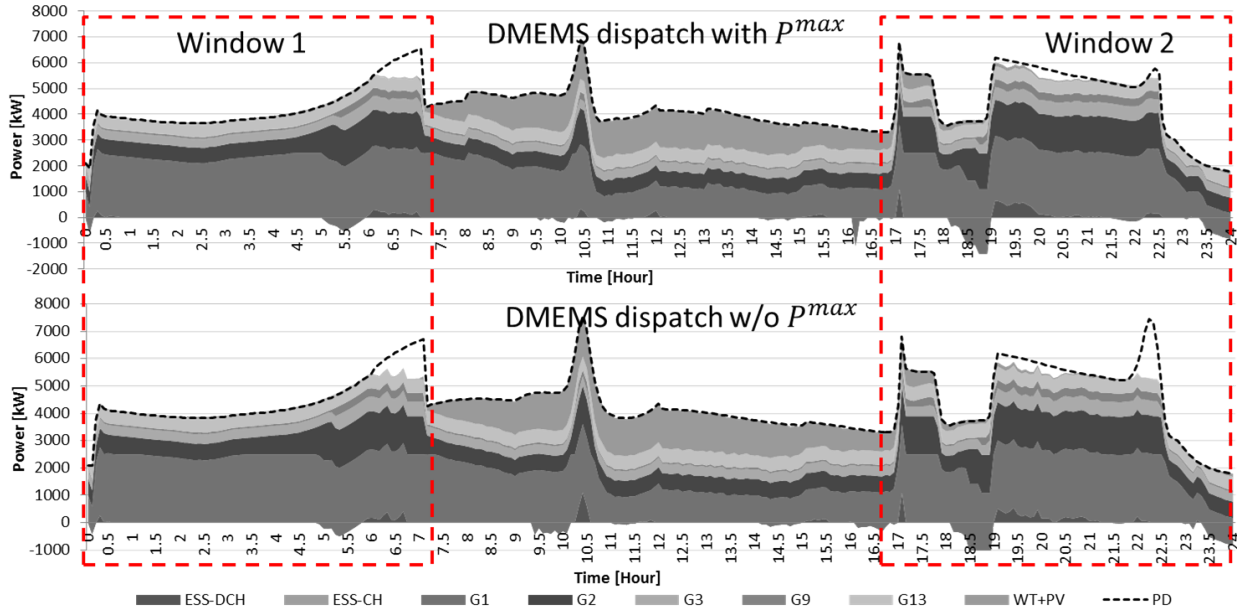

Figure 3.10: Optimal dispatch obtained from the DMEMS approach with and without P^{max}.

Table 3.4: Summary of Results for Deterministic and Stochastic load model.

Load Model	Objective function [$]	Energy served by ESS [kWh]	Total demand [kWh]	Load factor	Peak demand [kW]
Deterministic	19,941	2,416	103,822	0.631	6,851
Stochastic	20,098	2,480	104,626	0.641	6,799

- In Window 1 of Figure 3.9, observe that the ESSs are charged to store energy until hour 6, and are dispatched to meet the high demand between hours 6 and 7. On the other hand, for the DMEMS approach, as shown in Figure 3.10, the demand is not fully met by the DGs and ESSs from hour 6 to 7, thus requiring load curtailment, which is due to the ESSs not being optimally scheduled for charging during off-peak hours.

- In Window 2, between hours 22 to 22.5, a peak demand of 7.4 MW is observed when there is no P^{max} control, because the EHMS shifts its controllable demand to these hours when the TOU price is low. On the other hand, with P^{max} control, the EHMS manages the load demand such that the peak is reduced to 5.8 MW, hence reducing load curtailment significantly.

- When energy is available from RES between hours 7 and 17, the MEMS approach schedules more ESSs charging (Figure 3.9), which are dispatched to meet the demand in Window 2. However, in the DMEMS approach (Figure 3.10), the ESSs are not adequately charged to serve the peak demand, and hence load curtailment is required from hour 19 to 22.5 due to lack of generation from DGs. Even though load curtailment is still needed without P^{max} control in the MEMS approach, it is lower compared to that with the DMEMS framework.

3.4.2 Effect of Uncertainties in the RCLPE Model

As discussed in Section 3.3, there are errors associated with the NN-based smart load model. Therefore, to study the effect of these errors in the proposed dispatch approach, the errors λ_k in the output of the NN-based model are considered in the MEMS, based on the normal pdf obtained from the error histogram shown in Figure 3.5. Note that this pdf approximations overstates the actual error distribution in the model, thus representing a

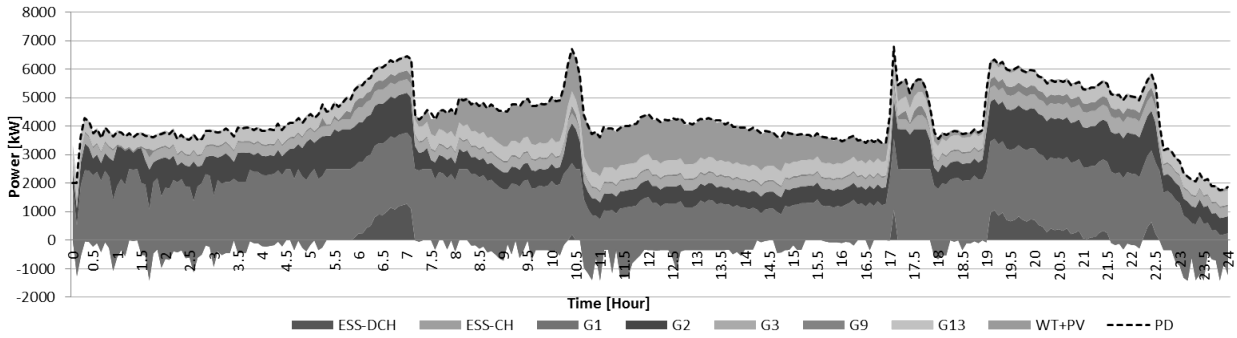

Figure 3.11: Optimal dispatch obtained from the MEMS approach including errors in the estimation of PD^{rc}.

worst case scenario for testing purposes. These errors are applied as a stochastic deviation parameter of the controllable demand as follows:

$$PD_{i,k}^{rc} = \widehat{PD}_{i,k}^{rc}(P_k^{max}) + \lambda_k \tag{3.26}$$

where $\widehat{PD}_{i,k}^{rc}$ represents the deterministic output of the NN model (3.24).

The MEMS model including (3.26) was solved for 100% EHMS loads with P^{max} control for 24 h of operation using the MPC approach, and the obtained results are compared with respect the previously obtained results with a deterministic load model, which does not consider uncertainties in the output of the RCLPE, in Table 3.4. Observe that there is less than 1% changes in the operating cost and peak demand; moreover, the change in the load factor is only 1.5%. Furthermore, from the dispatch solution shown in Figure 3.11, note that there are no significant changes in the dispatch compared to the schedule obtained for the base case with P^{max} control shown in Figure 3.9, showing that errors in the output of the RCLPE have little impact on the dispatch solutions obtained with the proposed MEMS.

3.5 Summary

In this chapter, an NN-based model of an EHMS was presented, to estimates the demand of controllable loads as a function of ambient temperature, TOU prices, time of the day, and peak demand limits. This developed mathematical model was integrated into a proposed comprehensive MEMS model, formulated considering UC operational and network flow

constraints simultaneously. The deviations in the forecast of RES and electricity demand were managed by adopting an MPC approach. To evaluate the proposed MEMS approach, an DMEMS approach was implemented by decomposing the EMS problem into UC and OPF subproblems.

The MEMS and DMEMS techniques were compared on a CIGRE benchmark system, demonstrating that, even though the MEMS method took longer to solve than the DMEMS approach, better overall dispatch results were obtained, with less load curtailment and better use of ESS resources, within feasible computational times for online applications. Furthermore, the solutions obtained with both EMS methodologies considers a smart loads highlighted the advantages of DR schemes, in particular with respect to reduction in peak demand, load curtailment, total costs, and improvements in load factors, demonstrating that the proposed DR scheme enhances the microgrid's load serving capability. Finally, it is shown that undesirable load spikes at low electricity price hours due to customer response can be mitigated with the proposed approach. The main content of this chapter was published in [65] and [66].

Chapter 4

A Practical EMS for Isolated Microgrids

From the measurements in the actual isolated microgrids, it is found that the voltage drops across feeders and the feeder losses are relatively small. Therefore, in this chapter, the need for considering the network is evaluated, in the context of developing practical EMS models for isolated microgrids.

Two practical EMS models are proposed and studied, considering the operational constraints of DERs, active-reactive power balance, unbalanced system configuration and loading, and voltage dependent loads. A novel linearization approach is proposed and validated based on the fact that, for isolated microgrids, due to the characteristics of feeders, network losses and voltage drops across feeders are relatively small. The proposed practical EMS models are compared with a typical decoupled UC and OPF based EMS with and without consideration of system unbalancing. The proposed practical and "standard" EMS models are tested and validated using a CIGRE medium voltage benchmark system and the real isolated microgrid of KLFN in Northern Ontario, Canada. The presented results demonstrate the effectiveness and practicability of the proposed EMS models.

4.1 Proposed Practical EMS Models

In a decoupled UC-OPF problem, it is possible to account for the impact of reactive power supply in the UC decisions when solving the three-phase OPF problem, as proposed in [17]. Thus, if the OPF is infeasible, the commitment decisions of the UC subproblem can be modified by forcing the commitment of the next available cheaper generator. This process is repeated until a feasible OPF solution is obtained that satisfies all system constraints; however, the UC-OPF solution in this case is sub-optimal. Furthermore, a three-phase OPF problem is a complex NLP problem that requires significant computation time. Since isolated microgrids are generally radial networks with relatively short and high-capacity

feeders, these networks do not usually play a significant role in microgrid energy management, as observed from measurements on actual remote microgrids [67]. Therefore, there is a need to reevaluate the representation of the distribution network in EMS models, while considering the need for voltage and reactive power management in the microgrid. Hence, practical EMS models are proposed next, which include detailed three-phase models of DG units, voltage dependent and unbalanced loads, reactive power balance constraints, and UC DER constraints, with and without linear approximations of the feeder equations.

4.1.1 Linearized UC-OPF Model (EMS-1)

The conventional UC-OPF is a complex MINLP optimization model [17], which may be transformed into by an MILP problem by linearizing the non-linear network equations, based on the fact that typical isolated microgrids typically have short-length and high-capacity feeders, and thus bus voltage magnitudes and angles do not change significantly from node to node.

Nodal Power Balance

The demand-supply balance at each bus considers the output from dispatchable generators and non-dispatchable PV and wind generator units, plus the total power demand from commercial and residential customers, taking into account the generation from ESS units. In this case, feeders can be modeled as follows [68]:

$$\vec{V}_{abc,i} = \vec{V}_{abc,j} + \vec{I}_{abc,i,j}\vec{Z}_{abc,i,j} \qquad \forall i,j \tag{4.1}$$

where

$$\vec{I}_{abc,i,j} = (\vec{V}_{abc,i} - \vec{V}_{abc,j})\vec{Y}_{abc,i,j} \qquad \forall i,j$$

$$\vec{Y}_{abc,i,j} = \vec{Z}^{-1}_{abc,i,j} \qquad \forall i,j$$

$$[Y]_{i,j} = \begin{bmatrix} Y^{aa}_{i,j} & Y^{ab}_{i,j} & Y^{ac}_{i,j} \\ Y^{ba}_{i,j} & Y^{bb}_{i,j} & Y^{bc}_{i,j} \\ Y^{ca}_{i,j} & Y^{cb}_{i,j} & Y^{cc}_{i,j} \end{bmatrix} \qquad \forall i,j$$

From these equations, the complex power injection at node i for phase l can be defined as follows:

$$\begin{aligned}\vec{\mathcal{S}}^{*}_{l,i,k} &= \vec{V}^{*}_{l,i,k}\sum_{j}\vec{I}_{l,i,j,k} = \vec{V}^{*}_{l,i,k}\sum_{j}\sum_{m}\vec{Y}^{l,m}_{i,j}(\vec{V}_{m,i,k}-\vec{V}_{m,j,k}) \\ &= \sum_{j,m} Y^{l,m}_{i,j}[V_{l,i,k}V_{m,i,k}e^{\mathrm{j}(\theta^{l,m}_{i,j}+\delta_{m,i,k}-\delta_{l,i,k})} - V_{l,i,k}V_{m,j,k}e^{\mathrm{j}(\theta^{l,m}_{i,j}+\delta_{m,j,k}-\delta_{l,i,k})}] \quad \forall l,i,k \quad (4.2)\end{aligned}$$

Thus, active and reactive power injection at node i for phase l can be obtained as follows:

$$\begin{aligned}&\sum_{g\in G_i} P_{l,g,k} + PV_{l,i,k} + PW_{l,i,k} - PD^{c}_{l,i,k}V^{\alpha^{c}_{k}}_{l,i,k} - PD^{r}_{l,i,k}V^{\alpha^{r}_{k}}_{l,i,k} + P^{LC}_{l,i,k} + \sum_{n\in N_i}(P^{dch}_{l,n,k} - P^{ch}_{l,n,k}) \\ &= \sum_{j,m} V_{l,i,k}Y^{l,m}_{i,j}[V_{m,i,k}\cos(\theta^{l,m}_{i,j}+\delta_{m,i,k}-\delta_{l,i,k}) - V_{m,j,k}\cos(\theta^{l,m}_{i,j}+\delta_{m,j,k}-\delta_{l,i,k})] \quad \forall l,i,k\end{aligned} \quad (4.3)$$

$$\begin{aligned}&\sum_{g\in G_i} Q_{l,g,k} - QD^{c}_{l,i,k}V^{\beta^{c}_{k}}_{l,i,k} - QD^{r}_{l,i,k}V^{\beta^{r}_{k}}_{l,i,k} + K_2P^{LC}_{l,i,k} \\ &= \sum_{j,m} V_{l,i,k}Y^{l,m}_{i,j}[V_{m,i,k}\sin(\theta^{l,m}_{i,j}+\delta_{m,i,k}-\delta_{l,i,k}) - V_{m,j,k}\sin(\theta^{l,m}_{i,j}+\delta_{m,j,k}-\delta_{l,i,k})] \quad \forall l,i,k\end{aligned} \quad (4.4)$$

In order to linearize (4.3) and (4.4), the following assumptions can be made:

- $V = 1+\Delta V$, where ΔV is small, i.e., $\Delta V^2 \approx 0$.
- $\Delta\delta_{i,j} \approx 0$, and thus $\sin(\Delta\delta_{i,j}) \approx \Delta\delta_{i,j}$, and $\cos(\Delta\delta_{i,j}) \approx 1$.
- $\Delta\delta_{l,m} \approx \gamma_{l,m}$, where $\gamma_{a,b} = 120^0, \gamma_{b,c} = 120^0$, and $\gamma_{c,a} = 120^0$.
- $V^{\alpha} \approx 1+\alpha\Delta V$, and $V^{\beta} \approx 1+\beta\Delta V$.

Based on these assumptions, the linearized active and reactive power balance equations can be linearized as follows:

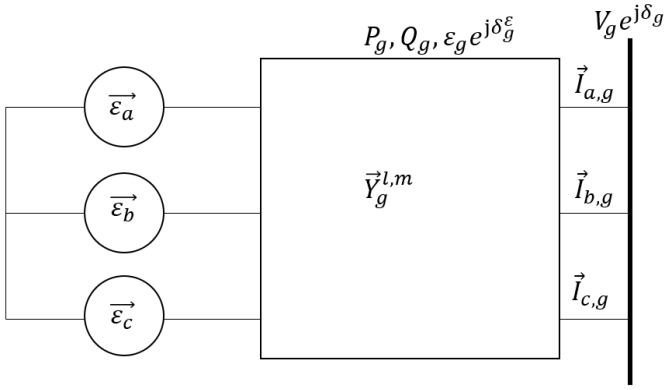

Figure 4.1: Generator model.

$$\begin{aligned}
&\sum_{g\in G_i} P_{l,g,k} + PV_{l,i,k} + PW_{l,i,k} + P^{LC}_{l,i,k} - PD^{c}_{l,i,k}(1+\alpha^{c}_{k}\Delta V_{l,i,k}) \\
&\qquad - PD^{r}_{l,i,k}(1+\alpha^{r}_{k}\Delta V_{l,i,k}) + \sum_{n\in N_i}(P^{dch}_{l,n,k} - P^{ch}_{l,n,k}) \\
&= \sum_{j,m} Y^{l,m}_{i,j}[(\Delta V_{m,i,k} - \Delta V_{m,j,k})\cos(\theta^{l,m}_{i,j} + \gamma_{l,m}) + (\delta_{m,j,k} - \delta_{m,i,k})\sin(\theta^{l,m}_{i,j} + \gamma_{l,m})] \quad \forall l,i,k
\end{aligned} \tag{4.5}$$

$$\begin{aligned}
&\sum_{g\in G_i} Q_{l,g,k} + K_2 P^{LC}_{l,i,k} - QD^{c}_{l,i,k}(1+\beta^{c}_{k}\Delta V_{l,i,k}) - QD^{r}_{l,i,k}(1+\beta^{r}_{k}\Delta V_{l,i,k}) \\
&= -\sum_{j,m} Y^{l,m}_{i,j}[(\Delta V_{m,i,k} - \Delta V_{m,j,k})\sin(\theta^{l,m}_{i,j} + \gamma_{l,m}) - (\delta_{m,j,k} - \delta_{m,i,k})\cos(\theta^{l,m}_{i,j} + \gamma_{l,m})] \quad \forall l,i,k
\end{aligned} \tag{4.6}$$

Generator Constraints

Directly-connected synchronous generators are modeled as a special case of series element as follows:

$$\begin{bmatrix} \vec{\mathcal{E}}_{abc,g,k} \\ \vec{I}_{abc,g,k} \end{bmatrix} = \begin{bmatrix} \mathrm{I} & \vec{Z}_{abc,g,k} \\ 0 & \mathrm{I} \end{bmatrix} \begin{bmatrix} \vec{V}_{abc,g,k} \\ \vec{I}_{abc,g,k} \end{bmatrix} \quad \forall g,k \tag{4.7}$$

where $\vec{\mathcal{E}}_{abc} = \begin{bmatrix}\vec{\mathcal{E}}_a & \vec{\mathcal{E}}_b & \vec{\mathcal{E}}_c\end{bmatrix}^T$. Z_{abc} is the per-phase impedance matrix of the machine, which can be estimated from the sequence impedances of the generator.

$$\vec{I}_{abc,g,k} = (\vec{\mathcal{E}}_{abc,g,k} - \vec{V}_{abc,g,k})\vec{Y}_{abc,g} \qquad \forall g,k \tag{4.8}$$

$$\vec{Y}_{abc,g} = \vec{Z}^{-1}_{abc,g} \qquad \forall g \tag{4.9}$$

$$[Y]_g = \begin{bmatrix} Y_g^{aa} & Y_g^{ab} & Y_g^{ac} \\ Y_g^{ba} & Y_g^{bb} & Y_g^{bc} \\ Y_g^{ca} & Y_g^{cb} & Y_g^{cc} \end{bmatrix} \qquad \forall g \tag{4.10}$$

As per Fig. 4.1, at the generator terminal, the currents in each phase can be determined from (4.8). Hence, the per phase complex power output of the generator can be determined as follows:

$$\begin{aligned}\vec{\mathcal{S}}^*_{l,g,k} &= \vec{V}^*_{l,g,k}\vec{I}_{l,g,k} = \vec{V}^*_{l,g,k}\sum_m \vec{Y}^{l,m}_g(\vec{\mathcal{E}}_{m,g,k} - \vec{V}_{m,g,k}) \\ &= \sum_m Y^{l,m}_g[V_{l,g,k}\mathcal{E}_{m,g,k}e^{\mathrm{j}(\theta^{l,m}_g + \delta^{\mathcal{E}}_{m,g,k} - \delta_{l,g,k})} - V_{l,g,k}V_{m,g,k}e^{\mathrm{j}(\theta^{l,m}_g + \delta_{m,g,k} - \delta_{l,g,k})}] \quad \forall l,g,k\end{aligned} \tag{4.11}$$

The active and negative power outputs can hence be expressed as:

$$P_{l,g,k} = \sum_m V_{l,g,k}Y^{l,m}_g[\mathcal{E}_{m,g,k}\cos(\theta^{l,m}_g + \delta^{\mathcal{E}}_{m,g,k} - \delta_{l,g,k}) - V_{m,g,k}\cos(\theta^{g}_{l,m} + \delta_{m,g,k} - \delta_{l,g,k})] \qquad \forall l,g,k \tag{4.12}$$

$$Q_{l,g,k} = \sum_m V_{l,g,k}Y^{l,m}_g[\mathcal{E}_{m,g,k}\sin(\theta^{l,m}_g + \delta^{\mathcal{E}}_{m,g,k} - \delta_{l,g,k}) - V_{m,g,k}\sin(\theta^{l,m}_g + \delta_{m,g,k} - \delta_{l,g,k})] \qquad \forall l,g,k \tag{4.13}$$

In order to linearize (4.12)-(4.13), one can assume that $V_{l,g,k} = 0.95$ p.u., because in isolated microrids with voltage dependent loads, the UC-OPF procedure will try to minimize the network voltage to reduce demand, thus reducing costs, and hence voltages will be close to their minimum value. Furthermore:

$$\delta^{\mathcal{E}}_{m,g,k} - \delta_{l,g,k} = \delta^{\mathcal{E}}_{m,g,k} - \delta^{\mathcal{E}}_{l,g,k} + \delta^{\mathcal{E}}_{l,g,k} - \delta_{l,g,k} \tag{4.14}$$

where $\delta^{\mathcal{E}}_{m,g,k} - \delta^{\mathcal{E}}_{l,g,k} = \gamma_{l,m}$, and thus:

$$\delta^{\mathcal{E}}_{m,g,k} - \delta_{l,g,k} = \gamma_{l,m} + \delta^{\mathcal{E}}_{l,g,k} - \delta_{l,g,k} = \gamma_{l,m} + \Delta\delta^{\mathcal{E}}_{l,g,k} \tag{4.15}$$

On the other hand, defining the variables $EX_{l,g,k} = \mathcal{E}_{l,g,k}\cos(\Delta\delta^{\mathcal{E}}_{l,g,k})$, and $EY_{l,g,k} = \mathcal{E}_{l,g,k}\sin(\Delta\delta^{\mathcal{E}}_{l,g,k})$, it follows that:

$$\mathcal{E}_{a,g,k} = \mathcal{E}_{b,g,k} = \mathcal{E}_{c,g,k} \qquad \forall g,k \tag{4.16}$$

$$\Delta\delta^{\mathcal{E}}_{a,g,k} \approx \Delta\delta^{\mathcal{E}}_{b,g,k} \approx \Delta\delta^{\mathcal{E}}_{c,g,k} \qquad \forall g,k \tag{4.17}$$

$$EX_{g,k} \approx EX_{a,g,k} \approx EX_{b,g,k} \approx EX_{c,g,k} \qquad \forall g,k \tag{4.18}$$

$$EY_{g,k} \approx EY_{a,g,k} \approx EY_{b,g,k} \approx EY_{c,g,k} \qquad \forall g,k \tag{4.19}$$

Thus, (4.12) and (4.13) can be expressed in linear form as follows:

$$\begin{aligned} P_{l,g,k} \approx \sum_m Y^{l,m}_g [&0.95 EX_{g,k}\cos(\theta^{l,m}_g + \gamma_{l,m}) - 0.95 EY_{g,k}\sin(\theta^{l,m}_g + \gamma_{l,m}) \\ &- (1 + \Delta V_{l,g,k} + \Delta V_{m,g,k})\cos(\theta^{l,m}_g + \gamma_{l,m}) + (\delta_{m,g,k} - \delta_{l,g,k})\sin(\theta^{l,m}_g + \gamma_{l,m})] \quad \forall l,g,k \end{aligned} \tag{4.20}$$

$$\begin{aligned} Q_{l,g,k} \approx -\sum_m Y^{l,m}_g [&0.95 EX_{g,k}\sin(\theta^{l,m}_g + \gamma_{l,m}) + 0.95 EY_{g,k}\cos(\theta^{l,m}_g + \gamma_{l,m}) \\ &- (1 + \Delta V_{l,g,k} + \Delta V_{m,g,k})\sin(\theta^{l,m}_g + \gamma_{l,m}) - (\delta_{m,g,k} - \delta_{l,g,k})\cos(\theta^{l,m}_g + \gamma_{l,m})] \quad \forall l,g,k \end{aligned} \tag{4.21}$$

Objective Function

The objective function representing the cost of the microgrid, including generation costs, start-up and shut-down costs of diesel generators, and high costs for load curtailment can be defined as:

$$\begin{aligned} J = \sum_{g,k} [&(d_g P^2_{g,k}\Delta t_k + e_g P_{g,k} + f_g W_{g,k})\Delta t_k + C^{sup}_g U_{g,k} \\ &+ C^{sdn}_g S_{g,k}] + \sum_{i,k} C^{LC} P^{LC}_{i,k}\Delta t_k \end{aligned} \tag{4.22}$$

Reserve Constraint

The following constraint guarantees that proper spinning reserves for the microgrid are provided by the committed generators:

$$\sum_{g}(\bar{P}_g W_{g,k} - P_{g,k}) \geq R^{sv} \sum_{l,i}[P^{PV}_{l,i,k} + P^{PW}_{l,i,k} + PD^{c}_{l,i,k}(1 + \Delta V_{l,i,k}\alpha^{c}_{k}) + (PD^{r}_{l,i,k})(1 + \Delta V_{l,i,k}\alpha^{r}_{k}) - P^{LC}_{l,i,k}] \quad \forall k \quad (4.23)$$

Generalized UC Constraints

These include limits on active power generation, ramp-up and ramp-down, minimum up-time and down-time constraints, and coordination constraints, as explained in Section 3.1.

ESS

These constraints include the energy balance constraint and constraints to prevent simultaneous charging/discharging, limits on SOC, and charging/discharging power, as follows:

$$SOC_{n,k+\Delta t_k} - SOC_{n,k} = \left(P^{ch}_{n,k}\eta^{ch}_{n} - \frac{P^{dch}_{n,k}}{\eta^{dch}_{n}}\right)\Delta t_k \qquad \forall n,k \qquad (4.24)$$

$$U^{ch}_{n,k} + U^{dch}_{n,k} \leq 1 \qquad \forall n,k \qquad (4.25)$$

$$\underline{SOC}_n \leq SOC_{n,k} \leq \overline{SOC}_n \qquad \forall n,k \qquad (4.26)$$

$$P^{ch}_{n,k} \leq \overline{PESS}_n U^{ch} \qquad \forall n,k \qquad (4.27)$$

$$P^{dch}_{n,k} \leq \overline{PESS}_n U^{dch} \qquad \forall n,k \qquad (4.28)$$

Grid Operational Constraints

This includes the following bus voltage constraint:

$$\underline{\Delta V} \leq \Delta V_{l,i,k} \leq \overline{\Delta V} \qquad \forall l,i,k \qquad (4.29)$$

Current limits are not considered in this model, because the short-length and high-capacity of feeders in isolated microgrids make these limits unnecessary, as demonstrated by the results discussed in the next section. However, these limits could be readily included if required without affecting the linearity of the model.

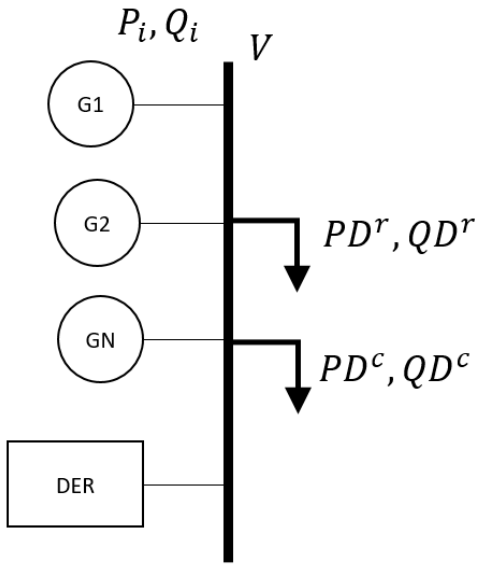

Figure 4.2: Single-node representation of an isolated microgrid.

4.1.2 Linearized UC-OPF Model (EMS-2)

As discussed before, in isolated microgrids, the voltage drop across the feeder and losses in the feeders are not significant, and hence one may assume that all the DERs and loads are basically connected to a single bus, as shown in Figure 4.2. This is consistent with what has been observed in real microgrids, where the feeder capacity is designed to be greater than the maximum system demand, as in case of the Huatacando microgrid in Chile [22], as well as the Bella Coola microgrid [69] and Hartley Bay microgrid [70] in British Columbia, Canada. However, it is necessary to consider unbalanced system loading, voltage dependent loads, and reactive power regulation in general. In this case, the objective function is the same as (4.22), but the model constraints change as discussed next.

Demand-Supply Balance

This constraint ensures that the total generation is equal to the total demand, for each phase, at every time interval, as follows:

$$\sum_{g} P_{l,g,k} + PV_{l,k} + PW_{l,k} + \sum_{n} (P^{dch}_{l,n,k} - P^{ch}_{l,n,k}) = PD^{c}_{l,k} V^{\alpha^{c}_{k}}_{l,k} + PD^{r}_{l,k} V^{\alpha^{r}_{k}}_{l,k} - P^{LC}_{l,k} \quad \forall l, k \quad (4.30)$$

Hence, assuming that $V = 1 + \Delta V$, where ΔV is small, so that it can be approximated by $V^{\alpha} \approx 1 + \alpha \Delta V$, (4.30) can be approximated by:

$$\sum_{g} P_{l,g,k} + PV_{l,k} + PW_{l,k} + \sum_{n \in \mathcal{N}} (P^{dch}_{l,n,k} - P^{ch}_{l,n,k}) \\ \approx PD^{c}_{l,k}(1 + \alpha^{c}_{k} \Delta V_{l,k}) + PD^{r}_{l,k}(1 + \alpha^{r}_{k} \Delta V_{l,k}) - P^{LC}_{l,k} \quad \forall l, k \quad (4.31)$$

Similarly for reactive power balance constraints:

$$\sum_{g} Q_{l,g,k} \approx QD^{c}_{l,k}(1 + \beta^{c}_{k} \Delta V_{l,k}) + QD^{r}_{l,k}(1 + \beta^{r}_{k} \Delta V_{l,k}) - K_2 P^{LC}_{l,k} \quad \forall l, k \quad (4.32)$$

Reserve Constraint

The following constraint guarantees that spinning reserve requirements for the microgrid are provided by the committed generators:

$$\sum_{g} \left(\bar{P}_g W_{g,k} - \sum_{l} P_{l,g,k} \right) \\ \geq R^{sv} \sum_{l} [PD^{c}_{l,k}(1 + \alpha^{c}_{k} \Delta V_{l,k}) + PD^{r}_{l,k}(1 + \alpha^{r}_{k} \Delta V_{l,k}) - P^{LC}_{l,k} + PV_{l,k} + PW_{l,k}] \forall k \quad (4.33)$$

Other Constraints

In addition to the above, the generator model (4.20)-(4.21), generalized UC constraints, ESS constraints, and voltage limit constraints defined for the EMS-1 model are also considered in this model.

In order to capture the deviations in forecast of RES and demand, the forecasts are updated at every time step implementing an MPC technique with a recalculation time of 5 min and a 24 h time horizon, as discussed in Section 3.2.3. The practical EMS models proposed here are MIQP problems, and are solved using the CPLEX solver in GAMS [56], on an Intel® Xeon® CPU L7555, 1.87 GHz 4-processor server. The UC subproblem of the decoupled UC-OPF model is also an MIQP problem solved with CPLEX, while the OPF subproblem is an NLP problem solved using the SNOPT solver [56], [59].

4.2 Results and Discussions

In order to evaluate the accuracy of the proposed practical EMS models, a power flow problem is solved using the generator dispatch obtained from these models and including slack active power ΔP and reactive power ΔQ variables at each node; the sum of these slack variables, for each EMS model, yield a total measure of the power flow accuracy of the linearized model. The same forecasting approach explained in Section 3.4 was used here to simulate the real application of the proposed models, and the real-time operation of the microgrid, considering the dispatch schedule obtained, is also evaluated by solving a three-phase power flow problem using the actual, i.e., not forcasted, demand and renewable generation, with the internal voltage angle and magnitude being kept fixed for the generator controlling the system frequency (slack bus), and fixed active and reactive power outputs for the rest of the DERs. Based on the change of power in the slack generator for this power flow problem, the actual microgrid operating costs can be calculated and compared for all EMS models.

The developed dispatch models are tested and validated on a modified CIGRE benchmark system [17], and on the real Northern Ontario-Canada isolated microgrid of KLFN to evaluate their practical application.

4.2.1 CIGRE Benchmark System

The same modified CIGRE benchmark system with 25% more ESS capacity used in Section 3.4, shown in Figure 3.6, is also used here to test and validate the proposed EMS models. The dispatch models are simulated for 24 h of operation with an MPC recalculation time of 5 min. For comparison purposes, four different EMS models are considered: EMS-1 (Case I), EMS-2 (Case II), unbalanced decoupled UC-OPF (Case III), and balanced decoupled UC-OPF (Case IV). It is assumed that generator G1 is responsible for frequency control because of its large capacity.

Table 4.1 presents a summary of results obtained for all the EMS models. The values of ΔP and ΔQ are presented in % of the total demand, and the maximum observed errors over the 24 h period are shown. Observe that the EMS-1 model (Case I) yields the least operating cost dispatch, with maximum errors in active and reactive power injection of 0.6% and 3%, respectively. The EMS-2 model (Case II) yields a solution with larger errors as compared to Case I, at lower computational costs, as expected. It is important to note that the dispatch solutions obtained from the decoupled UC-OPF with and without the unbalanced condition, i.e., Case III and Case IV, respectively, resulted in higher estimated

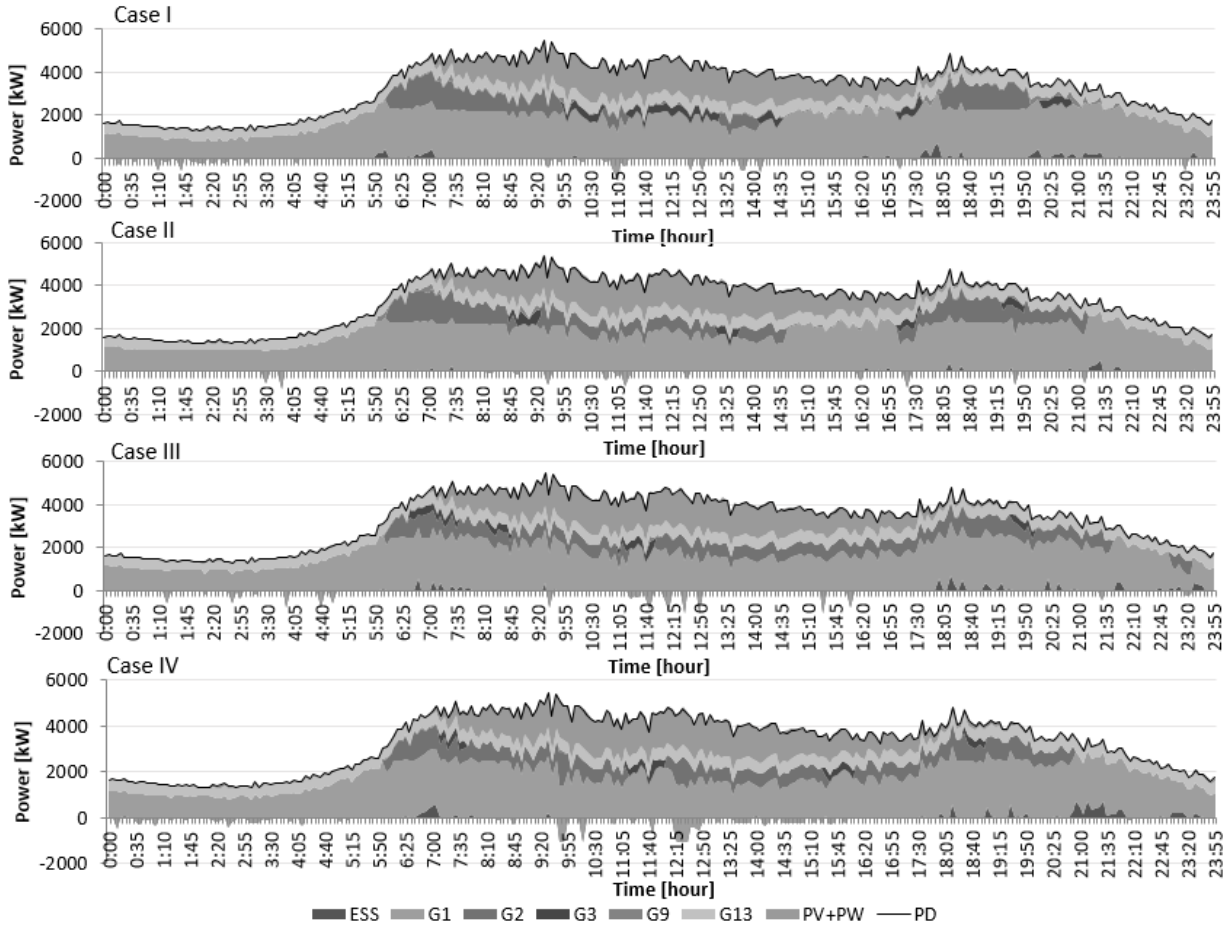

Figure 4.3: Dispatch for all four EMS cases for the CIGRE test system.

Table 4.1: Summary of Results for CIGRE system

Case	EMS Operating Cost [$]	Actual Operating Cost [$]	Max. ΔP [%]	Max. ΔQ [%]	Total Computation Time [s]
I	12,775	12,750	0.6	3	10,800
II	12,828	12,705	1.1	6	2,760
III	13,037	12,975	0	0	18,600
IV	12,970	12,907	3.6	4.12	9,960

and acutal operating costs as compared to the proposed practical EMS models, at much higher computational costs, as expected. The power flow errors in Case IV are due to the fact that a balanced power flow model was used in the dispatch solution, but the system is in fact unbalanced. None of the feeders reached their current capacity limits.

Figure 4.3 presents the plots of dispatch for all the models considering the modified CIGRE test system. Note that G1 and G13 are committed for the entire 24 hour operating horizon, in all cases. However, during hours 15-17, G9 is committed in Cases I and II in order to meet the reactive power requirements, since it has a low minimum generation limit, but has a high operating cost. On the other hand, in Cases III and IV, G2 or G3 replace G9 during hours 15-17, because these are the next available cheaper units; however, this results in higher operating costs overall, thus showing that the proposed practical EMS methods yield more optimal solutions than the decoupled UC-OPF approaches. The latter is due to the fact that the decoupling and NLP OPF subproblem in the UC-OPF models yield sub-optimal solutions, while the EMS-1 and -2 are more optimal because of the coupling of UC and OPF, and the MIQP mathematical modeling.

4.2.2 Kasabonika Lake First Nation System

The KLFN system model used, shown in Figure 4.4, with DER and feeder data given in Appendix B, allows to evaluate the performance of the proposed EMS models in a real existing microgrid in a Northern Canada. The measured generation data from existing 12.4 kW roof-top PV panels and 30 kW wind turbines are used in these simulations. A solar PV plant of 250 kW, as shown in Figure 4.4, will be installed at Bus 3; however, in this work, this plant is not considered, as it is not yet installed, and it is not needed to demonstrate the effectiveness of the proposed EMS models. There are 3 diesel units, operated one at a time as per the utility's dispatch rules, with the largest unit being of 1.5 MW capacity. The commercial demand is represented by the data measured from the Store (STR), the School (SCL), the Police Station (PLC), the Nurse Station (NRS), and the Water Treatment Plant (WTP). The total residential demand at an hour is calculated from the measured total generation net of the total commercial demand, assuming that losses are not really significant in this microgrid, given the length and capacity of the feeders. Note that a 100% unbalance condition is considered, where load on one phase is twice the load in the other two phases, as is the actual case during the summer months for two phases; hence, the assumed unbalancing represents a more extreme condition than in the actual system.

Table 4.2 presents the summary of results obtained from the EMS models for the KLFN system. Observe that, similarly to the CIGRE test system, the EMS-1 model provides the

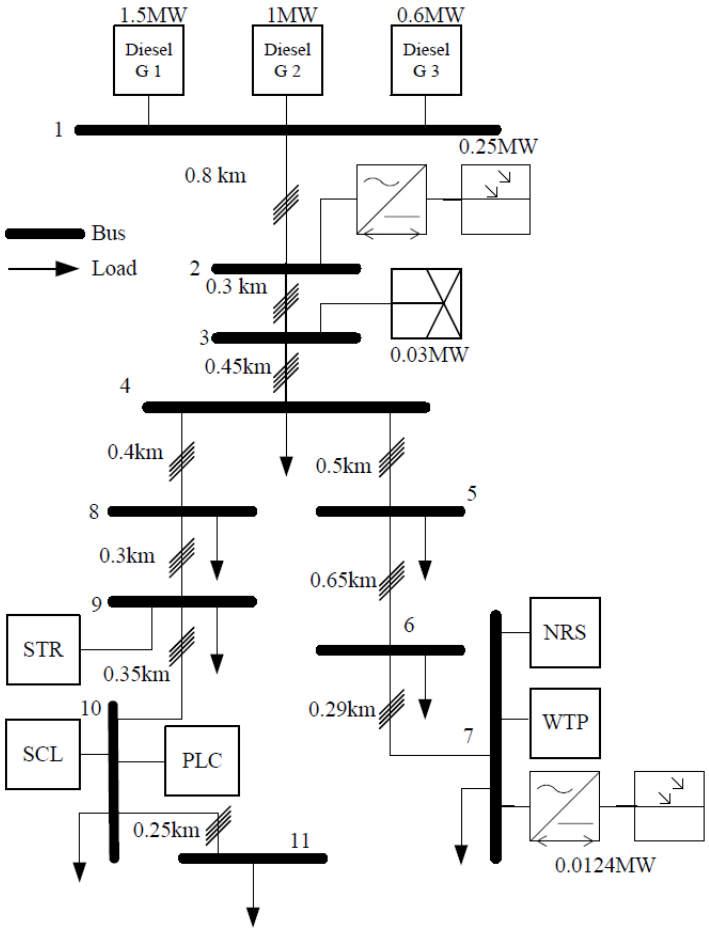

Figure 4.4: Kasabonika Lake First Nation system.

Table 4.2: Summary of Results for KLFN system

Case	EMS Operating Cost [$]	Actual Operating Cost [$]	Max. ΔP [%]	Max. ΔQ [%]	Total Computation Time [s]
I	12,928	12,863	0.24	0	13,000
II	12,979	12,958	0.25	0	1,980
III	14,457	14,415	0	0	5,640
IV	14,452	14,573	17	25	5,660

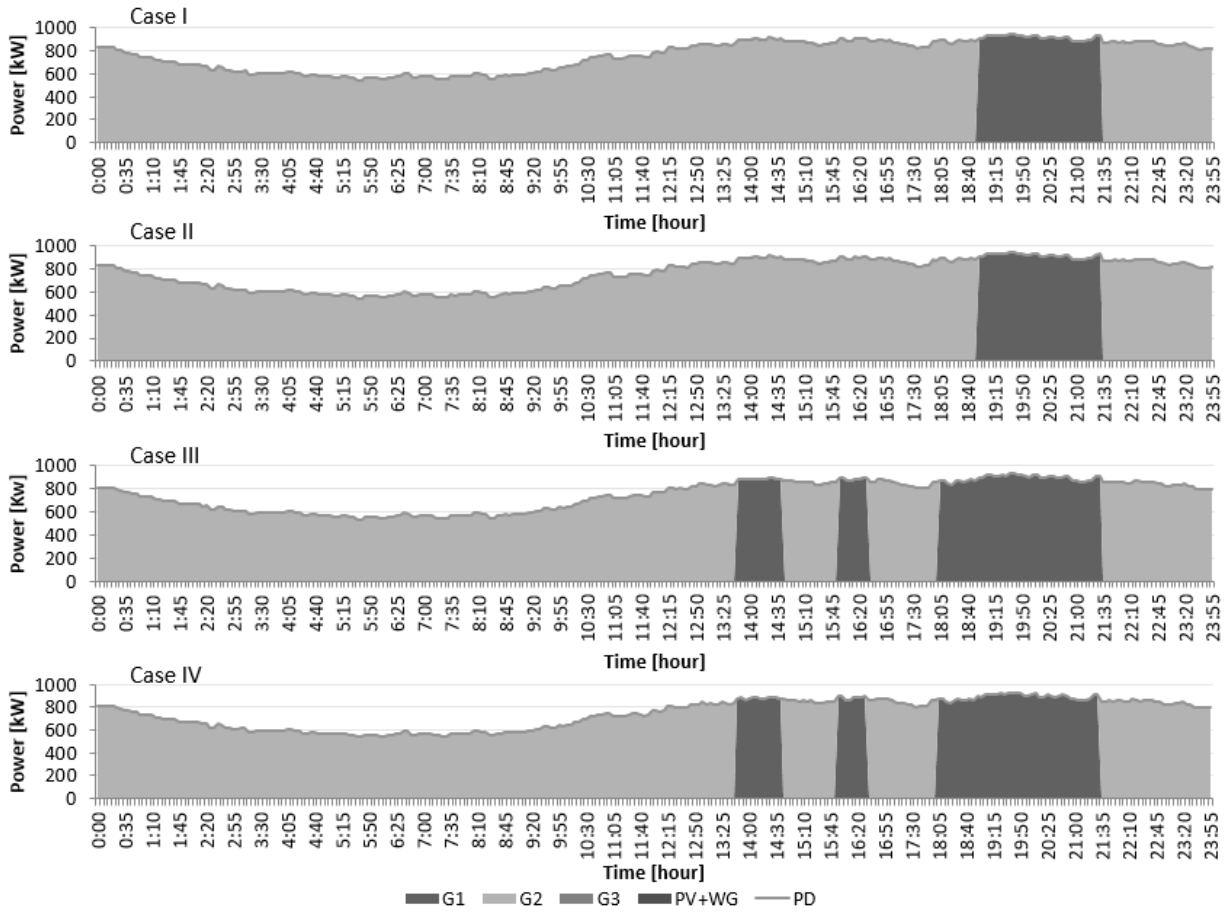

Figure 4.5: Dispatch for all cases for the KLFN system.

least cost dispatch, with the EMS-2 following closely, with negligible values of ΔP and ΔQ in both cases. The latter can be attributed to the relatively smaller system size of KLFN microgrid as compared to the CIGRE microgrid; this is also the reason for the low computational burden of Cases III and IV. Note that there is a significant difference of around 10% in the operating costs of the practical EMS models Cases I and II with the decoupled UC-OPF models (Cases III and IV). Observe also that in spite of the 100% unbalanced condition, there is no significant difference in operating costs between Case III and Case IV, since only one generator is dispatched at a time, with negligible differences in the generator active power output between the two cases.

Figure 4.5 depicts the stacked area plot of the calculated dispatch considering each of

the EMS models for KLFN system. There were only two main generators participating in the dispatch, G1 and G2, with G1 operating during the peak hours only. For the practical EMS models (Cases I and II), G1 was dispatched only during hours 19-22 while for the decoupled UC-OPF models (Cases III and IV), G1 was dispatched during hours 14, 16, and 18-22, since the UC subproblems in the decomposed EMS approach (Cases III and IV) do not consider voltage dependency of the loads, thus committing more capacity. Generator G1 mostly operates near its minimum generation limit, which is the least efficient operating point of the generator; therefore, there is significant difference in the operating cost in Cases I and II compared to Cases III and IV.

4.3 Summary

In this chapter, two novel and practical EMS models were proposed by linearizing UC-OPF models with and without the grid, and considering DER operational constraints, active-reactive power balance, voltage-dependent loads, and unbalanced system condtions. Furthermore, the decoupled UC-OPF models were studied both with and without considering unbalanced loading. All the EMS models were tested and validated using a modified CIGRE benchmark system, highlighting the benefits of the proposed practical EMS models in terms of reduction in operating costs by more efficiently dispatching the system units, at reduced computational costs. Additionally, the EMS models were tested and validated on the KLFN isolated microgrid, showing that a significant reduction in operating costs with accurate and realistic dispatch can be obtained with the proposed practical EMS models.

The results show that approximating the network is a valid approach for isolated microgrids, as the power flow errors are relatively low. Thus, the proposed practical EMS model with a single node approximation of the system is shown to yield reasonable results, while considering voltage-dependent loads, active-reactive power management, and unbalanced system conditions, and hence should the preferred approach for EMS applications in practice. Note that in practice, a simple linear UC approach is used for generators dispatch, which yields significant network error and high-cost dispatches; therefore, the proposed EMS method could be a better dispatch approach for isolated microgrid in practice. The main content of this chapter has been submitted for publication in [71].

Chapter 5

Modeling and Impact of Electric Thermal Storage Systems

In this chapter, a mathematical model of the ETS system is developed and integrated into an EMS for isolated microgrids, using a decoupled UC-OPF EMS approach, to dispatch fossil-fuel-based generators, ESS, and ETS charging. The proposed ETS-EMS framework is tested and studied on a modified CIGRE medium voltage benchmark system, which comprises various kinds of DERs, and on the real KLFN isolated microgrid system. It is shown that the ETS significantly reduces operating costs, and allows for better integration of intermittent wind and solar sources.

5.1 Mathematical Modeling

5.1.1 Electric Thermal Storage System Model

The schematic of house heating with an ETS system is depicted in Fig. 5.1. The thermal demand of the house is estimated based on the ambient temperature T^0 and the temperature set point T_s, using the Smart Residential Load Simulator (SRLS) [72], [73]. As discussed in Section 2.5, an ETS system comprises an electric heating element that converts the electric input $P^{ETS^{EL}}$ into thermal output $P^{ETS^{TH}}$, which is stored in high density bricks [52]. The estimated thermal demand P_s^{TH} obtained using the SRLS is considered as the thermal discharge set point for the ETS. The ETS system discharges the stored thermal energy to meet the thermal demand of the house P^{TH}. In steady state, P^{TH} would be equal to P_s^{TH}, with P^{TH} representing the thermal demand of typical Northern community households in the equations given next.

For the model of the ETS system, the following discrete time equations are used:

$$E_{k+1}^{ETS} = E_k^{ETS} + (P_k^{ETS^{TH}} - P_k^{TH})\Delta t_k - L_k^{ETS^{TH}} \quad \forall k \tag{5.1}$$

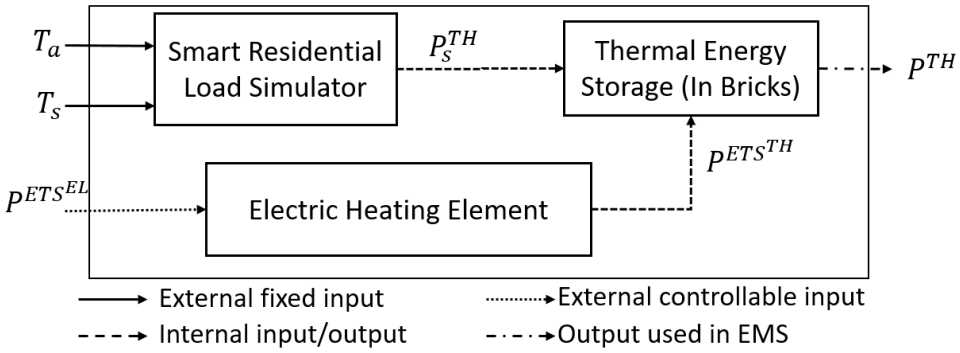

Figure 5.1: Schematic of room heating with ETS system.

where:

$$L_k^{ETS^{TH}} \geq (1-\eta_S)E_k^{ETS}\Delta t_k - P_k^{TH}\Delta t_k \forall k \in \{\mathcal{T}\colon (1-\eta_S)\bar{E}^{ETS} \geq \underline{P}^{TH}\} \tag{5.2}$$

$$L_k^{ETS^{TH}} \geq 0 \qquad \forall k \in \{\mathcal{T}\colon (1-\eta_S)\bar{E}^{ETS} \geq \underline{P}^{TH}\} \tag{5.3}$$

$$L_k^{ETS^{TH}} = 0 \qquad \forall k \in \{\mathcal{T}\colon (1-\eta_S)\bar{E}^{ETS} \leq \underline{P}^{TH}\} \tag{5.4}$$

Note here that the self-discharge of the ETS is described by $(1-\eta_S)E_k^{ETS}$, while $L_k^{ETS^{TH}}$ represents the effective self-discharge of the system. Since the thermal demand P^{TH} is estimated considering the room temperature to be the same as the temperature set point, when thermal demand is higher than the self-discharge $(1-\eta_S)E_k^{ETS}$, P^{TH} will be the same as the sum of the thermal discharge and self-discharge of the ETS. Thus, the effective self-discharge of ETS $L_k^{ETS^{TH}}$ is zero, as in (5.4). However, when P_k^{TH} is less than $(1-\eta_S)E_k^{ETS}$, $L_k^{ETS^{TH}}$ will be greater than zero, as in (5.3), and can be calculated using (5.2).

The conversion from electric to thermal power that is fed into the thermal energy storage can be defined as follows:

$$P_k^{ETS^{TH}} = \eta_{ETS} P_k^{ETS^{EL}} \qquad \forall k \tag{5.5}$$

$$E_k^{ETS} \leq \bar{E}^{ETS} \qquad \forall k \tag{5.6}$$

$$P_k^{ETS^{EL}} \leq \bar{P}^{ETS^{EL}} \qquad \forall k \tag{5.7}$$

5.1.2 Microgrid EMS Model with ETS

The widely used approach of decomposing the EMS problem into UC and OPF subproblems, is used here to obtain efficient solutions suitable for online applications, as discussed in Section 3.2.1. The mathematical models of the UC and OPF subproblems are discussed next.

UC Subproblem

The objective function of this subproblem is to minimize the operating cost of the microgrid, including generation costs, start-up and shut-down costs of diesel generators, costs of the ETS effective losses, and the significantly high costs associated with load curtailment, and can be defined as follows:

$$J = \sum_{g,k}[(d_g P_{g,k}^2 \Delta t_k + e_g P_{g,k} + f_g W_{g,k})\Delta t_k + C_g^{sup} U_{g,k} + C_g^{sdn} S_{g,k}] + \sum_{i,k}[C^{LC} P_{i,k}^{LC} \Delta t_k + \chi_i \mu_i C^L L_k^{ETS^{TH}}] \quad (5.8)$$

where x_i represents the number of electric heating units at Bus i, while μ_i denotes % share of electric heating replaced by ETS at Bus i.

The model constraints are the following:

- *Demand-Supply Balance:* This constraint ensures that the total generation is equal to the total power demand at every time interval:

$$\sum_g P_{g,k} + \sum_i (PV_{i,k} + PW_{i,k}) + \sum_n (P_{n,k}^{dch} - P_{n,k}^{ch}) = \sum_i [PD_{i,k}^r + PD_{i,k}^c + \chi_i \mu_i P_k^{ETS^{EL}} + \chi_i (1-\mu_i) P_k^{TH} - P_{i,k}^{LC}] \quad \forall k \quad (5.9)$$

- *Reserve Constraint:* The following constraint guarantees that spinning reserve requirements for the microgrid are provided by the committed generators:

$$\sum_g (\bar{P}_g W_{g,k} - P_{g,k}) \geq R^{sv} \sum_i [PD_{i,k}^r + PD_{i,k}^c + \chi_i \mu_i P_k^{ETS^{EL}} + \chi_i (1-\mu_i) P_k^{TH} - P_{i,k}^{LC} + PV_{i,k} + PW_{i,k}] \quad \forall k \quad (5.10)$$

- *Generalized UC Constraints:* These constraints represent active power generation, ramp-up and ramp-down, minimum up-time and down-time limits, and coordination constraints, as discussed in Section 3.1.

- *Energy Storage System:* The following ESS constraints include the energy balance constraint (4.24) and constraints to prevent simultaneous charging/discharging (4.25), limits on SOC (4.26), and charging/discharging power (4.27) and (4.28).

- *Electric Thermal Storage:* The ETS constraints include the energy balance equations (5.1)-(5.5), and the limits on stored energy and charging power (5.6) and (5.7).

OPF Subproblem

This subproblem objective function is the minimization of the operating cost of the microgrid, subject to active and reactive power balance constraints at each node, limits on active and reactive power generation of the controllable DERs, ESS constraints, ETS constraints (5.1)-(5.7), and other grid operating constraints such as bus voltage limits. The objective function and constraints of the OPF are presented next.

- *Objective Function:* The objective is to minimize the operating cost of the microgrid, including generation costs and costs associated with load curtailment and ETS effective losses, as follows:

$$J = \sum_{g,k}[(d_g P_{g,k}^2 \Delta t_k + e_g P_{g,k} + f_g \widehat{W}_{g,k})\Delta t_k + C_g^{sup}\widehat{U}_{g,k} + C_g^{sdn}\widehat{S}_{g,k}] + \sum_{i,k}[C^{LC} P_{i,k}^{LC} \Delta t_k + \chi_i \mu_i C^L L_k^{ETS^{TH}}] \quad (5.11)$$

- *Power Balance:* The following power balance equation at each bus considers the output from DG, PV and wind units, and the total power demand of loads from commercial and residential customers, taking into account ESS charging and dis-

charging, and ETS charging:

$$\sum_{g\in G_i} P_{g,k} + PV_{i,k} + PW_{i,k} + \chi_i \mu_i P_k^{ETS_{EL}} + \chi_i(1-\mu_i)P_k^{TH} - PD_{i,k}^c V_{i,k}^{\alpha_k^c} - [PD_{i,k}^r - P_{i,k}^{LC}]V_{i,k}^{\alpha_k^r} + \sum_{n\in N_i}(P_{n,k}^{dch} - P_{n,k}^{ch}) = \sum_j V_{i,k}V_{j,k}Y_{i,j}\cos(\theta_{i,j}+\delta_{j,k}-\delta_{i,k}), \forall k,i,j \quad (5.12)$$

$$\sum_{g\in G_i} Q_{g,k} - QD_{i,k}^c V_{i,k}^{\beta_k^c} - (QD_{i,k}^r - K_2 P_{i,k}^{LC})V_{i,k}^{\beta_k^r} + \sum_{n\in N_i}(QC_{n,k}) = -\sum_j V_{i,k}V_{j,k}Y_{i,j}\sin(\theta_{i,j}+\delta_{j,k}-\delta_{i,k}) \quad \forall k,i,j \quad (5.13)$$

Here, residential and commercial loads are modeled as exponential functions of voltage.

- *Reserve Constraint:* Even though the commitment decisions of DERs are obtained from the UC subproblem considering spinning reserves, reserve constraints still need be included in the OPF subproblem to ensure proper operating margins. Thus, equation (5.10) is modified in the OPF as follows:

$$\sum_g(\bar{P}_g - P_{g,k})\widehat{W}_{g,k} \geq R^{sv}\sum_i[PV_{i,k} + PW_{i,k} + PD_{i,k}^c V_{i,k}^{\alpha_k^c} + \chi_i\mu_i P_k^{ETS} + \chi_i(1-\mu_i)P_k^{TH} + (PD_{i,k}^r - P_{i,k}^{LC})V_{i,k}^{\alpha_k^r}] \quad \forall k \quad (5.14)$$

  Note that $\widehat{W}_{g,k}$ in (5.14) denotes the optimal UC decisions which are applied in the OPF as fixed parameters.

- *Grid Operational Constraints:* These include (3.5)-(3.8), (3.18), and (3.19) with the binary variables $W_{g,k}, U_{g,k}$ and $S_{g,k}$ obtained from the UC solution being same treated as parameters $\widehat{W}_{g,k}, \widehat{U}_{g,k}$ and $\widehat{S}_{g,k}$. These constraints impose limits on active/reactive power generation and voltage at each node, plus feeder current limits.

- *Energy Storage System:* The ESS constraints are (3.13) to (3.17).

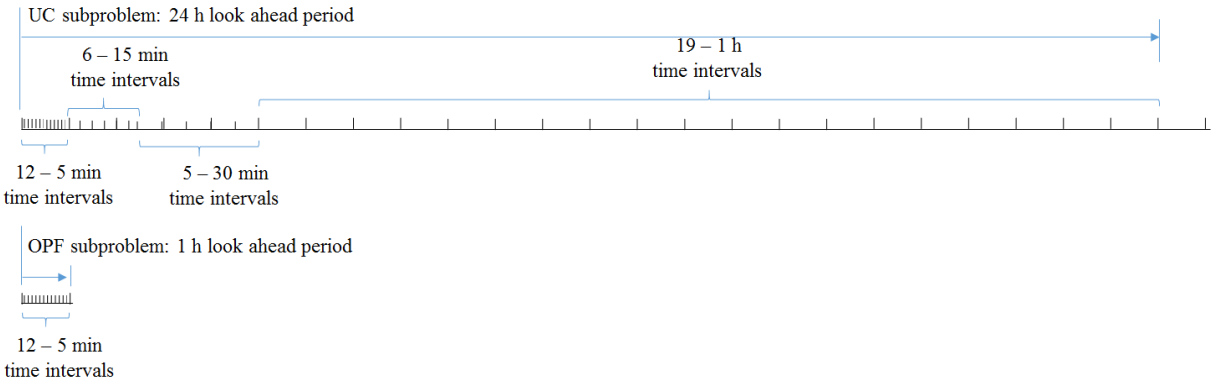

Figure 5.2: MPC time horizons.

5.2 Results and Discussions

In order to account for the deviations in the forecast of the RES and demand, an MPC technique is used with recalculation time of 5 min and time horizons as shown in Figure 5.2, as discussed in Section 3.2.3. The EMS model is coded in GAMS [59], with the UC subproblem being an MIQP problem solved using the CPLEX solver [56], in which the maximum absolute relative gap is set at 1%, which corresponds to a maximum difference of 1% between the best possible integer solution and the global optimal non-integer solution. The OPF subproblem is an NLP problem solved using the SNOPT solver.

The developed ETS-EMS model is tested and validated using the modified CIGRE benchmark system, shown in Figure 3.6. The model is also tested on the real isolated microgrid of KLFN shown in Figure 4.4 to evaluate the practical application and possible actual benefits of ETS. The MPC based ETS-EMS approach is simulated on both systems for 6 days, from January 25 to 30, 2015, considering the same ambient temperature profile for both test systems (KLFN data from [74] was used). The demand, wind, and solar profiles for the KLFN system are real measured data, while for the modified CIGRE test system these data are provided in [17] for a single day, which are then perturbed considering normal pdfs to simulate different days. To simulate forecast errors, normal pdfs were used to perturb the actual profiles, as discussed in Section 3.4. The ETS system self-discharge rate $(1-\eta_S)$ used for these studies is 0.2 %/h [38].

Table 5.1: Summary of Results for CIGRE system

Case	Operating Cost of Microgrid	Peak Demand	Energy Curtailed	Dispatch Share [%]	
	[$]	[MW]	[kWh]	ESS	G3
I	148,718	6.76	293	1.4	4
II	117,136	6.43	0	0.5	2.6
III	116,735	6.47	0	0.34	1.9

5.2.1 CIGRE Benchmark System

For the presented studies, 50% of the total residential demand is assumed to be electric heating demand [75]. The electric heating demand profile is obtained by using the Smart Residential Load Simulator [72], [73], considering typical parameters of detached single houses in Canada [76].

The following three cases are analyzed:

- Case I: No ETS system.
- Case II: 50% of the electric heating demand is provided by ETS.
- Case III: 100% of the electric heating demand is provided by ETS.

Table 5.1 presents a summary of the results for all cases for the modified CIGRE benchmark system. Observe that there is a significant difference in the operating cost of the microgrid between Case I and the other two cases, where electric heating is provided by the ETS system, because of the load curtailment required in Case I. Thus, with the introduction of ETS systems, the peak demand is reduced by 4.9% and 4.3% in Cases II and III, respectively. Observe that the share of energy supplied by the ESS and the most expensive generator (G3) in the total energy dispatch is reduced significantly from Case I to Case III, which further reduces the operating costs, and demonstrates the diminishing role of ESS when ETS is introduced. It should be mentioned that for this benchmark system, the feeder current limits were enforced but did not become active.

Figure 5.3 presents stacked-area plots of the optimal dispatch for the first day obtained for all the cases considered. The negative areas in these plots correspond to the charging of the ESS, and the dark grey line depicts the total demand including electric heating. The black dotted line denotes the total demand including the electric heating load and including

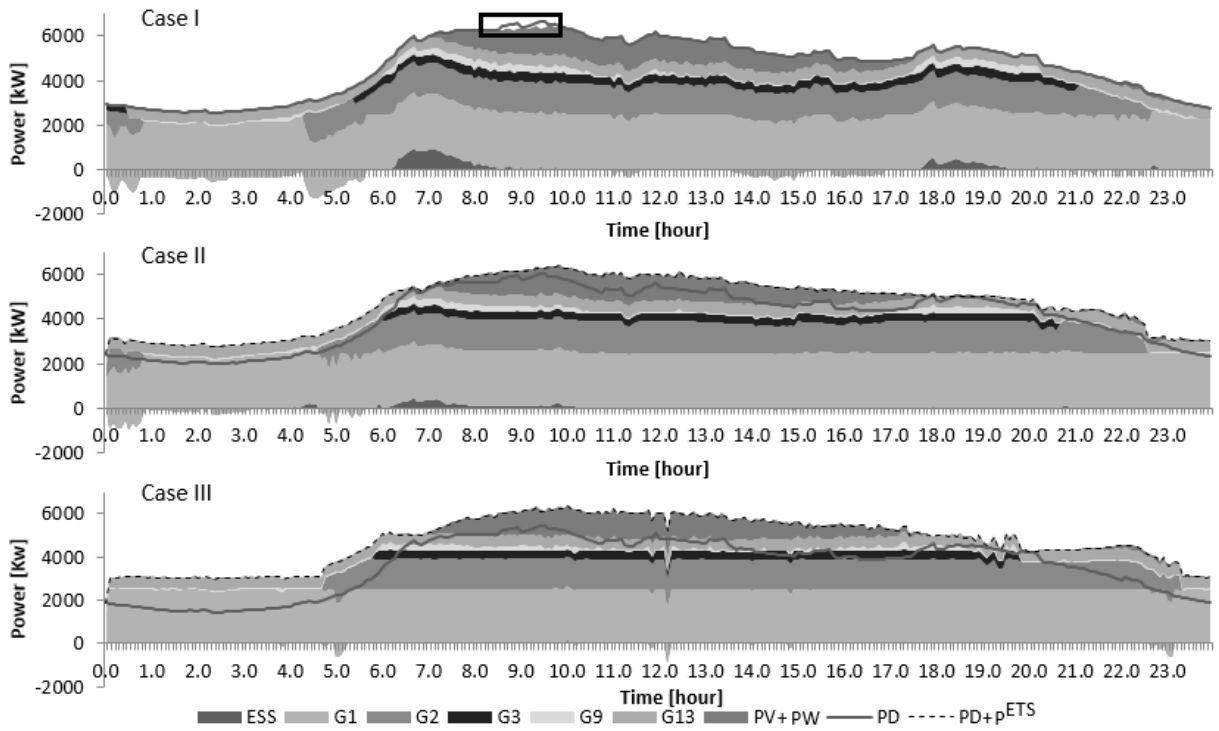

Figure 5.3: Dispatch for all three cases for the CIGRE test system.

the ETS charging power. Finally, the white area below the demand line corresponds to load curtailment. The following can be observed in these plots:

- In Case I, load curtailment during hours 9 and 10 takes place due to insufficient generation capacity.
- In Case II, a significant reduction in use of ESS can be observed due to the introduction of the ETS systems. In Case III, the use of ESS is almost negligible.
- With the introduction of ETS system, the use of the most expensive generator G3 is reduced. Thus, in Case I, the share of G3 in the dispatch is 4%, which is reduced to 2.6% in Case II and further reduced to 1.9% in Case III.

Figure 5.4 depicts the ETS charging power, the ETS energy levels, and the thermal demand for Case III. Note that in the time Windows 1 and 5, the ETS is charged during the off-peak hours, while in on-peak hours in Windows 2 and 4, the ETS is not charged,

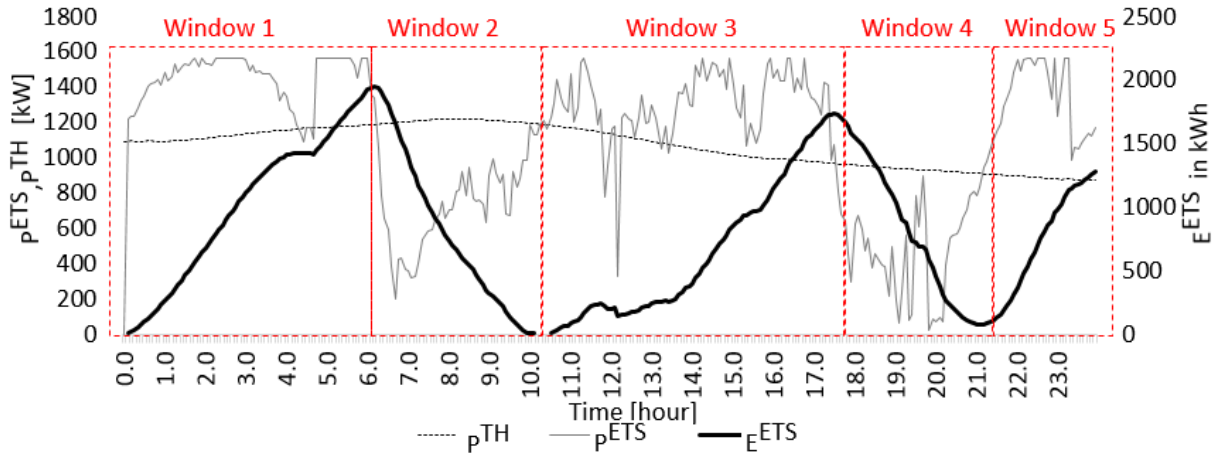

Figure 5.4: ETS charging power and energy, and thermal demand for the CIGRE test system.

using the stored energy to meet the thermal demand. In Window 3, when energy from RES is available, the ETS is charged again. This matches the dispatch and use of ETS discussed in [38].

5.2.2 Kasabonika Lake First Nation System

The KLFN system model used here allows to evaluate the potential contribution of ETS systems in a real existing Northern community microgrid. As the KLFN community is planning to build a new 250 kW PV plant, the system is analyzed with and without this solar plant, considering feeder current limits, to study the impact of ETS on RES integration.

In this system, 30% of the total residential electricity demand is assumed to be from electric heating demand [77]. The electric heating demand profile is obtained in this work using the Smart Residential Load Simulator [72], [73], considering parameters of a typical KLFN house and measured ambient temperature data [74].

As in the CIGRE system, the following three cases are analyzed:

- Case I: No ETS system.
- Case II: 50% of the electric heating demand replaced by ETS.

Table 5.2: Summary of Results for KLFN system

250 kW PV Plant	Case	Operating Cost of Microgrid	Peak Demand	Total ON Time [h]	
		[$]	[kW]	G2	G3
No	I	45,724	771	97	47
	II	43,574	734	89	55
	III	40,220	790	73	71
Yes	I	42,632	771	90	54
	II	36,710	725	65	79
	III	32,898	772	49	95

- Case III: 100% of the electric heating demand replaced by ETS.

Table 5.2 shows the results for all these cases, with and without the 250 kW PV plant. Note the significant reduction in operating costs by increasing the penetration of ETS in both scenarios; then, without the PV plant, the maximum cost reduction is 12%, and with the PV plant, a cost reduction of up to 22.8% is possible. Observe that the peak demand is not reduced in this system, which, however, is only around 50% of the maximum capacity of the system. As with the modified CIGRE benchmark system, feeder current limits were not reached, given that the feeder capacities are typically designed to be larger than the system peak demand in remote microgrids, as discussed in Section 4.1.1.

In Figures 5.5 and 5.6, the stacked-area plots of the optimal dispatch obtained for all the cases and both scenarios of PV plant are depicted for the first day. The following observations can be made:

- The demand can be met by one of the two smaller generators at all times, since in the considered days, the demand was not high enough to dispatch the new 1.5 MW generator G1.
- With the increase of ETS penetration, the total time G3 is ON increases (see Table 5.2), which highlights the efficient operation of generators, since G3 operates near its maximum capacity with increased ON time, so that the total ON time of G2, which operates at low efficient operating point due to low demand compared to its capacity, is decreased.
- Because of inclusion of ETS when the system has no significant penetration of renewable power, generators G2 and G3 operate about the same amount of time, near

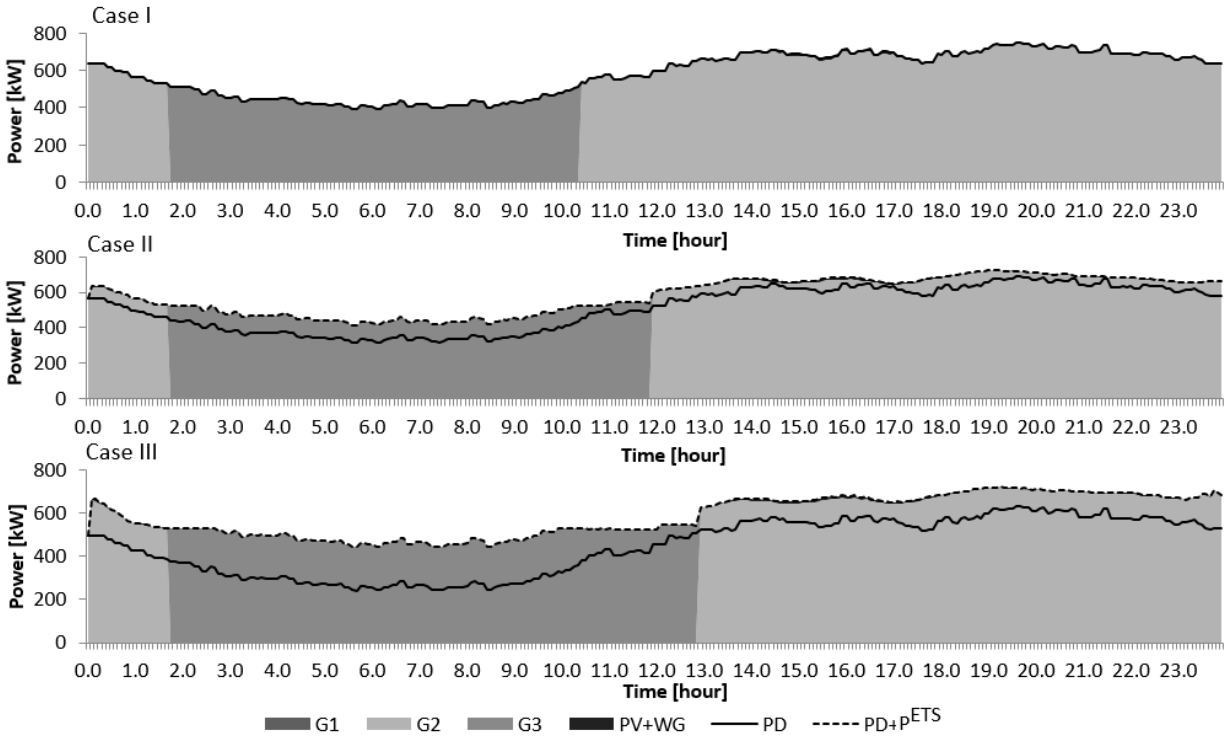

Figure 5.5: Dispatch for all cases for the KLFN system without 250 kW PV plant.

their optimal operating point. As the PV power penetration is increased, the smaller generator is used more, as expected [77].

To analyze the reduction of cost with respect to ETS penetration, the share of ETS is increased from 0% to 100% in steps of 10% in the scenario with the 250 kW PV plant. The impact of this increase on the operating costs is shown in Figure 5.7, where it can be observed that the operating cost steadily decreases as the ETS penetration increases. These results support the introduction of ETS systems in the KLFN community.

5.2.3 Sensitivity Study

In order to analyze the impact of the location, capacity and the number of ETS units on operating costs, a sensitivity study is presented here, for the KLFN isolated microgrid, using actual measured electricity demand and output from PV and wind generators. The 6-day dispatch problem was repeated considering various commercially available ETS unit

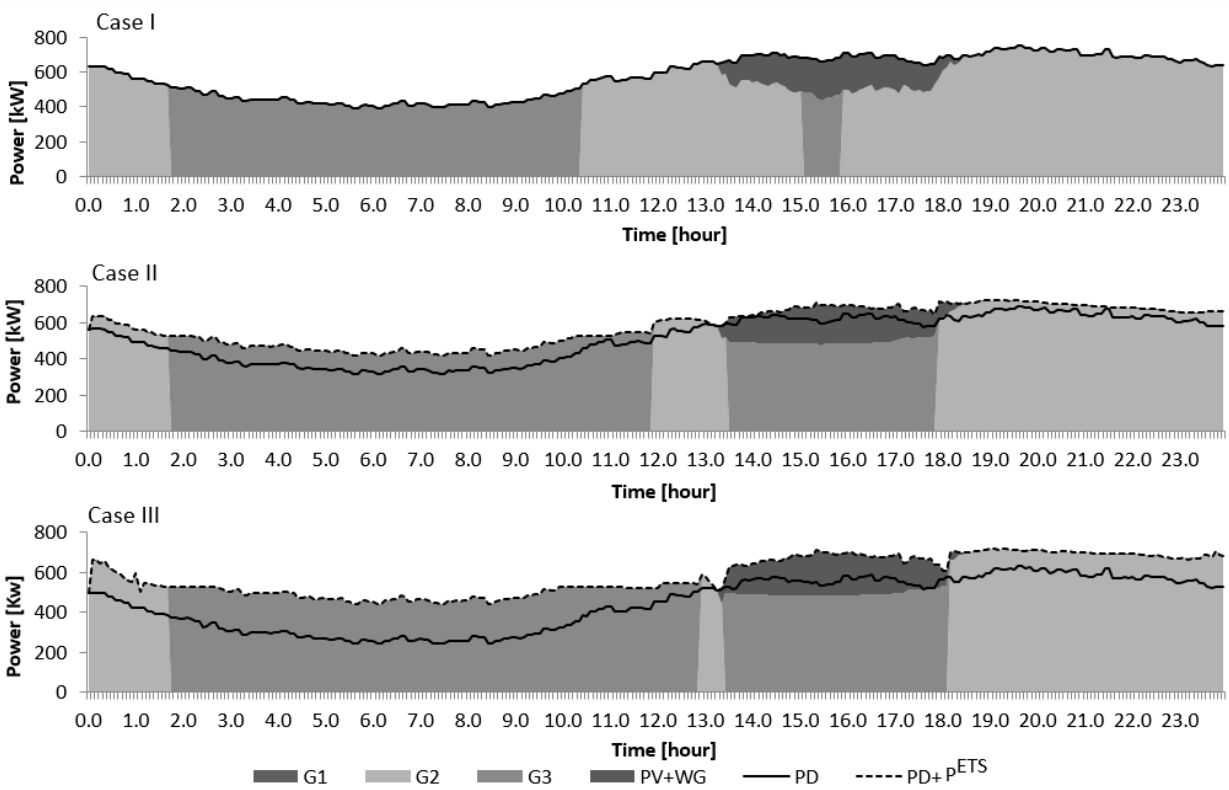

Figure 5.6: Dispatch for all cases for the KLFN system with 250 kW PV plant.

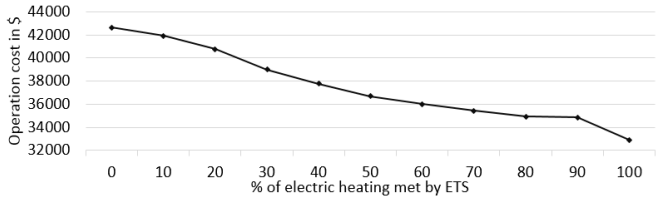

Figure 5.7: Percentage of electric heating replaced by ETS systems versus operating costs for the KLFN system.

capacities of 20 kWh, 27 kWh, 33 kWh, and 40 kWh [52], and varying the number of ETS units from 4 to 40, depending on the ETS capacity. Figure 5.8 shows that the total operating cost decreases with the number of ETS units in a approximately linear manner for all ETS capacities. Also note that the overall 6-day least operating cost is obtained with 20 units of 40 kWh ETS, while for the other ETS unit capacities, the minimum operating

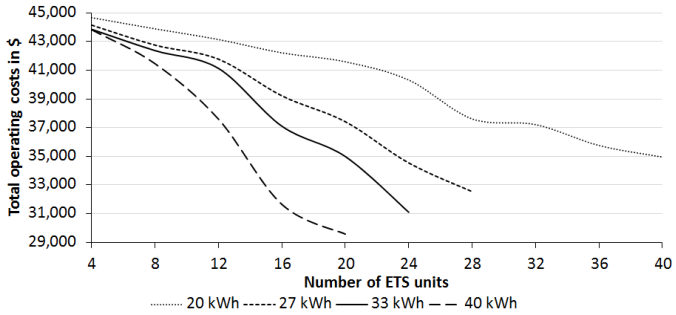

Figure 5.8: Variation of total operating cost with number of ETS units for the KLFN System.

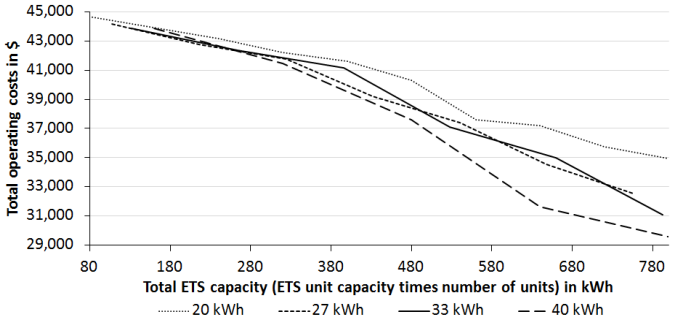

Figure 5.9: Variation of total operating cost with total ETS capacity for the KLFN System.

cost increases with decreasing in the ETS capacity.

Figure 5.9 shows the variation of total operating cost with total ETS capacity for the different ETS unit capacities considered. Observe that the 40 kWh ETS is the cheapest option in most cases due to its larger charging power limits, as compared to all other ETS unit capacities.

To analyze the impact of the location of ETS systems, the 6-day dispatch problem was solved assuming that 50% of the households with electric heating have a 40 kWh ETS, and changing the number of houses per bus with ETS. As shown in Figure 5.10, two ETS distributions per bus are considered; in Case 1, the ETS are located at Buses 4-9 only, which are closer to the generators, while in Case 2, the ETS are located at Buses 9-11, which are farthest from the generators. As expected, because of the typical size of the KLFN isolated microgrid, the operating costs obtained for the two cases are more or less the same, indicating that the location of ETS systems do not significantly impact the operating costs of the considered microgrid.

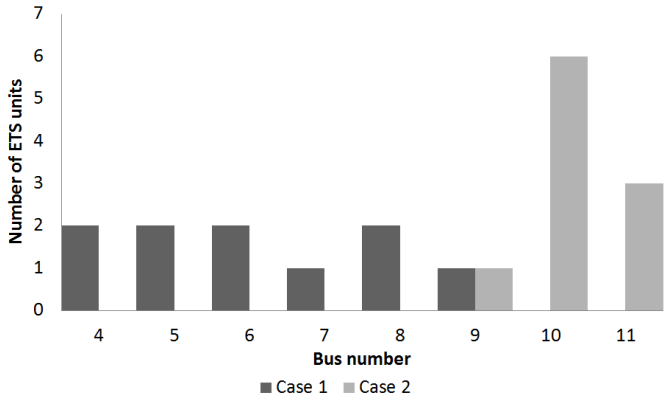

Figure 5.10: Distribution of number of ETS units at various buses for the KLFN System.

5.3 Summary

A mathematical model for an ETS system was presented and integrated into a decoupled UC-OPF microgrid EMS model, with an MPC approach to account for the deviations in the forecast of RES and demand. The proposed ETS-EMS framework was tested and validated using a modified CIGRE benchmark system, highlighting the benefits of integration of ETS systems in terms of reduction in operating costs, load curtailment, and use of ESS. Additionally, the ETS-EMS model was tested with the real KLFN isolated microgrid, showing a possible reduction in operating costs of up to 23%, demonstrating that the higher the penetration of RES, the more reduction in operating costs, with diesel units operating closer to their optimal point. A sensitivity study was also performed to analyze the impacts of the location, number, and unit capacity of the ETS systems on the operating costs of KLFN microgrid, illustrating that the location has negligible impact on operating costs, while the operating costs decrease linearly with the number of ETS units, and as the capacity of the ETS units increase, the operating cost decreases. The main content of this chapter has been published in [78].

Chapter 6

A Sustainable Microgrid EMS

From the review of the literature, it is observed that there are no reported attempts to analyze the impact of DR on pollutant emissions from fossil-fuel-based DG units in a microgrid. Thus, in this chapter, the emission models of the fossil-fuel-based generator, which can be integrated into EMS models are presented. Constant energy demand shifting load models are also considered and integrated into the EMS to examine the impact of DR on the system emission and operating cost. The impact of including the emission models on the operation of an isolated microgrid, emissions, and costs, are studied considering different operating strategies. The proposed operating strategies are validated on the modified CIGRE medium voltage benchmark microgrid system, demonstrating the effectiveness of the proposed EMS and studying the impact of DR on emissions and costs.

6.1 Mathematical Modeling

6.1.1 Emission Model of Generators

Emission models of fossil-fuel-based DG units are proposed here, representing the mathematical relationship between the loading level of DG units and the associated amount of pollutant emissions, namely, carbon dioxide (CO_2), nitrogen oxide (NO_x) and carbon monoxide (CO). Thus, the emissions at different loading levels of DG units can be obtained as follows:

$$E_{p,g}(P_g) = \psi_{p,g}(P_g) L_g(P_g) \qquad \forall p, g \tag{6.1}$$

The amount of pollutant emissions per unit fuel combustion $\psi_{p,g}$ can be found in [79].

The equivalent CO_2 emission from each pollutant can be determined by multiplying the Global Warming Potential Index (GWPI) of the pollutant ξ_p, given in [80], with the respective pollutant emissions, as follows:

$$E_{p,g}^{CO_2}(P_g) = \xi_p E_{p,g}(P_g) \qquad \forall p, g \tag{6.2}$$

The equivalent CO_2 emission from a DG unit can then be determined by summing the equivalent CO_2 emissions of each pollutant as follows:

$$E_g^{\mathrm{CO_2}}(P_g) = \sum_p E_{p,g}^{\mathrm{CO_2}}(P_g) \qquad \forall g \tag{6.3}$$

Therefore, $E_g^{\mathrm{CO_2}}(P_g)$ can be expressed using (6.1) and (6.2) as follows:

$$E_g^{\mathrm{CO_2}}(P_g) = \sum_p \xi_p \psi_{p,g}(P_g) L_g(P_g) \qquad \forall g \tag{6.4}$$

where it can be observed that the emission from a DG unit is directly dependent on its loading level.

The equivalent CO_2 emission from a DG unit operating at a given loading level at time k can also be expressed in general form as follows [7]:

$$E_{g,k}^{\mathrm{CO_2}}(P_{g,k}) = (d_g^{em} P_{g,k}^2 \Delta t_k + e_g^{em} P_{g,k} + f_g^{em} W_{g,k})\Delta t_k + C_g^{em-sup} U_{g,k} + C_g^{em-sdn} S_{g,k} \quad \forall g,k \tag{6.5}$$

which is a generic quadratic function depicting the relationship of equivalent CO_2 emissions with the DG loading level. Note also that (6.5) includes equivalent CO_2 emissions associated with DG unit start-up and shut-down, where the start-up emission coefficient C_g^{em-sup} denotes the amount of CO_2 emission during the DG unit start-up, which is assumed equivalent to 5 min of full load operation of the DG unit, while the shut-down coefficient C_g^{em-sdn} denotes the CO_2 emission during shut-down operation, which is assumed equivalent to 2.5 min full load operation of the DG unit [7]. From (6.4) and (6.5), the coefficients d_g^{em}, e_g^{em}, and f_g^{em} can be determined using a simple curve-fitting technique. Hence, the mathematical model for CO_2 emission from a DG unit given by (6.5) can be integrated into the microgrid UC model as discussed next.

6.1.2 Microgrid UC Model

The model is developed from the perspective of the operator, who seeks to minimize the operating costs of the microgrid, including generation costs, and start-up and shut-down costs. Such objective can be expressed as in (3.1):

$$J_{op} = \sum_{g,k} [(d_g P_{g,k}^2 \Delta t_k + e_g P_{g,k} + f_g W_{g,k})\Delta t_k + C_g^{sup} U_{g,k} + C_g^{sdn} S_{g,k}] \tag{6.6}$$

In addition, the constraints discussed next can be defined to represent the operational constraints of the microgrid.

- *Demand Supply Balance:* The following constraints ensure that the total generation meets the total demand of the microgrid at each time step, similarly to (3.21):

$$\sum_g P_{g,k} + \sum_i (PV_{i,k} + PW_{i,k}) + \sum_n (P^{dch}_{n,k} - P^{ch}_{n,k}) = \sum_i [PD^c_{i,k} + PD^r_{i,k} + PD^{rs}_{i,k}] \qquad \forall k \quad (6.7)$$

  In this case, it is assumed that a part of the residential load PD^{rs}_k is controllable and hence is an optimization variable, as it can be shifted to other hours. The rest of the load, which is uncontrollable, can be obtained using a forecasting engine.

- *Reserve Constraints:* These constraints ensure that the spinning reserve requirement is met by the dispatched generators, similarly to (3.22) as follows:

$$\sum_g (\bar{P}_g W_{g,k} - P_{g,k}) \geq R^{sv} \sum_i [PD^c_{i,k} + PD^r_{i,k} + PD^{rs}_{i,k} + PV_{i,k} + PW_{i,k}] \qquad \forall k \quad (6.8)$$

- *DR Constraints:* The controllable demand PD^{rs}_k is a power-shifting demand that can be shifted and recovered within the same day, considering the maximum and minimum limits of the shiftable demand. This can be modeled as follows:

$$\sum_k PD^{rs}_{i,k} \Delta t_k \geq 0 \quad \forall i \quad (6.9)$$

$$\underline{PD}^{rs}_i \leq PD^{rs}_{i,k} \leq \overline{PD}^{rs}_i \quad \forall i,k \quad (6.10)$$

- *UC Constraints:* These constraints include active and reactive power generation limits, ramp-up and ramp-down constraints, minimum up-time and down-time constraints, and coordination constraints, as discussed in detail in Section 3.1.

- *Energy Storage System:* The ESS constraints include the energy balance constraint (4.24), and constraints to prevent simultaneous charging/discharging (4.25), limits on SOC (4.26), and charging/discharging power (4.27) and (4.28).

6.1.3 Operating Strategies

The following five different operating strategies are considered to study the optimal dispatch of microgrid DG units and the role of DR in system emissions and costs:

- *Operating Cost Minimization (Case I or Base Case)*: The operating costs of the microgrid includes generation cost, and start up and shut down costs as given in (6.6). This case represents the current EMS practice in isolated microgrids, and is not sustainable from a long-term perspective. The next four cases include the proposed emission models, thus representing sustainable models.

- *Emission Cost Minimization (Case II)*: The equivalent CO_2 emission cost for fossil-fuel-based DG units is obtained by multiplying the social cost of equivalent CO_2 emissions Γ with the total equivalent CO_2 emissions from generation, start-up and shut-down operations, as per (6.5), and is given by:

$$J_{em} = \Gamma \sum_{g,k} [(d_g^{em} P_{g,k}^2 \Delta t_k + e_g^{em} P_{g,k} + f_g^{em} W_{g,k}) \Delta t_k + C_g^{em-sup} U_{g,k} + C_g^{em-sdn} S_{g,k}] \tag{6.11}$$

- *Minimization of Emission and Operating Costs (Case III)*: In order to consider the pollutant emissions and the operating cost of DG units simultaneously in the formulation of the EMS objective function, one of the strategies is to minimize the algebraic sum of equivalent CO_2 emission costs and operating costs. The key feature of this multi-objective strategy is that it does not require prior knowledge of the aspiration levels of these conflicting objectives, their minimum or maximum values, nor the weights associated with them to obtain an optimal dispatch. Such an objective function can be expressed as follows:

$$J_{oc} = J_{op} + J_{em} \tag{6.12}$$

- *Pareto-optimality of Operating and Emission Costs (Case IV)*: In this case, the objective function is formulated considering both the operating costs and emission costs as a normalized function to obtain the Pareto-optimal solution between the two objectives based on the compromise programming method (as discussed in Section 2.5.6), as follows:

$$J_{cp} = \sqrt{\left(\frac{J_{op} - \underline{J}_{op}}{\bar{J}_{op} - \underline{J}_{op}}\right)^2 + \left(\frac{J_{em} - \underline{J}_{em}}{\bar{J}_{em} - \underline{J}_{em}}\right)^2} \tag{6.13}$$

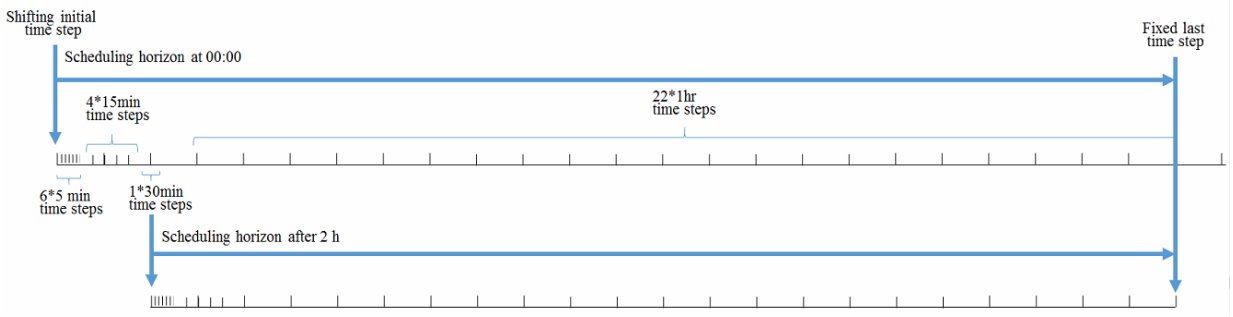

Figure 6.1: Scheduling time horizon using a receding horizon approach.

- *Minimization of Deviation of Operating and Emission Costs (Case V)*: In this case, the objective function seeks to minimize the weighted sum of two quantities: the deviations in the operating costs from its aspiration level, and the deviation in the equivalent CO_2 emission costs from its aspiration level based on the goal programming method (as discussed in Section 2.5.6), as follows:

$$J_{gp} = wD_1 + (1-w)D_2 \tag{6.14}$$

where

$$D_1 = J_{op} - A_1 \tag{6.15}$$

$$D_2 = J_{em} - A_2 \tag{6.16}$$

and A_1 and A_2 are the aspiration levels of operating and emission costs, respectively. The aspiration levels are the desired target values of the objective function such as operating cost or emissions, which are set by the system operator, planner, or policy maker. In the present work, the aspiration level of the operating cost A_1 is considered to be the minimum operating cost obtained from Case I, while the aspiration level of emission cost A_2 is set at the minimum emission cost obtained from Case II. These are stiff targets to achieve simultaneously, and represent the "ideal" solution, which the model "aspires" to attain.

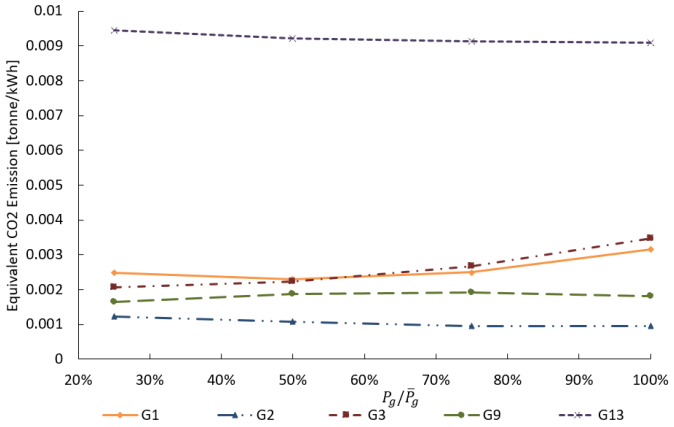

Figure 6.2: Emission characteristics of DG units.

6.2 Results and Discussions

An MPC approach is adopted here to account for the deviations in the forecast of RES and demand, where the dispatch problem is resolved considering updated forecast of the generation from RES at every 5 minute recalculation time interval, as explained in [17] and Section 3.2.3. The obtained UC dispatch of DERs is valid only for the next time interval. Moreover, in order to balance the shiftable demand over a day and also to maintain the SOC level at the end of the day, the time horizon is considered to be receding at every recalculation iteration, in which the initial time step is shifted forward by one time interval, while the last time step is kept fixed, as depicted in Figure 6.1. The proposed operating strategies for the proposed EMS model are tested on the CIGRE medium voltage benchmark network depicted in Figure 3.6. The social cost of equivalent CO_2 emissions Γ is assumed to be 37 \$/tonne [81].

The emission data sheet of the respective generators and their emission factors [79], [82] yield the equivalent CO_2 emission characteristics of the five DG units illustrated in Figure 6.2, from which the corresponding co-efficients of the equivalent CO_2 emission functions shown in Table 6.1 can be obtained. Note in Figure 6.2 that DG unit G13 accounts for the highest equivalent CO_2 emission in tonne/kWh, and its emission level is significantly higher compared to the other DG units; units G3, G1, G9 and G2 follow suit in decreasing order of emissions.

As discussed earlier, five distinct operating strategies (UC objective functions) are considered to examine the microgrid EMS model performance. In order to study the impact of

Table 6.1: Parameters of the DG emission characteristics

DG units	**G1**	**G2**	**G3**	**G9**	**G13**
$\bar{P}_g$, MW	2.5	1.4	0.8	0.31	0.5
d_g^{em}	1.2228	0.0234	4.3792	0	0.0088
e_g^{em}	-0.48236	0.8114	-0.4755	1.8849	8.9722
f_g^{em}	1.4235	0.1505	0.3449	-0.0087	0.0594
C_g^{em-sup}	0.0712	0.1075	0.0165	0.0479	0.3788
C_g^{em-sdn}	0.0356	0.0537	0.0082	0.0239	0.1894

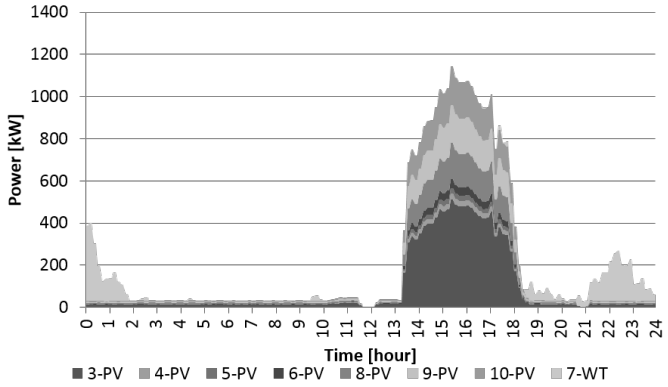

Figure 6.3: Solar PV and wind generation profiles.

DR on pollutant emissions, all these cases are also compared to corresponding simulations without DR by forcing $PD_{i,k}^{rs} = 0 \quad \forall i, k$.

All the models were coded and solved in GAMS [59], on an Intel® Xeon® CPU L7555, 1.87 GHz 4-processor server. In Cases I, II, III and V, the objective functions are quadratic functions, and hence these are MIQP problems, which can be solved using the CPLEX solver [56]. On the other hand, Case IV has a non-linear objective function, and hence is an MINLP problem, which can be solved using the DICOPT solver [56]. All case studies, with and without DR, were simulated for 24 hours of system operation using the MPC approach, with a recalculation time of 5 minutes.

The wind and solar PV profiles shown in Figure 6.3 were used here, based on actual measured data from wind and solar plants in the KLFN community microgrid [67], instead of the profiles used in prvious chapters just to obtian solutions with different RES outputs. The demand profiles were the same as those used in [17]. To simulate forecast, normal pdfs were used to perturb the actual profiles, as discussed in Section 3.4.

Table 6.2: Summary of microgrid EMS operating strategies

	Cases	I	II	III	IV	V
Without DR	J_{op} [$]	15,198	18,996	17,547	16,730	16,707
	J_{em} [$]	10,351	5,422	6,538	7,869	7,276
	Emissions [Tonne]	279.8	146.6	176.7	212.7	199.6
	Reduction in emissions [%]	0	48	37	24	29
	Increase in op. costs [%]	0	25	15	10	10
	Average CPU time per MPC iteration [s]	6.67	22.7	36.25	8.12	5
With DR	J_{op} [$]	14,971	18,906	17,862	16,394	16,491
	J_{em} [$]	10,593	5,103	5,982	7,865	7,443
	Emissions [Tonne]	286.3	137.9	161.7	212.6	201.2
	Reduction in emissions [%]	0	52	44	26	30
	Increase in op. costs [%]	0	26	19	9.5	10
	Average CPU time per MPC iteration [s]	13.75	43.12	47.08	8.12	17.29

Table 6.2 presents the EMS results obtained without and with DR, including the total equivalent CO_2 emissions in each case and its % reduction with respect to Case I. Figures 6.4 and 6.5 present plots of normalized operating costs $\widetilde{J}_{op}$ versus normalized emission costs $\widetilde{J}_{em}$ for all the cases without and with DR, respectively, where these normalized costs are defined as follows:

$$\widetilde{J}_{op} = \frac{J_{op} - \underline{J}_{op}}{\bar{J}_{op} - \underline{J}_{op}} \tag{6.17}$$

$$\widetilde{J}_{em} = \frac{J_{em} - \underline{J}_{em}}{\bar{J}_{em} - \underline{J}_{em}} \tag{6.18}$$

Figures 6.6 and 6.7 present the share of individual DG units in the microgrid EMS dispatch without and with DR, respectively. Finally, Figures 6.8 to 6.12 depict stacked area plots of the equivalent CO_2 profiles for each DG unit, for all cases, without and with DR. The

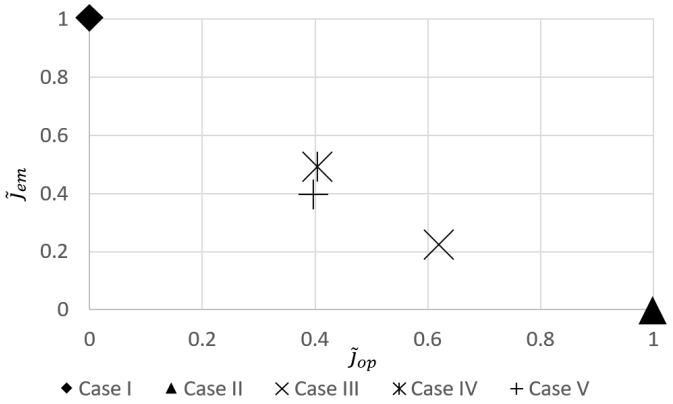

Figure 6.4: Normalized operating costs vs. normalized emission costs without DR.

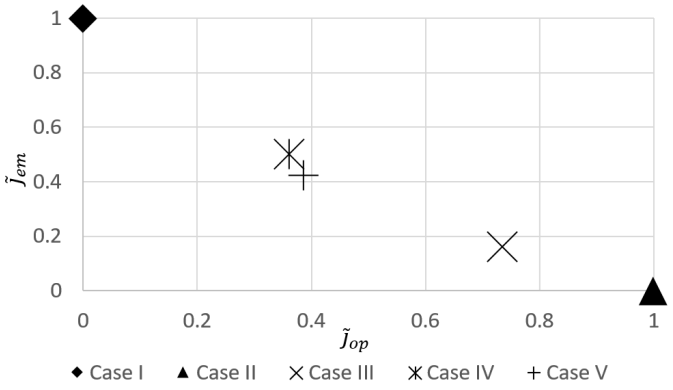

Figure 6.5: Normalized operating costs vs. normalized emission costs with DR.

following observations can be made for Table 6.2 and Figures 6.4-6.12:

- Case I yields the least operating cost dispatch but incurs the highest emission cost, which is to be expected, since in this case emissions are not considered. On the other hand, and as expected, Case II yields the least emission cost dispatch with the highest operating cost, both with and without DR. These cases account for the two extreme points in Figures 6.4 and 6.5.
- In Case I with DR, observe that operating costs are reduced by 1.5%, while emission costs increase by 2.3% (Table 6.2) with respect to Case I without DR. This is because the shiftable demand is dispatched at off-peak hours, so that the dispatch share of the cheapest unit G1 is increased, while the dispatch from G2, which has least emissions

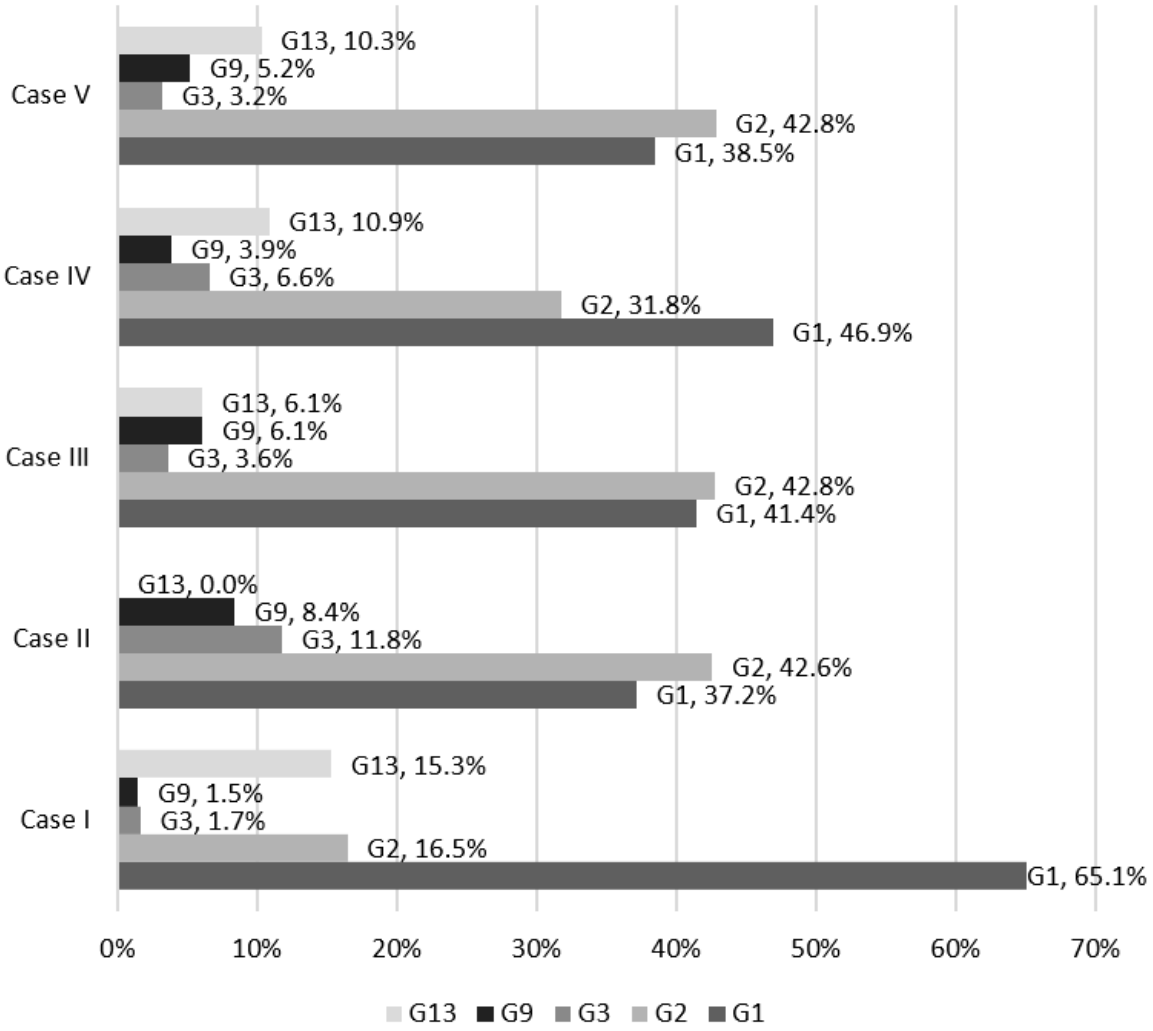

Figure 6.6: Dispatch contribution of DG units without DR.

(Figure 6.2), is reduced (Figures 6.6 and 6.7). The major changes in emissions with DR for Case I are highlighted in Figure 6.8, where the emissions during off-peak hours (hours 0 to 6) and also during on-peak hours (hours 18 to 20) are increased, while a reduction in emissions is observed during peak hours 7 to 10.

- In Case II with inclusion of DR, the emission and operating costs are reduced by 5.8% and 0.5%, respectively (Table 6.2), with respect to Case II without DR. The reason for this significant reduction is that the dispatch share of low emission units G2, G1,

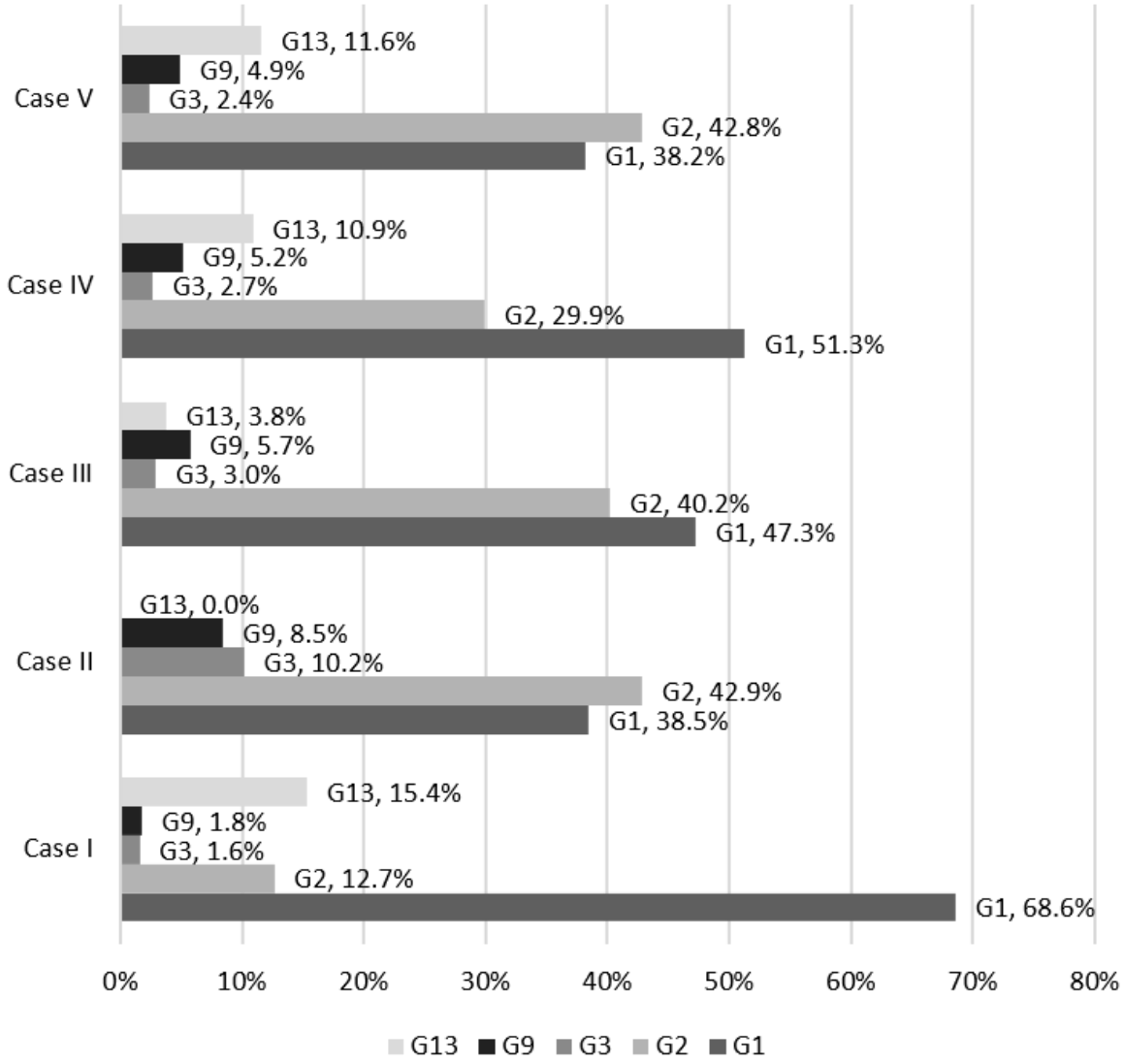

Figure 6.7: Dispatch contribution of DG units with DR.

and G9 are increased, whereas unit G13, which has the highest emission (Figure 6.2), is not committed, as the controllable demand is shifted to off-peak hours (Figures 6.6 and 6.7). These observations can also be made in Figure 6.9, during the highlighted off-peak hours, which shows reduction in emissions from G3 due to a reduced dispatch of this unit at these hours due to DR.

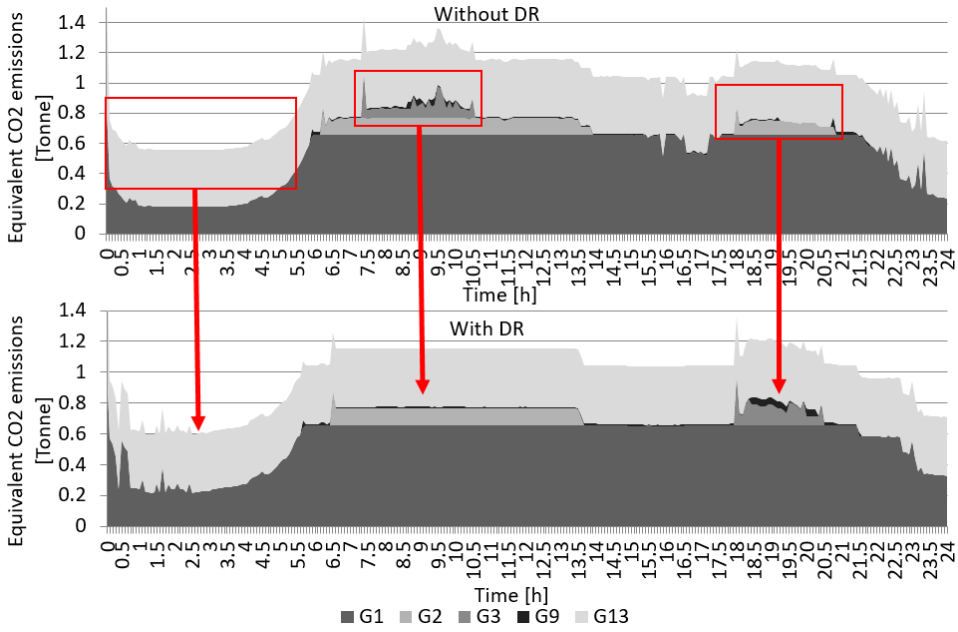

Figure 6.8: Case I emission profiles of DG units without and with DR.

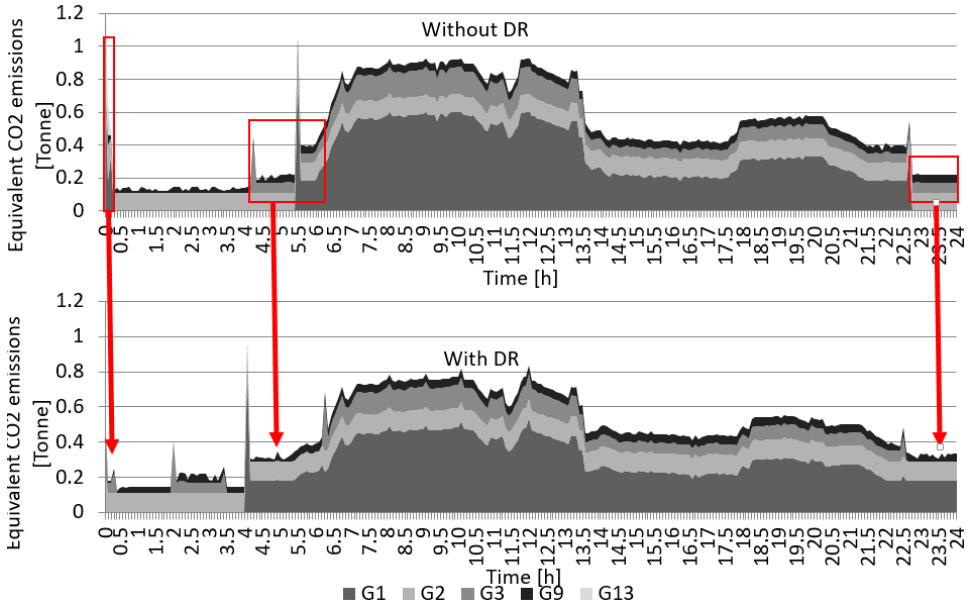

Figure 6.9: Case II emission profiles of DG units without and with DR.

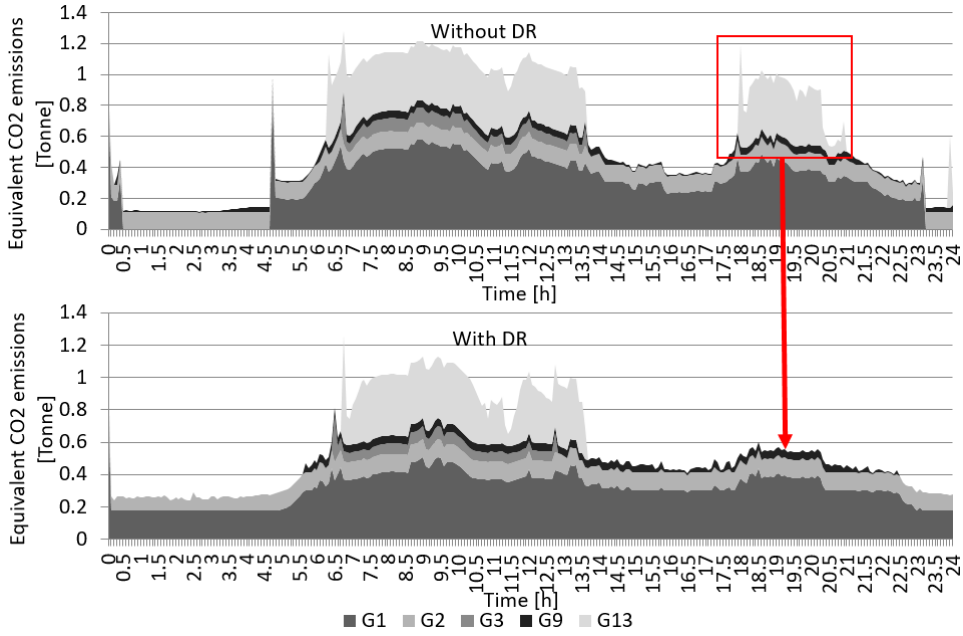

Figure 6.10: Case III emission profiles of DG units without and with DR.

- In Case III, note that the introduction of DR reduces the sum of operating and emission costs, as compared to the case without DR, with the operating costs increasing by 1.8%, while the emission costs decrease by 8.5% (Table 6.2). This can be attributed to the reduction in dispatch of G13, which has the highest emissions and the least operating costs, when DR is introduced. This is also depicted and highlighted for hours 18 to 21 in Figure 6.10.

- Case IV yields a dispatch to minimize deviations from the optimal operating and emission costs. Observe in Figures 6.4 and 6.5 that normalized operating costs are 0.4 and 0.36, and normalized emission costs are 0.49 and 0.5, without and with DR, respectively. Note in Table 6.2 that with DR, both operating and emission costs are reduced by 2% and 0.1% with respect to Case IV without DR, respectively, because the dispatch share of G1 and G9 is increased, since G1 is the cheapest unit while G9 is a low-emission unit (Figures 6.6 and 6.7). On the other hand, the dispatch share of unit G3, which has high emissions (Figure 6.2), is reduced in coordination with the shifting of the controllable demand (Figures 6.6 and 6.7). The reduction in emissions due to less use of G3 is also highlighted in Figure 6.11. The reason for the higher reduction in operating cost as compared to the emission cost is that, in

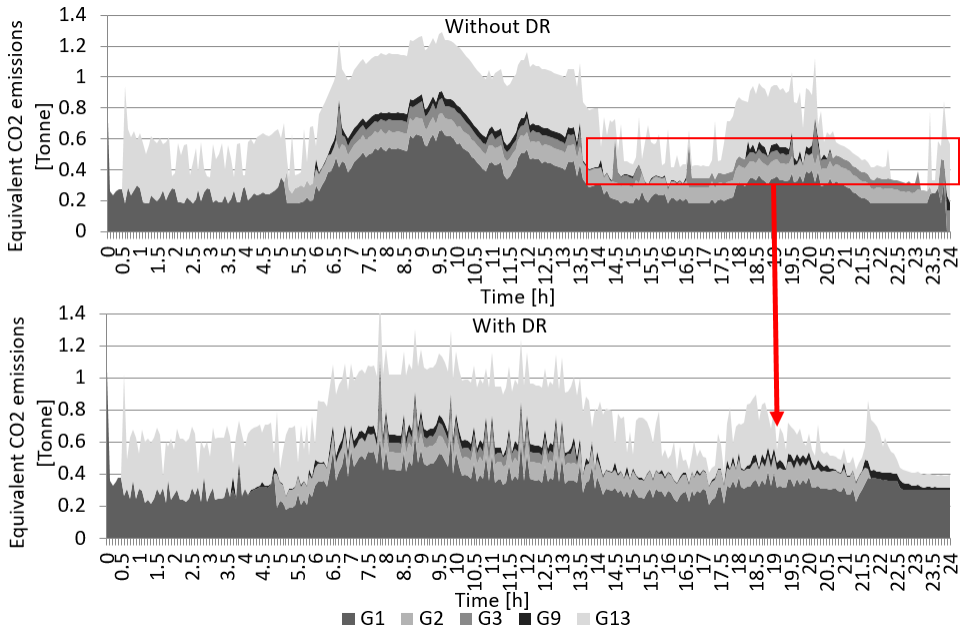

Figure 6.11: Case IV emission profiles of DG units without and with DR.

the objective function, $\frac{1}{\bar{J}_{op}-\underline{J}_{op}}$ is larger than $\frac{1}{\bar{J}_{em}-\underline{J}_{em}}$, which are the multiplication factors for each cost component in (6.13).

- In Case V, the best combination of weights for least operating and emission cost is obtained by running the microgrid EMS model with different values of w. The variations of normalized operating and emission costs with respect to w are depicted in Figures 6.13 and 6.14, where the curves intersect at $w = 0.54$ and $w = 0.535$. With these values, observe Figures 6.4 and 6.5 that the normalized operating and emission costs are closest to those obtained in Case IV, for both without and with DR. Note also that with DR for $w = 0.535$, the operating cost is reduced by 1.2% while emission cost is increased by 0.8% with respect to the case without DR (Table 6.2), due to the increase in dispatch share of unit G13, which has the highest emission but least operating cost (Figure 6.7). The increase in emissions with DR due to dispatch of G13 is also observed in Figure 6.12.

- It is important to note in Table 6.2 that with the consideration of the equivalent CO_2 emission model, the total equivalent CO_2 emissions are reduced from 24% to 48% without DR and from 26% to 52% with DR compared to Case I (Base case), which does not include the emission function of DG unit, demonstrating the environmental

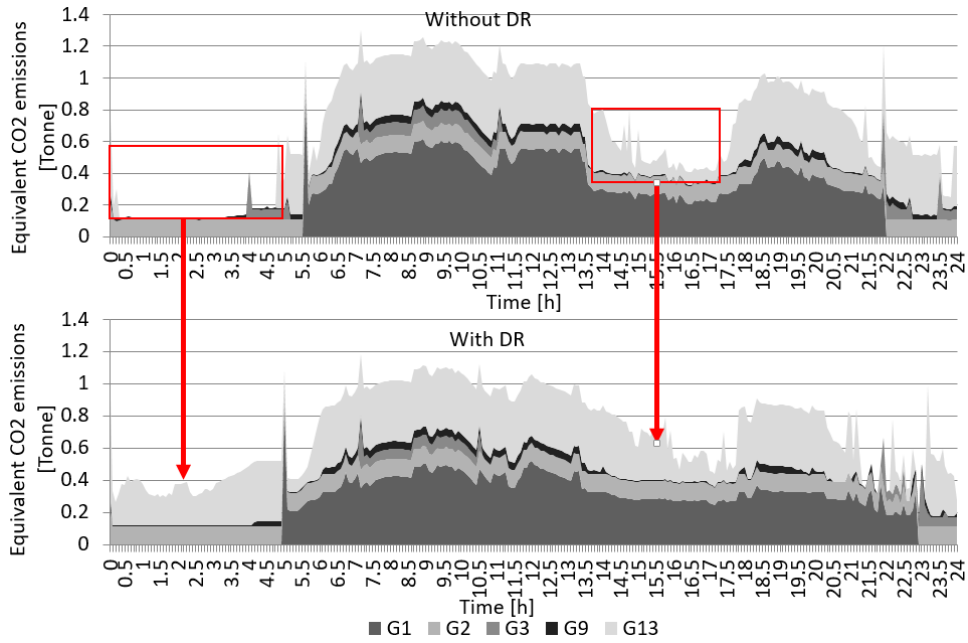

Figure 6.12: Case V emission profiles of DG units without and with DR.

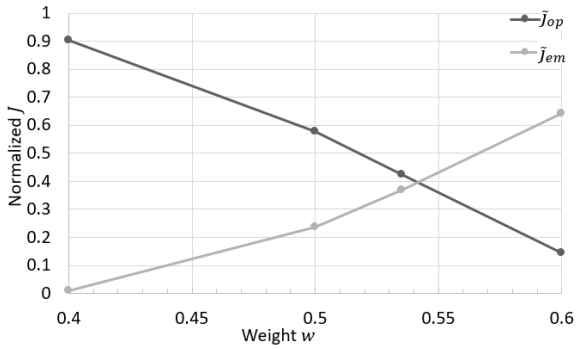

Figure 6.13: Variation of J with weight w without DR

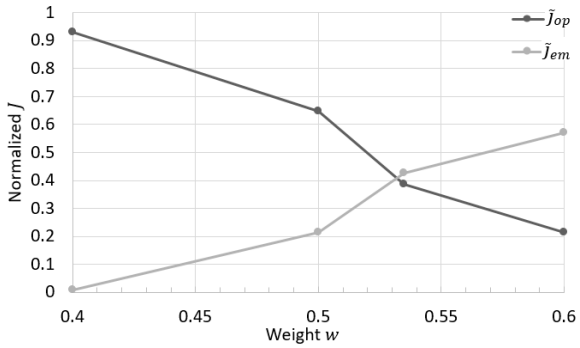

Figure 6.14: Variation of J with weight w with DR.

benefits of the proposed EMS models. However, there is an increase in operating cost in Cases II to V, from 10% to 25 % without DR, and 9.5% to 26% with DR, compared to the operating costs in Case I, reflecting the impact of emission reductions in operating costs in the test system. Observe that among all operating strategies, Case IV provides the dispatch with least increase in operating cost with significant reduction in emissions compared to Case I, also showings the positive impact on both cases of DR.

The average computation (CPU) times per iteration of the MPC algorithm to obtain the 24 hour UC dispatch for all the cases, with and without DR, are shown in Table 6.2. Observe that the CPU time increases in most of the cases when DR is included; however, the average computation time per MPC iteration is less than the required 5 min recalculation time, and hence the proposed approach can be implemented online in practical applications.

6.3 Summary

In this chapter, equivalent CO_2 emission functions were developed for DG units based on their emission factors and the GWPI of pollutants, and these equivalent CO_2 emission models were included in a microgrid EMS formulation; demand shifting loads were also included in the EMS model. To study the impact of equivalent CO_2 emission and operating costs simultaneously in microgrid dispatch, different operating strategies were developed, validated, and tested on a CIGRE microgrid benchmark system by using an MPC approach, considering the deviations in the forecast of demand and renewable generation.

The obtained results demonstrate that, with inclusion of DR, equivalent CO_2 emissions depend on the operating strategy, as the impact of DR on operating costs and equivalent CO_2 emission costs is different. From the presented studies, it can be concluded that the operating strategy that corresponds to Pareto-optimality of operating and emission costs provides the best possible compromise between the operating and equivalent CO_2 emission costs, reducing both costs with inclusion of DR. The operating strategy which minimizes the sum of both costs indeed yields the least total costs; however, inclusion of both costs in the objective function does not guarantee reduction of these costs with DR. On the other hand, the operating strategy which minimizes the deviations in the aspiration levels of the two costs, with best possible weights, yields the dispatch solution closest to the Pareto-optimal solution. The main content of this chapter was published in [83].

Chapter 7

Conclusion

7.1 Summary and Conclusions

The research presented in this thesis focuses on the development of EMS for isolated microgrids considering their different aspects and relevant issues. The motivations to carry out the research were presented in Chapter 1, and the main research objectives were outlined based on a critical review of the literature.

In Chapter 2, the background topics related to the present research carried out in this thesis were reviewed. The definitions and the concept of microgrids were explained. The basic EMS for isolated microgrids including UC and OPF models were then outlined, presenting the objective functions and associated constraints. DR schemes were also discussed in the context of isolated microgrids, and the structure and features of ETS system were outlined. Finally, a brief overview of the optimization methods along with the MPC technique were presented.

In Chapter 3, the mathematical models for controllable (smart) loads were proposed, which were then integrated into a novel EMS framework for an isolated microgrid that considered UC and OPF constraints simultaneously. The deviations in forecast of generation from RES-based DGs and loads were accounted for using the MPC approach. The novel microgrid EMS framework presented, yields optimal dispatch decisions for dispatchable generators, ESS, and the optimal peak demand cap for controllable loads. Finally, the impacts of DR on microgrid operation with the proposed EMS framework were studied, showing the benefits in the terms of reduction in operating costs, peak demand, and load curtailment.

In Chapter 4, practical EMS models were presented, which considered the operational constraints of the DERs, active-reactive power balance, unbalanced system configuration and loading, and voltage dependent loads. Deviations in the forecast of RES and demand were taken into account using an MPC technique. Considering the large size and short length of the feeders, a novel linearization approach was presented and applied to the

network equations. Furthermore, the proposed practical EMS models were compared with the typical decoupled UC and OPF based EMS models with and without consideration of the unbalanced system conditions. The simulation results showed that the proposed practical EMS models attained computationally, and cost effective, dispatch solution.

In Chapter 5, a mathematical model of the ETS system was proposed and integrated into an EMS for isolated microgrids, in which the problem was divided into UC and OPF subproblems, to dispatch fossil-fuel-based generators, ESS, and ETS charging. To account for the deviations in the forecast of RES and demand, an MPC technique was used. The proposed framework evaluated and analyzed the impact of the ETS system on the operation of isolated microgrids. The simulation results showed that the ETS system significantly reduced operating costs, allowing for better integration of intermittent wind and solar resources.

In Chapter 6, equivalent CO_2 emission functions were developed for DG units based on their emission factors and the GWPI of pollutants. These models were then integrated within a microgrid EMS model. An MPC approach was used to account for deviations in the forecast of RES and demand. Constant energy, demand shifting load models were also integrated into the EMS to examine the possible impact of DR on the total system emissions and operating costs of the microgrid. Different multi-objective operating strategies were considered to minimize both operating and emission costs simultaneously. The simulation results showed that with DR, the emission cost can increase, while reducing the operating cost.

The main conclusions of the presented work are:

- A comparison between the UC+OPF integrated and decoupled UC-OPF EMS models showed that even though the integrated model took longer time to solve, better dispatch results can be obtained, with less load curtailment, and efficient use of ESS resources, within feasible computational times for real-time applications.

- With the inclusion of smart load models into the EMS framework, reduction in peak demand, load curtailment, and total costs, as wellas improvements in load factor can be achieved. It is also demonstrated that the proposed DR integrated EMS approach enhances the microgrid's load serving capability.

- Smart loads, under the influence of TOU prices, can cause undesirable load spikes at low electricity price hours due to customer response. This issue can be mitigated with the proposed approach of dispatching the smart load with a peak demand cap.

- The need for detailed network consideration in microgrid EMS is evaluated, demonstrating that the single node approximation of the network is sufficient; however, voltage-dependent loads, active-reactive power management, and unbalanced system conditions need to be included.

- With the integration of ETS system into the microgrid EMS model, the operating cost, load curtailment, and use of ESS can be reduced, while diesel units can operate closer to their efficient and economic operating point.

- A sensitivity study, analyzing the impact of the location, number, and unit capacity of ETS systems illustrates that the location has negligible impact on operating cost, while the operating cost decreases almost linearly with the number of ETS units, and the unit capacity.

- The pollutant emissions may increase with the inclusion of DR into EMS models with operating cost minimization objective; therefore, the impact of DR on equivalent CO_2 emissions needs to be considered. Among the various mutli-objective operating strategies, the Pareto optimality of both operating and emission costs obtains the best compromised solution, and also reduces both costs with inclusion of DR.

7.2 Contributions

The main contributions of this thesis are the following:

- A mathematical model for smart loads has been developed using supervised NN learning, as a function of ambient temperature, TOU price, time of the day, and peak demand constraints imposed by the MGO.

- A comprehensive mathematical formulation of the EMS for isolated microgrids, incorporating the developed smart load model, has been proposed simultaneously considering OPF and UC constraints.

- Two different mathematical models, referred to as practical EMS for isolated microgrids, have been proposed and studied, both neglecting feeders and considering an approximate feeder representation. Both models include UC constraints, a three-phase linearized generator model, voltage dependency of the loads, and unbalanced system conditions. It was shown, based on comparisons with respect to decoupled UC-OPF based EMS models, considering balanced and unbalanced conditions, that

the proposed single-node practical EMS model yields economic and computationally efficient solutions.

- A new mathematical model of ETS systems has been proposed considering stored thermal energy, charging electric input, thermal demand, and effective heating losses. This model is then integrated into the microgrid EMS model taking into account UC and OPF constraints, to analyze the impact of ETS systems on the operation of isolated microgrids.

- Equivalent CO_2 emission functions have been developed for DG units based on their emission factors and the GWPI of pollutants. Demand-shifting load models along with emission models have been integrated into the UC to examine the possible impact of DR on the total system emissions and costs. Multi-objective UC models have been developed to study the impact of microgrid operation on emissions and costs for different operating strategies.

The main contents of this thesis have been published in [65], [66], [78], [83]. The main contents of Chapter 4 has been reported in a paper currently under review for publication [71].

7.3 Future Work

Based on the work presented in this thesis, further research may be pursued on the following subjects:

- Hardware implementation of the proposed EMS models to study their performance in conjunction with primary controls in an experimental microgrid setup could be carried out. This would allow to study their practical implementation in a microgrid, and their integration with existing microgrid controllers.

- Since only heating ETS systems were considered in these studies, it would be relevant to develop models for cooling ETS system, and integrate them into an EMS to study their impact in microgrids.

- The integration of primary ETS controllers with the microgrid EMS could be also studied to increase RES penetration.

References

[1] R. Lasseter, "Microgrid," in *Proc. IEEE Power Engineering Soc. Winter Meet.*, vol. 1, Jan. 2002, pp. 305–308.

[2] "Status of remote/off-grid communities in Canada," Natural Resources Canada, Tech. Rep., Aug. 2011. [Online]. Available: https://www.nrcan.gc.ca/sites/www.nrcan.gc.ca/files/canmetenergy/files/pubs/2013-118_en.pdf

[3] M. Arriaga, C. A. Cañizares, and M. Kazerani, "Northen lights: Access to electricty in Canada's northern and remote communities," *IEEE Power Energy Mag.*, vol. 12, no. 4, pp. 50–59, Jul/Aug 2014.

[4] F. Katiraei, R. Iravani, N. Hatziargyriou, and A. Dimeas, "Microgrids management: Controls and operation aspects of microgrids," *IEEE Power Energy Mag.*, vol. 6, no. 3, pp. 54–65, May/Jun 2008.

[5] IEEE-PES Task Force on Microgrid Control, "Trends in microgrid control," *IEEE Trans. Smart Grid*, vol. 5, no. 4, pp. 1905–1919, Jul. 2014.

[6] "Assessment of demand response and advanced metering," FERC Staff Report, Tech. Rep., Dec. 2012. [Online]. Available: http://www.ferc.gov/legal/staff-reports/12-20-12-demand-response.pdf

[7] C. Chen, S. Duan, T. Cai, B. Liu, and G. Hu, "Smart energy management system for optimal microgrid economic operation," *IET Renewable Power Generation*, vol. 5, no. 3, pp. 258–267, 2011.

[8] H. Kanchev, F. Colas, C. Lazarov, and B. Francois, "Emission reduction and economical optimization of an urban microgrid operation including dispatched PV-based active generators," *IEEE Trans. Sustainable Energy*, vol. 5, no. 4, pp. 1397–1405, Oct. 2014.

[9] W. Hu, P. Wang, and H. B. Gooi, "Towards optimal energy management of microgrids via robus two-stage optimization," *IEEE Trans. Smart Grid,* pre-print, pp. 1–13, Jun. 2016.

[10] S. Y. Derakhshandeh, A. S. Masoum, S. Deilami, M. A. S. Masoum, and M. E. H. Golshan, "Coordination of generation scheduling with PEVs charging in industrial microgrids," *IEEE Trans. Power Syst.*, vol. 28, no. 1, pp. 102–111, Feb. 2013.

[11] S. Conti, R. Nicolosi, S. A. Rizzo, and H. H. Zeineldin, "Optimal dispatching of distributed generators and storage systems for MV islanded microgrids," *IEEE Trans. Power Delivery*, vol. 27, no. 3, pp. 1243–1251, May 2012.

[12] Y. Levron, J. M. Guerrero, and Y. Beck, "optimal power flow in microgrids with energy storage," *IEEE Trans. Power System*, vol. 28, no. 3, pp. 3326–3234, Aug. 2013.

[13] M. M. A. Abdelaziz, M. F. Shaaban, H. E. Farag, and E. F. El-Saadany, "A multistage centralized control scheme for islanded microgrids with PEVs," *IEEE Trans. Sustainable Energy*, vol. 5, no. 3, pp. 927–937, Jul. 2014.

[14] P. P. Vergara, J. C. Lopez, L. C. da Silva, and M. J. Rider, "Security-constrained optimal energy managment system for three-phase residential microgrids," *Electr. Pow. Syst. Res.*, vol. 146, pp. 371–382, May 2017.

[15] P. P. Vergara, J. C. Lopez, M. J. Rider, and L. C. da Silva, "Optimal operation of unbalanced three-phase islanded droop-based microgrids," *IEEE Trans. Smart Grid,* pre-print, pp. 1–13, Sep. 2017.

[16] R. Findeisen, "Nonlinear model predictive control: A sampled-data feedback persepective," Ph.D. dissertation, Univ. Stuttgart, Stuttgart, Germany, 2004.

[17] D. E. Olivares, C. A. Cañizares, and M. Kazerani, "A centralized energy management system for isolated microgrids," *IEEE Trans. Smart Grid*, vol. 5, no. 4, pp. 1864–1875, Jul. 2014.

[18] D. E. Olivares, J. D. Lara, C. A. Cañizares, and M. Kazerani, "Stochastic-predictive energy management system for isolated microgrids," *IEEE Trans. Smart Grid*, vol. 6, no. 6, pp. 2681–2693, Nov. 2015.

[19] K. Dietrich, J. M. Latorre, L. Olmos, and A. Ramos, "Demand response in an isolated system with high wind integration," *IEEE Trans. Smart Grid*, vol. 27, no. 1, pp. 20–29, Feb. 2012.

[20] Q. Jiang, M. Xue, and G. Geng, "Energy management of microgrid in grid-connected and stand-alone modes," *IEEE Trans. Power System*, vol. 28, no. 3, pp. 3380–3389, Aug. 2013.

[21] K. H. Youssef, "Power quality constrained optimal management of unbalanced smart microgrids during scheduled multiple transitions between grid-connected and islanded modes," *IEEE Trans. Smart Grid*, vol. 8, no. 1, pp. 457–464, Jan. 2017.

[22] R. Palma-Behnke, C. Benavides, F. Lanas, B. Severino, L. Reyes, J. Llanos, and D. Saez, "A microgrid energy management system based on the rolling horizon strategy," *IEEE Trans. Smart Grid*, vol. 4, no. 2, pp. 996–1006, Jun. 2013.

[23] A. Parisio, E. Rikos, and L. Glielmo, "A model predictive control approach to microgrid operation optimization," *IEEE Trans. Control Syst. Technol.*, vol. 22, no. 5, pp. 1813–1827, Sep. 2014.

[24] M. Ross, C. Abey, F. Bouffard, and G. Joós, "Multiobjective optimization dispatch for microgrids with a high penetration of renewable generation," *IEEE Trans. Sustainable Energy*, vol. 6, no. 4, pp. 1306–1314, Oct. 2015.

[25] C. Deckmyn, J. V. de Vyver, T. L. Vandoorn, B. Meersman, J. Desmet, and L. Vandevelde, "Day-ahead unit commitment model for microgrids," *IET Generation, Transmission & Distribution*, vol. 11, no. 1, pp. 1–9, Jan. 2017.

[26] N. Zhang, Z. Hu, D. Dai, S. Dang, M. Yao, and Y. Zhou, "Unit commitment model in smart grid environment considering carbon emissions trading," *IEEE Trans. Smart Grid*, vol. 7, no. 1, pp. 420–427, Jan. 2016.

[27] B. Marti, "Emissions of power delivery systems," Master's thesis, Swiss Federal Institute of Technology (ETH), Zurich, 2005.

[28] I. J. Raglend and N. P. Padhy, "Solutions to practical unit commitment problems with operational, power flow and environmental constraints," in *Proc. IEEE Power Engineering Soc. General Meet.*, Jun. 2006.

[29] W. R. Coleman and C. M. Grastataro, "American electric power system electric thermal storage program: An evaluation of performance within the home," *IEEE Trans. Power App. Syst.*, vol. PAS-100, no. 12, pp. 4741–4749, Dec. 1981.

[30] L. Hughes, "Meeting residential space heating demand with wind-generated electricity," *Ren. Energy*, vol. 35, pp. 1765–1772, 2010.

[31] N. T. Janssen, R. A. Peterson, and R. W. Wies, "Improved frequency regulation on hybrid wind-diesel microgrids using self-sensing electric thermal storage devices," in *Proc. IEEE Australasian Universities Power Engineering Conference (AUPEC),* Curtin University, Perth, Australia, Sep.-Oct. 2014, pp. 1–6.

[32] S. Wong, G. Gaudet, and L.-P. Proulx, "Capturing wind with thermal energy storage - Summerside's smart grid approach," *IEEE Power Energy Technol. Syst. J.,* pre-print, pp. 1–9, Oct. 2017.

[33] A. Molina, A. Gabaldonó, C. Álvarez, J. A. Fuentes, and E. Gómez, "A physically based load model of residential electric thermal storage: Application to LM programs," *Int. J. Energy Res.*, vol. 24, no. 1, pp. 1–6, 2004.

[34] K. J. Kircher and K. M. Zhang, "Model predictive control of thermal storage for demand response," in *Proc. IEEE American Control Conference,* Chicago, IL, USA, 2015, pp. 956–961.

[35] N. Good, E. Karangelos, A. Navarro-Espinosa, and P. Mancarella, "Optimization under uncertainty of thermal storage-based flexible demand response with quantification of residential users' discomfort," *IEEE Trans. Smart Grid*, vol. 6, no. 5, pp. 2333–2342, Sep. 2015.

[36] M. Ali, J. Jokisalo, K. Siren, and M. Lehtonen, "Combining the demand response of direct electric space heating and partial thermal storage using LP optimization," *Elect. Power Syst. Res.*, vol. 106, pp. 160–167, Jan. 2014.

[37] Y. Tang and J. Zhong, "Operation strategies and performance of air-conditioning systems with thermal energy storages in power systems," in *Proc. IEEE Power Systems Computation Conference (PSCC),* Genova, Italy, Jun. 2016.

[38] S. Wong and J. Pinard, "Opportunities for smart electric thermal storage on electric grids with renewable energy," *IEEE Trans. Smart Grid,* pre-print, pp. 1–9, Jan. 2016.

[39] Z. Bao, Q. Zhou, Z. Yang, Q. Yang, L. Xu, and T. Wu, "A multi time-scale and multi energy-type coordinated microgrid scheduling solution-part i: Model and methodology," *IEEE Trans. Power System*, vol. 30, no. 5, pp. 2257–2266, Nov. 2014.

[40] D. T. Ton and M. A. Smith, "The U.S. Department of Energy's microgrid initiative," *The Electricity Journal*, vol. 25, no. 8, pp. 84–94, Oct. 2012.

[41] C. W. Gellings, "The concept of demand-side management for electric utilities," in *Proc. IEEE*, vol. 73, no. 10, Oct. 1985, pp. 1468 – 1470.

[42] "Benefits of demand response in electricity markets and recommendations for achieving them," U.S. Department of Energy, Tech. Rep., Feb. 2006. [Online]. Available: http://energy.gov/sites/prod/files/oeprod/DocumentsandMedia/DOE_Benefits_of_Demand_Response_in_Electricity_Markets_and_Recommendations_for_Achieving_Them_Report_to_Congress.pdf

[43] J. Zhang, B. M. Hodge, A. Florita, S. Lu, H. F. Hamann, and V. Banunarayanan, "Demand response: An introduction," Rocky Mountain Institute, Boulder, Colorado, Report, Apr. 2006. [Online]. Available: http://www.smartgridinformation.info/pdf/2440_doc_1.pdf

[44] Peaksaver PLUS. [Online]. Available: https://saveonenergy.ca/Consumer/Programs/PeaksaverPlus.aspx

[45] M. Wrinch, G. Dennis, T. H. M. EL-Fouly, and S. Wong, "Demand response implementation for improved system efficiency in remote communities," in *Proc. IEEE Electric Power and Energy Conference (EPEC),* London, Ontario, Canada, Oct. 2011, pp. 1–5.

[46] Managing costs with time-of-use rates. [Online]. Available: https://www.oeb.ca/rates-and-your-bill/electricity-rates/managing-costs-time-use-rates

[47] S. Chan, K. Tsui, H. Wu, Y. Hou, Y.-C. Wu, and F. F. Wu, "Load/price forecasting and managing demand response technologies," *IEEE Signal Processing Mag.*, vol. 29, no. 5, pp. 68–85, Aug. 2012.

[48] M. Geidl, G. Koeppel, P. Favre-Perrod, G. Andersson, and K. Frohlich, "Energy hub for the future," *IEEE Power Energy Mag.*, vol. 5, no. 1, pp. 24–30, Jan/Feb 2007.

[49] M. C. Bozchalui, S. A. Hashmi, H. Hassen, C. A. Cañizares, and K. Bhattacharya, "Optimal operation of residential energy hubs in smart grids," *IEEE Trans. Smart Grid*, vol. 3, no. 4, pp. 1755–1766, Dec. 2012.

[50] C. McParland, "Home network technologies and automating demand response," Berkeley National Laboratory, Technical Report, Dec. 2008.

[51] J. McLellan. Automated home / energy management. [Online]. Available: http://apps1.eere.energy.gov/buildings/publications/pdfs/building_america/ns/ahem_8_home_automation_trends.pdf

[52] STEFFES ETS room unit specifications. [Online]. Available: http://www.steffes.com/electric-thermal-storage/room-units/

[53] W. L. Winston and M. Venkataramanan, *Introduction to Mathematical Programming.* 4th ed. Curt Hinrichs, 2003.

[54] J. Nocedal and S. J. Wright, *Numerical Optimization.* 2nd ed. Springer.

[55] E. Castillo, A. J. Canejo, P. Pedregal, R. Garcia, and N. Alguacil, *Building and Solving Mathematical Programming Models in Engineering and Science.* Wiley, 2002.

[56] (2015, May) GAMS - The solver manuals. [Online]. Available: http://www.gams.com/dd/docs/solvers/allsolvers.pdf

[57] P. Belotti, C. Kirches, S. Leyffer, J. Linderoth, J. Luedtke, and A. Mahajan, "Mixed-Integer Non-linear Optimization," Argonne National Laboratory, Illinois, U.S.A., Technical report, Nov. 2012. [Online]. Available: http://www.mcs.anl.gov/papers/P3060-1112.pdf

[58] I. E. Grossmann, "Review of nonlinear mixed-integer and disjunctive programming techniques," *Optimization and Engineering*, vol. 3, no. 3, pp. 227–252, Sep. 2002.

[59] R. E. Rosenthal, "GAMS - A user's guide," Tech. Rep., May 2015. [Online]. Available: http://www.gams.com/dd/docs/bigdocs/GAMSUsersGuide.pdf

[60] J. Malczeswski and C. Rinner, *Multiobjective Optimization Methods. In: Multicriteria Decision Analysis in Geographic Information Science. Advances in Geographic Information Science.* Springer, Berlin, Heidelberg, 2015.

[61] R. J. Yinger, "Behavior of Capstone and Honeywell microturbine generators during load changes, Ernest Orlando Lawrence Berkeley National Lab." Tech. Rep., Feb. 2004. [Online]. Available: http://www.certs.lbl.gov/pdf/49095.pdf

[62] F. Scarselli and A. C. Tsoi, "Universal approximation using feedforward neural networks: A survey of some existing methods, and some new results," *Journal on Neural Networks*, vol. 11, no. 1, pp. 15–37, Jan. 1998.

[63] M. Beale, M. T. Hogan, and H. B. Demuth, "Neural network toolbox," Neural Network Toolbox, The Math Works, pp. 5–25, 1992.

[64] K. Rudion, A. Orths, Z. Styczynski, and K. Strunz, "Design of benchmark of medium voltage distribution network for investigation of DG integration," in *Proc. IEEE PES Gen. Meet.*, Jun. 2006.

[65] B. V. Solanki, A. Raghurajan, K. Bhattacharya, and C. A. Cañizares, "Including smart loads for optimal demand response in integrated energy management systems for isolated microgrids," *IEEE Trans. Smart Grid*, vol. 8, no. 4, pp. 1739–1748, Jul. 2017.

[66] B. V. Solanki, K. Bhattacharya, and C. A. Cañizares, "Integrated energy management system for isolated microgrids," in *Proc. IEEE Power Systems Computation Conference (PSCC),* Genova, Italy, Jun. 2016.

[67] M. Arriaga, A. Madhavan, X. Wu, C. A. Cañizares, and M. Kazerani, "Database of electrical grid and microgrid systems in Canada's northern and remote communities," Hatch Ltd. Contract, ecoII NRCan project, Department of Electrical & Computer Engineering, University of Waterloo, Tech. Rep., Mar. 2014.

[68] C. Goldman and M. Kito, "Review of demand-side bidding programs: Impacts, costs, and cost-effectiveness," National Technical Information Service, U.S. Department of Commerce, Technical Report, May 1994.

[69] A. Hajimiragha and M. R. D. Zadeh, "Research and development of a microgrid control and monitoring system for remote community of Bella Coola: Challenges, solutions, achievements and lessons learned," in *Proc. IEEE Int. Conf. on Smart Energy Grid Eng. (SEGE)*, Aug. 2001.

[70] "The first Canadian smart remote microgrid: Hartley Bay, BC," Natural Resources Canada, Tech. Rep. [Online]. Available: http://www.nrcan.gc.ca/sites/www.nrcan.gc.ca/files/canmetenergy/files/pubs/2013-035_en.pdf

[71] B. V. Solanki, C. A. Cañizares, and K. Bhattacharya, "Practical energy management systems for isolated microgrids," *IEEE Trans. Smart Grid,* submitted Jan 2018, pp. 1–8.

[72] E. Pouresmaeil, J. M. Gonzalez, C. A. Cañizares, and K. Bhattacharya, "Development of a smart residential load simulator for energy management in smart grids," University of Waterloo, Waterloo, Canada, Tech. Rep. [Online]. Available: https://uwaterloo.ca/power-energy-systems-group/sites/ca.power-energy-systems-group/files/uploads/files/srls.pdf

[73] Smart residential load simulator. [Online]. Available: https://uwaterloo.ca/power-energy-systems-group/downloads/smart-residential-load-simulator-srls

[74] Weather historical data. [Online]. Available: http://climate.weather.gc.ca/historical_data/search_historic_data_e.html

[75] Household consumption. [Online]. Available: http://www.hydroquebec.com/residential/energy-wise/electricity-consumption-by-use.html

[76] "Households and the environment: Energy use," Statistics Canada - Environment Accounts and Statistics Division, Tech. Rep. 11-526-S, 2011. [Online]. Available: http://www.statcan.gc.ca/pub/11-526-s/11-526-s2013002-eng.pdf

[77] M. Arriaga, "Long-term renewable energy electricity planning for remote communities," Ph.D. dissertation, University of Waterloo, Waterloo, Ontario, Canada, 2015.

[78] B. V. Solanki, K. Bhattacharya, and C. A. Cañizares, "A sustainable energy management system for isolated microgrids," *IEEE Trans. Sustainable Energy*, vol. 8, no. 4, pp. 1507–1517, Oct. 2017.

[79] "Compilation of air pollutant emission factor," U.S. Environmental Protection Agency, NC, Tech. Rep., Jan. 1995. [Online]. Available: https://www3.epa.gov/ttn/chief/ap42/index.html

[80] "Climate change 2007: The physical science basis," Intergovernmental Panel on climate change (IPCC), Tech. Rep., 2007.

[81] "Social cost of carbon," U.S. Environmental Protection Agency, NC, Tech. Rep., Dec. 2015. [Online]. Available: http://www3.epa.gov/climatechange/Downloads/EPAactivities/social-cost-carbon.pdf

[82] "Exhaust emission data sheet 2500DQLE," Cummins Power Generation, Tech. Rep. [Online]. Available: https://powersuite.cummins.com

[83] P. S. Sauter, B. V. Solanki, C. A. Cañizares, K. Bhattacharya, and Sören Hohmann, "Electric thermal storage system impact on northern communities' microgrids," *IEEE Trans. Smart Grid,* pre-print, pp. 1–12, Sep. 2017.

APPENDICES

Appendix A

Modified CIGRE Medium-Voltage Test System Data

Table A.1: Line Parameters

Node from-to	R_{ph} [Ω]	X_{ph} [Ω]	B_{ph} [μS]	R_0 [Ω]	X_0 [Ω]	B_0 [μS]
1-2	0.208	0.518	4.596	0.421	2.160	1.884
2-3	0.173	0.432	3.830	0.351	1.800	1.570
3-4	0.106	0.264	2.336	0.214	1.098	0.958
4-5	0.097	0.242	2.145	0.197	1.008	0.879
5-6	0.266	0.665	5.898	0.541	2.772	2.418
6-7	0.042	0.104	0.919	0.084	0.432	0.377
7-8	0.289	0.721	6.396	0.586	3.006	2.622
8-9	0.055	0.138	1.226	0.112	0.576	0.502
9-10	0.133	0.333	2.949	0.270	1.386	1.209
10-11	0.057	0.143	1.264	0.116	0.594	0.518
11-4	0.085	0.212	1.877	0.172	0.882	0.769
3-8	0.225	0.562	4.979	0.456	2.340	2.041
1-12	0.846	2.112	18.729	1.716	8.802	7.677
12-13	0.517	1.292	11.452	1.049	5.382	4.694
13-8	0.346	0.864	7.660	0.702	3.600	3.140

Table A.2: Load Parameters

Node	Apparent Power [kVA]						Power Factor	
	Phase A		Phase B		Phase C		Res	Com
	Res	Com	Res	Com	Res	Com		
1	344.00	80.00	172.00	180.00	200.00	180.00	0.90	0.80
2	100.00	200.00	50.00	200.00	0.00	200.00	0.95	0.85
3	0.00	80.00	200.00	80.00	50.00	80.00	0.90	0.80
4	200.00	0.00	100.00	0.00	100.00	0.00	0.90	1.00
5	200.00	50.00	172.00	200.00	0.00	50.00	0.95	0.85
6	50.00	0.00	100.00	0.00	172.00	0.00	0.95	1.00
7	0.00	100.00	100.00	100.00	0.00	100.00	0.95	0.95
8	100.00	0.00	150.00	0.00	0.00	200.00	0.90	0.90
9	100.00	0.00	150.00	0.00	100.00	0.00	0.95	1.00
10	150.00	0.00	100.00	0.00	250.00	0.00	0.90	1.00
11	50.00	150.00	50.00	150.00	0.00	150.00	0.95	0.85
12	0.00	145.00	0.00	145.00	0.00	145.00	0.95	0.85
13	0.00	90.00	0.00	90.00	172.00	90.00	0.90	0.90

Table A.3: Synchronous Generator Parameters

Unit No	S_{base} [kVA]	V_{base} [kV]	$\bar{P}$ [kW]	$\underline{P}$ [kW]	$\vec{Z}_g^{l,l}$ [p.u.]	$\vec{Z}_g^{l,m}$ [p.u.]	$\vec{Z}_g^{m,l}$ [p.u.]
1	3125	0.48	2500	1000	1.0815j	-0.8390-0.5153j	0.8390-0.5153j
2	1750	0.48	1400	600	1.0815j	-0.8390-0.5153j	0.8390-0.5153j
3	1000	0.48	800	350	1.0815j	-0.8390-0.5153j	0.8390-0.5153j

Table A.4: ESS Parameters

ESS Unit No	$\bar{P}$ [kW]	η^{ch} [%]	η^{dch} [%]
1	750	86	86
2	41.25	55	55
3	265	55	55
4	250	86	86
5	17.5	55	55

Table A.5: Generator Parameters

DG Unit No	d [US$/kWh^2]	e [US$/kWh]	f [US$]	C^{sup} [US$]	C^{sdn} [US$]	R [kW/min]	T^{up} [min]	T^{dn} [min]
1	0.0000088	0.197	40.04	83.6	13.464	250	60	60
2	0	0.226	22.44	39.6	7.304	140	60	60
3	0	0.253	6.6	13.2	4.664	100	30	30
4	0	0.253	0	6.468	1.2672	60	30	30
5	0.0000976	0.00552	0.018414	0.829	0	100	30	30

Table A.6: Generator Emission Characteristics

DG Unit No	d^{em} [tonne/kWh^2]	e^{em} [tonne/kWh]	f^{em} [tonne]	C^{em-sup} [tonne]	C^{em-sdn} [tonne]
1	1.2228	-0.48236	1.4235	0.0712	0.0356
2	0.0234	0.8114	0.1505	0.1075	0.0537
3	4.3792	-0.4755	0.3449	0.0165	0.0082
4	0	1.8849	-0.0087	0.0479	0.0239
5	0.0088	8.972	0.0594	0.03788	0.1894

Appendix B

Kasabonika Lake First Nation System Data

Table B.1: Line Parameters

Node from-to	R_{ph} [Ω]	X_{ph} [Ω]	B_{ph} [μS]	R_0 [Ω]	X_0 [Ω]	B_0 [μS]
1-2	0.2688	0.3984	3.1576	0.5744	1.2416	1.368
2-3	0.1008	0.1494	1.1841	0.2154	0.4656	0.513
3-4	0.1512	0.2241	1.77615	0.3231	0.6984	0.7695
4-5	0.168	0.249	1.9735	0.359	0.776	0.855
5-6	0.2184	0.3237	2.56555	0.4667	1.0088	1.1115
6-7	0.09744	0.14442	1.14463	0.20822	0.45008	0.4959
4-8	0.1344	0.1992	1.5788	0.2872	0.6208	0.684
8-9	0.1008	0.1494	1.1841	0.2154	0.4656	0.513
9-10	0.1176	0.1743	1.38145	0.2513	0.5432	0.5985
10-11	0.084	0.1245	0.98675	0.1795	0.388	0.4275

Table B.2: Synchronous Generator Parameters

Unit No	S_{base} [kVA]	V_{base} [kV]	$\bar{P}$ [kW]	$\underline{P}$ [kW]	$\vec{Z}_g^{l,l}$ [p.u.]	$\vec{Z}_g^{l,m}$ [p.u.]	$\vec{Z}_g^{m,l}$ [p.u.]
1	2750	0.48	1500	600	1.0331j	-0.7419-0.5j	0.7419-0.5j
2	1875	0.48	1000	400	1.0331j	-0.7419-0.5j	0.7419-0.5j
3	1000	0.48	600	240	1.0755j	-0.7967-0.5227j	0.7967-0.5227j

Table B.3: Generator Parameters

DG Unit No	d [US$/kWh^2]	e [US$/kWh]	f [US$]	C^{sup} [US$]	C^{sdn} [US$]	R [kW/min]	T^{up} [min]	T^{dn} [min]
1	0.000123	1.0027	107.3	83.6	13.464	150	30	30
2	0	0.5	88.06	39.6	7.304	100	30	30
3	0.0000187	0.171	37.69	13.2	4.664	60	30	30